Master Thesis, Department of Geosciences

Geomechanical characterization of shale caprock of the Longyearbyen CO2 storage pilot

Mohsin Abbas

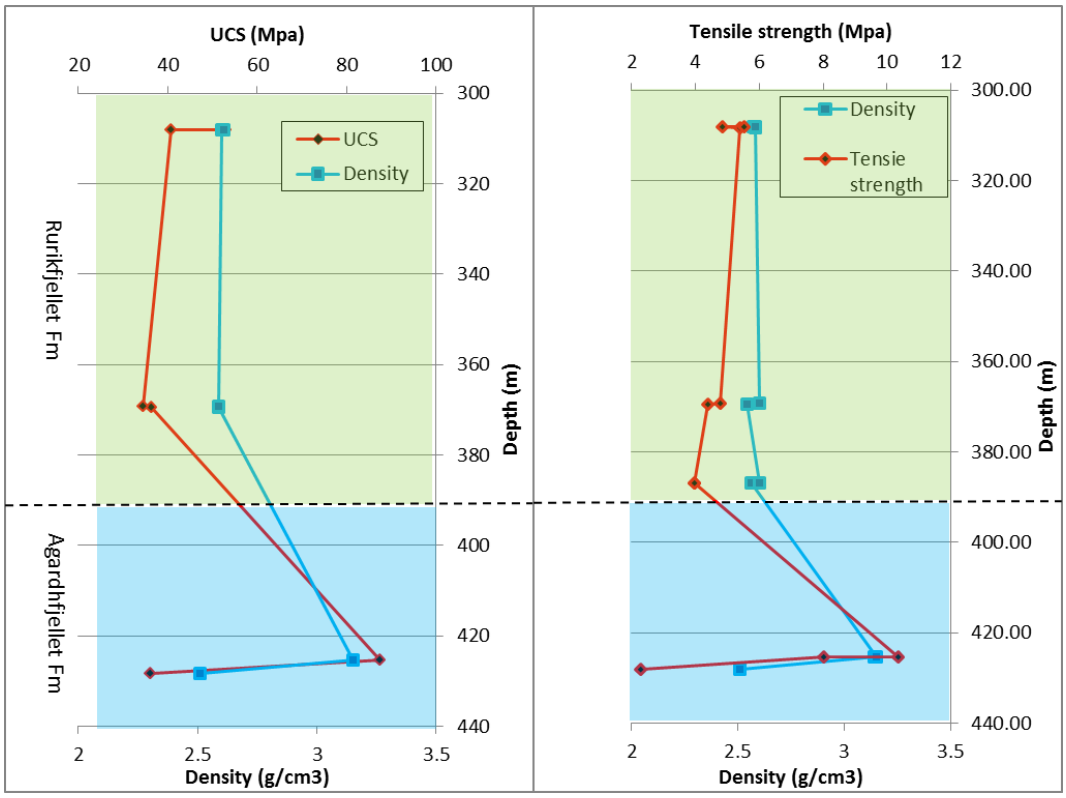

UNIVERSITY OF OSLO
FACULTY OF MATHEMATICS AND NATURAL SCIENCES

Geomechanical characterization of shale caprock of the Longyearbyen CO2 storage pilot

Mohsin Abbas

Master Thesis in Geosciences

Discipline: Geophysics

Department of Geosciences

Faculty of Mathematics and Natural Sciences

University of Oslo

June 2015

Supervisors: **Nazmul Hague Mondol (UiO), Bahman Bohloli (NGI) and Elin Skurtveit (NGI)**
This work is published digitally through DUO – Digitale Utgivelser ved UiO
http://www.duo.uio.no
It is also catalogued in BIBSYS (http://www.bibsys.no/english)

Preface

This thesis is submitted to the Department of Geoscience, University of Oslo (UiO) in candidacy of the M.Sc. degree in Geophysics.

This study has been carried out at Norwegian Geotechnical Institute (NGI) and Department of Geoscience, University of Oslo (UiO) from August 2014 to May 2015 under supervision of Nazmul Haque Mondol (UiO & NGI), Bahman Bohloli (NGI) and Elin Skurtveit (NGI).

Acknowledgements

I am very grateful and would like to thank my supervisors; Nazmul Haque Mondol (UiO & NGI), Bahman Bohloli (NGI) and Elin Skurtveit (NGI) for their motivation, support, guidelines and precious time throughout the research. Thanks to NGI for providing me caprock samples and access to their rock mechanical laboratory to perform Geomechanical tests.

I would like to thank many NGI people especially Lars Grande, Magnus Soldal, Reidar Otter and Sven Vangbæk for their help in the laboratory work and acquisition and processing of data.

I would like to thank Salahalldin Akhavan, Maarten Aerts and Berit Løken Berg at the Department of Geoscience, UiO for their help for SEM and XRD analyses. I am also thankful to administrative and academic staff of the Department of Geoscience for their continuous support throughout the thesis.

I would to thank my study colleagues, especially Truong Tran, Eivind Bernhard Larsen and Fredrik Magnussen for their great help and time.

SUCCESS (Subsurface CO_2 Storage- Critical Elements and Superior Strategy) FME center is acknowledged for financial support of this work and UNIS CO_2 Lab Pilot is acknowledged for providing data and core samples.

A special thanks to my elder brother Nadeem Abbas, my parents and other family members for their continuous financial and moral support, prayers and encouragement during these two years of my Master's study in Norway.

Mohsin Abbas

Abstract

Mechanical anisotropy and deformation behavior of cap rock is very important for safe subsurface storage of CO2. This is achieved partly by performing mechanical testing of core samples. In this study, a combined approach including mechanical testing and characterization of material is applied to evaluate strength parameters of two caprocks from the Longyearbyen (LYB) CO2 storage site. The study area is located 6 km east of the main town Longyearbyen in Central Spitsbergen, Norway. The caprock of the CO2 storage site comprises two geological formations (Agardhfjellet and Rurikfjellet) dominated by shale of Late Jurassic to Early Cretaceous age.

Core samples from well Dh-6 targeting both of the formations of overburden/caprock from 308 to 428.28 m of depth are utilized for rock mechanical testing. These tested cores were well preserved in paraffin and kept in a controlled temperature room. Ten disc shaped and six cylindrical shaped core plugs of certain dimensions (following ISRM and ASTM standards) were prepared for Brazilian and Uniaxial Compressive Strength (UCS) tests. Several important geomechanical parameters such as tensile strength, uniaxial compressive strength and Young's modulus and acoustic velocity (both P- and S-wave velocities) were measured utilizing the two standard mechanical tests. Also the caprock samples were characterized using XRD and SEM techniques.

The estimated tensile strength, σt, for whole set of tested plugs from caprock unit (depth range 308-428.28 m), ranges from 2.29 to 10.35 MPa. Two plugs; AFF-32A-BR and AFF-32B-BR from Agardhfjellet formation (depth range 425.28-425.43m) have exceptionally higher tensile strength of 10.35 and 8.01 MPa respectively, also their density is very high (3.15 g/cm3). Reason for this anomaly is the high content of Siderite (FeCO3) up till 80.19% (measured by XRD analysis) and high compaction because these plugs belong to a detachment zone.

Calculated uniaxial compressive strength, σc, Young' modulus, *E*, and P- and S-waves velocities ranges for the whole tested depth (308-428.28m) from caprock unit are; 34.58-87.37 MPa, 5.17-44.34 GPa and Vp (3551.20-5677.06 m/s) & Vs (1510.15-4100.01 m/s) respectively. A tested plug AFF-32-UCS from depth range 425.28-425.43 m has exceptionally higher values of all measured parameters from UCS test. Reasons for these anomalies from this depth are same as described for higher density and tensile strength from the same depth.

Results from this study can be used to assess the strength and preliminary quality checks for the safe CO2 storage into the reservoir. For instance estimated vertical tensile strength and behavior of rock specimen under tension can be utilized to avoid hydro-fracturing when the caprock is subjected to extra fluid pressure due to injection. Also index test data from UCS tests can also be used for various aspects of modeling caprock integrity.

Table of contents

Preface I

Acknowledgements III

Abstract V

List of Figures IX

Chapter 1 IX

Chapter 2 IX

Chapter 3 IX

Chapter 4 X

Chapter 5 XI

List Tables XIII

Chapter 1 XIII

Chapter 3 XIII

Chapter 4 XIII

Chapter 5 XIII

Chapter 1: Introduction 1

1.1 Background and motivation 1

1.2 Research focus 1

1.3 The Study area 2

1.4 Database and software 3

1.5 Limitations, implications and future works 3

1.6 Chapter descriptions 4

Chapter 2: Geology of the study area 5

2.1 Regional geologic setting 5

2.2 Structure and tectonic 7

2.3 Stratigraphy 10

2.3.1 Adventdalen Group 10

2.3.2 Kapp Toscana group 13
Chapter 3: Materials and research methodology 14
3.1 Available materials 14
3.1.1 Core sample inventory 14
3.1.2 Sample preparation 15
3.2 Characterization of material 17
3.2.1 Density 17
3.2.2 Mineralogical analysis 18
3.2.3 Mineral quantification 19
3.2.4 Microstructure analysis and mineral identification 20
3.3 Mechanical testing 27
3.3.1 Brazilian Test 27
3.3.2 Uniaxial compressive strength test 30
3.4 Work flow 35
Chapter 4: Tensile strength Analysis 37
4.1 Results 37
4.1.1 Rurikfjellet formation 38
4.1.2 Agardhfjellet formation 42
4.2 Discussion 44
4.2.1 Pre- and post-test analysis of tested plugs 44
4.2.2 Load-time curves and corresponding tensile strength analysis 47
4.2.3 Tensile strength and density versus depth analysis 49
4.2.4 Comparison with previous studies 50
Chapter 5: Uniaxial compressive strength and velocity analyses 53
5.1 Results 53
5.1.1 Uniaxial compressive strength test 53
5.1.2 Velocity measurements 59
5.2 Discussion 61

5.2.1 Pre- and post-test analysis 61

5.2.2 Load-time plots and featured UCS strength based analysis 63

5.2.3 UCS and density versus depth profile 65

5.2.4 Stress versus axial strain and Young's modulus (E) analysis..... 65

5.2.5 Velocity analysis 66

5.2.6 Comparison with previous work 67

Chapter 6: Summary and conclusions 71

6.1 Summary 71

6.2 Conclusions 72

References 74

Appendix I (Extended abstract)..... 77

List of Figures

Chapter 1

Fig.1.1: Location of the Longyearbyen CO2 Storage Lab and wells with reference to geographical map of Svalbard (modified from Bohloli B. et al. (2014). 2

Chapter 2

Fig. 2.1 Geological Map of Svalbard showing BFZ and LFZ bounding Central Spitsbergen basin. The LYB CO2 Filed Pilot is marked by black square (modified from Nøttvedt et al. (1993). 5

Fig. 2.2: Stage 1: Stratigraphy of Upper Paleozoic sequences of the Barents Shelf (Worsley, 2008)..... 6

Fig. 2.3: Tectonic activity and uplift in the Barents Sea (modified from Dimakis et al. (1998)). 8

Fig. 2.4: Map showing major structural elements of the Barents Sea with location of Svalbard (modified from (Worsley, 2008) 9

Fig. 2.5: Map showing major structural elements of central Spitsbergen including location of study area. Abbreviations: BFZ-Billeforden Fault Zone; LFZ- Lomfjorden Fault Zone (Ogata et al., 2014b). 9

Fig. 2.6: Lithostratigraphic chart showing the stratigraphy of Svalbard and Barents Sea.The study area, is marked by red square (modified from UiO Natrual history museum (2015)). .. 11

Fig. 2.7: Well log correlation with stratigraphy, depositional environment, ages. Figure shows all the wells and CO2 sealing and storage units (modified from Braathen et al. (2012a)..... 12

Chapter 3

Fig. 3.1: Image on the upper left side is a plug for Brazilian test and down left side is a plug for UCS test. Image on the right side is the core sample. 16

Fig. 3.2: Diffractogram of sample RFF-32. 18

Fig. 3.3: Scanned and zoomed area of thin section RFF-8 with spectrums is shown. 19

Fig. 3.4: SEM images at various scales: (a) Identified minerals are shown at 100 µm scale, (b) identified minerals at 40 µm scale, (c) very clear identification of pyrite minerals at 100 µm and (d) identified minerals and porosity (black color) at 200 µm scale..... 21

Fig. 3.5: Area measurements of thin section from sample RFF-8; Red: porosity, Blue: heavy minerals and Green: rest of the minerals. 22

Fig. 3.6: SEM images: (a) Site of interest at 50 um scale showing most of the identified minerals, (b) Image at 600 um is not a clear picture to see the various grains but blank spaces are very visible and (c) Image at 200 um scale where particles are more visible with few blank spaces and very tiny fractures. 23

Fig. 3.7: Area measurements from two selected sites on thin section from sample RFF-18 ... 24

Fig. 3.8: SEM images of sample AFF-32: (a) Electron image at 600µm scale showing prominent distribution of Siderite, Muscovite and Pyrite, (b) Electron image at 100µm scale showing most of the identified minerals and there grain shapes are also visible, (c) Electron image at 90 µm scale showing very prominent Dolomite and Pyrite grains with few other minerals and (d) SEM image at 40 µm scale showing Kaolinite surrounded by Pyrite ring and clearly visible Quartz grains. 25

Fig. 3.9: Area measurements from a selected site of interest (sample AFF-32). 26

Fig. 3.10: Schematic illustration of Brazilian test (modified from Bresciani et al. (2004)). 27

Fig. 3.11: (a) Apparatus for Brazilian test at NGI lab and (b) Steel jaws for holding a sample. 28

Fig. 3.12: Schematic diagram of load application to measure Brazilian tensile strength of the plugs loaded in perpendicular and parallel directions to the bedding planes. 29

Fig. 3.13: Graph showing the load vs time plot and peak load at the first break. 30

Fig. 3.14: Uniaxial compressive strength test conditions (JCRM, 2011). 30

Fig. 3.15: (a) Apparatus for UCS test at NGI lab, (b) Steel platens while holding a plug during test. 31

Fig. 3.16: (a) Graph showing the Load vs time plot and peak load at 1st break and (b) Graph showing stress-curve of sample RFF-8A-UCS. 32

Fig.3.17: Axial strain gauge (NGI lab) 33

Fig. 3.18: False deformation curve 33

Fig. 3.19: An example of time picking for velocity measurements using the NGI's time pick script. 34

Fig. 3.20: Visual explanation of zero correction to get the actual travel time through a sample (T_o = travel time in the steel platens, Tr = total travel time from one transducer to another and Ts = travel time of signal in the length of sample). 35

Fig. 3.21: Work flow for this study. 36

Chapter 4

Fig. 4.1: Load-time plot (part1) of samples from Rurikfjellet Formation. 38

Fig. 4.2: Load-time plot (Part 2) of samples from Rurikfjellet Formation. 39

Fig. 4.3: Fracture pattern recorded for four different test plugs (part 1) from Rurikfjellet Formation. 40

Fig. 4.4: Fracture pattern recorded for three different test plugs (part 2) from Rurikfjellet Formation. 41

Fig. 4.5: Tensile strength versus depth of entire set of plugs from Rurikfjellet Formation. 42

Fig. 4.6: Load-time plots of samples from Agardhfjellet Formation. 43

Fig. 4.7: Fracture pattern recorded for the different tests from Agardhfjellet Formation. 44

Fig. 4.8: Tensile strength and density are plotted versus depth for Rurikfjellet and Agardhfjellet formations. 49

Fig. 4.9: Comparison of tensile strength and density of this study with previous work performed at NGI. Plot on the left side is tensile strength versus depth and on the right side is density versus depth 50

Fig. 4.10: Load-time plots of plugs loaded parallel (left side) and perpendicular (right side) to the bedding planes (data from Bohloli B. et al. (2014)). 51

Fig. 4.11: Comparison of tensile strength of this study with previously measured data at NGI for different rocks from different depths (modified from NGI (2012)) 52

Chapter 5

Fig. 5.1: Load-time plots of plugs from Rurikfjellet formation. 55

Fig. 5.2: Stress-axial strain plots of plugs from Rurikfjellet formation. 56

Fig. 5.3: Load-time plots of two plugs from Agardhfjellet formation (depth range 425.28-428.28m). 57

Fig. 5.4: Stress-strain (axial) curves of plugs from Agardhfjellet formation. 58

Fig. 5.5: Stress versus velocity: (a) stress versus Vp and (b) stress versus Vs of four plugs from Rurikfjellet formation (depth 308-369.53m). 60

Fig. 5.6: Velocity versus stress: (a) Vp versus stress and (b) Vs versus stress plots of plugs from Agardhfjellet formation (depth 425.28-428.28m). Decrease of velocities at very high stresses may be related to initiation of fractures inside the sample. 61

Fig. 5.7: UCS and density versus depth profiles for whole tested plugs from both formations (depth 308-428.28m). 65

Fig. 5.8: UCS and E versus P-wave velocity of entire set of tested plugs from Rurikfjellet and Agardhfjellet formations. 67

Fig. 5.9: Comparison of UCS and Young's modulus of this study with previous work at NGI is shown. 68

Fig. 5.10: Comparison of UCS of this study with previously made UCS versus depth correlation profile by(NGI, 2012) 69

Fig. 5.11: A comparison of calculated Young's modulus of this study with a previously made Young's modulus versus depth profile by (NGI, 2012) 70

List Tables

Chapter 1

Table 1.1: List of data from previous work..... 3

Chapter 3

Table 3.1: List of studied core samples from well Dh-6. 14

Table 3.2: Pictures of selected sample with their IDs and description of the cores. 15

Table 3.3: Summary of prepared plugs for mechanical thin section and XRD study. 16

Table 3.4: Calculated densities of selected samples..... 17

Table 3.5: Summary of bulk mineralogy of the selected samples. 20

Table 3.6: List of identified minerals for sample RFF-8..... 20

Table 3.7: Identified minerals in RFF-18 during SEM. 22

Table 3.8: list of identified minerals from thin section (sample AFF-32). 24

Chapter 4

Table 4.1: Summary of results from Brazilian tests and parameters of all the plugs used for testing. 37

Table 4.2: Overview of Brazilian test plugs from Rurikfjellet formation. 38

Table 4.3: Brief overview of test plugs from Agardhfjellet Formation. 42

Table 4.4: Pre- and post-test pictures of tested plugs from Rurikfjellet Formation. 45

Table 4.5: Pre- and post-test summary of plugs from Agardhfjellet Formation. 47

Chapter 5

Table 5.1: Results of entire dataset from UCS test and parameters of plugs are listed. 53

Table 5.2: A general overview of Rurikfjellet formation..... 54

Table 5.3: Highlights of Agardhfjellet formation 57

Table 5.4: Summary of P- and S-wave velocity measurements..... 59

Table 5.5: Visual summary of pre- and post-test plugs from Rurikfjellet formation..... 62

Table 5.6: Visual summary of pre- and post-test images of plugs from Agardhfjellet formation. 63

Chapter 1: Introduction

1.1 Background and motivation

Injected CO2 is trapped in geological formations under the caprock by a number of different mechanisms: structural trapping (under caprock anticline), stratigraphic trapping (under impermeable layers), solubility trapping (CO2 dissolving in pore water), mineral trapping (CO2 trapped by chemical reactions) and capillary trapping, each with its own timescale of effectiveness. Interaction between CO2 and reservoir and cap rock may change the geomechanical and geochemical properties of the caprock, leading to changes its integrity such as porosity, fracturing and permeability and so lead to leak CO2 from the reservoir. Caprock integrity refers to the geomechanical properties of the caprock that controlled by lithology, pre-existing planes of weakness, regional stresses and orientation and magnitude of induced stresses due to fluid injection or withdrawn.

Braathen et al. (2012a) assessed geological conditions of Longyearbyen (LYB) CO2 storage site. Anell et al. (2014) discussed regional geology, faults and fracture systems of the LYB CO2 storage. Ogata et al. (2011) and (2014b) reported the natural fractures in the CO2 reservoir and their importance for the CO2 movement in the reservoir. Bælum et al. (2012) presented subsurface structures of LYB CO2 storage area. Recently, Bohloli B. et al. (2014) reported the evaluation caprock on the basis of laboratory experiments and in-situ injection tests. The motivation of this work is to extend Bohloli et al. 2014 work to acquire additional data to understand properties of two caprock formations (Agardhfjellet and Rurikfjellet) from the LYB CO2 storage. Detail mineralogical characterization of caprocks and assessment of caprock integrity using two standard laboratory tests (Brazilian and Uniaxial Compressive Strength) are of prime interest in this study.

1.2 Research focus

The research has strong focused on characterization of two caprock formations (Agardhfjellet and Rurikfjellet) and to determine their rock mechanical properties employing Brazilian and Uniaxial Compressive Strength (UCS) tests. The tasks of the research are highlighted bellow:

- Quantification of minerals and their microstructure
- Calculation of indirect tensile strength from the Brazilian test
- Calculation of Uuniaxial Compressive Strength from the UCS tests and measured their corresponding acoustic velocity
- Assessment of the caprock integrity combining result from uniaxial compressive, shear and tensile strengths and mineralogical analysis.

Estimation of tensile strength for a caprock can be very important aspect, especially when it is subjected to a fluid injection into the storage reservoir. Cap rock can undergo hydrofracturing when the pore fluid pressure reaches the equal level or surpass the maximum limit of tensile strength. To avoid hydrofracturing it is very critical to determine tensile strength for the safety of caprock.

1.3 The Study area

The LYB CO2 Storage Laboratory is located 6 km east of the main town Longyearbyen in Central Spitsbergen, Norway (Fig.1.1). This lab is considered to be the flagship from the archipelago of the Svalbard that offers great and exciting opportunities for geoscience studies and research (Sand et al., 2014). Archipelago of Svalbard is located in between Norway and North Pole in Arctic Ocean. It consists of a chain of the islands (Spitsbergen, Nordaustlandet, Barentsøya, Edgeøya, Kong Karls Land, Prins Karls Forland, and Bjørnøya) between Arctic Ocean, Barents Sea, Greenland Sea and Norwegian Sea (Fig.1.1).

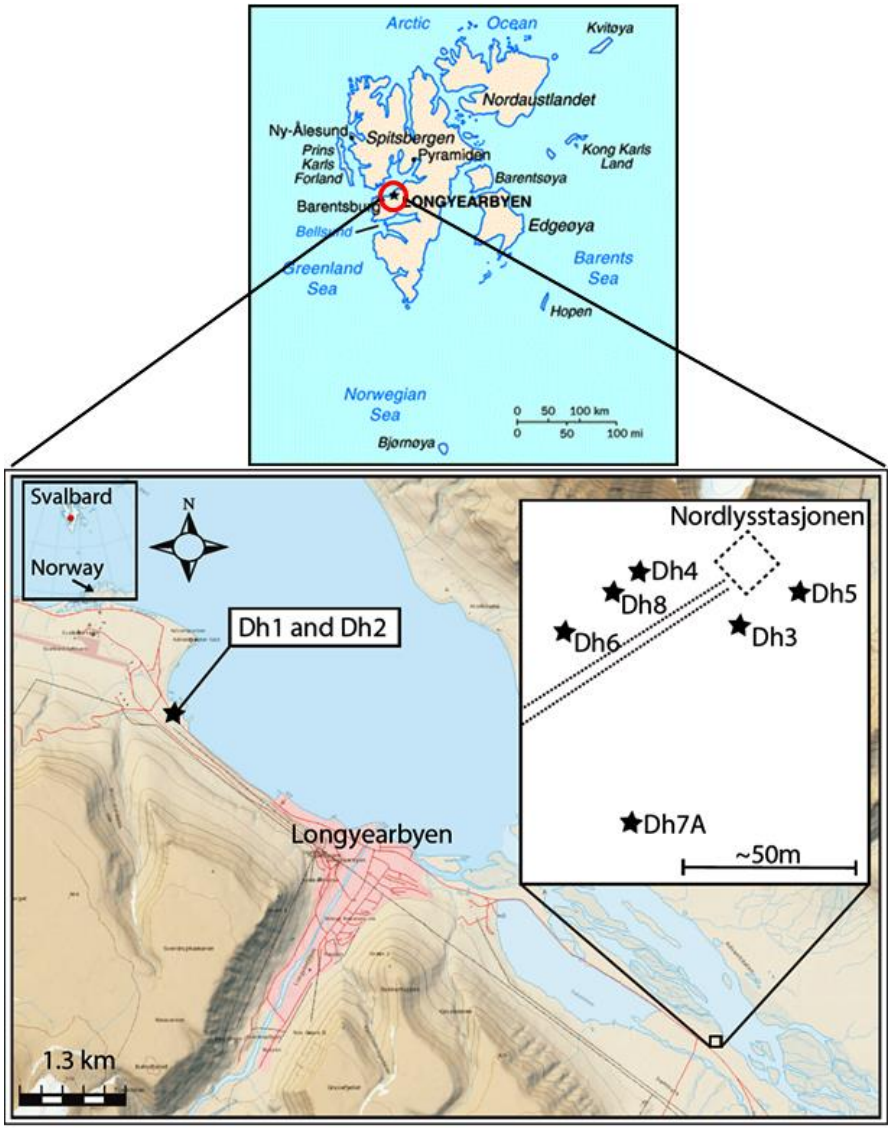

Fig.1.1: Location of the Longyearbyen CO2 Storage Lab and wells with reference to geographical map of Svalbard (modified from Bohloli B. et al. (2014).

A total of eight boreholes (Dhs 1-8) have been drilled in this study area, also called Longyearbyen Well Park. The main purpose of these wells is to acquire information of mechanical and physical properties of overburden, cap rocks and reservoir rocks, more specifically the pattern of fluid flow within the storage reservoir for CO2 in-situ conditions. The current study involves Dh-6 borehole (TD 435.00 meters) targeting two caprock formations of Agardhfjellet and Rurikfjellet belong to Janusfjellet subgroup (subgroup of Adventdalen Group) of Late Jurrassic to Early Cretaceous age (Braathen et al., 2012b).

1.4 Database and software

A total eight core plugs were selected from well Dh-6 from a depth range of 308.00-428.28 meters. All core samples were provided by the Longyearbyen CO2 lab sealed off and stored in the Norwegian Geotechnical Institute (NGI). Data from previous works (Bohloli et al. 2014) collected by the NGI are also utilized in this research (Table 1.1).

Table 1.1: List of data from previous work

Data provider	Reference document	Data type
NGI	20081351-00-19-R	Estimated unconfined compressive and tensile strengths
	20081351-00-25-R	Estimated horizontal and vertical tensile strength
	20120649-02-R	Effective vertical and horizontal stress from triaxial tests

For this study mainly Microsoft office 2010 (Excel, Word and PowerPoint) software is utilized to make tables, plots, writing and presentations. Other softwares such as GeoGebra (a free software provided by geogebra.org) is used to plot Mohr-coulomb failure criterion and the Matlab script time_picker developed by Inge Viken at NGI is used to pick arrival times of P- and S-waves to calculate velocity.

1.5 Limitations, implications and future works

This research has been carried out in limited time and resources. The main source to evaluate the integrity of cap rock unit is core samples and the availability of these cores in terms of quantity and dimensions was very limited. As we know that the more number of samples we test from different depth levels for a formation, the more accurate results we get. But it was not limited in this thesis especially for lower part of the cap rock (Agardhfjellet formation). We had only two cores and they were very different in all aspects, so it is not appropriate to evaluate the entire formation on the basis of limited samples.

It was similar scenario to study the microstructure (grain orientation, shape and microfractures) using SEM analysis technique. Due to limited materials to make thin sections and very short availability of lab resources in term of time detail investigation is somehow restricted. It could be better to compare experimental results to well log data. Due to unavailability of logs in the target depth in well Dh-6 no compare and justify of experimental results have been shown in this study.

To consider limitations that mentioned earlier still this study provides important geomechanical properties (e.g. uniaxial strength, tensile strength and Young's modulus, -P and S-wave velocities) and material characterization provides useful information. The outcomes from the study can be useful not only to evaluate the cap rock integrity of CO2 storage but can also be implemented on petroleum related cap rocks. The test procedures and analysis of Geomechanical properties can be useful for many engineering problems such as subsurface excavations, fracking in the reservoirs for recovery and production enhancement and unconventional shale gas production.

Also some additional work could have been done to make this study work even better and few recommendations are; Geomechanical testing of more core samples from Agardhfjellet formation, fractures study at macro and micro level for both Rurikfjellet and Agardhfjellet formation, Isotropically Consolidated Undrained (CIU) Triaxial Compression Test to define

Mohr-coulombs failure criterion for the entire caprock unit (along with UCS test and Brazilian test information that we have estimated for this study) .

1.6 Chapter descriptions

The thesis has been divided into six chapters. The first chapter is a general overview of the whole study that includes background and motivation, research focus, a brief description of the study area, description of database and softwares. Moreover, several limitations and implications of this study are briefly mentioned at the end.

Chapter two is highlighted geological background of the study area from regional to local scale. The general geology of the study area described under three categories including regional geologic setting, structure and tectonic and stratigraphy.

Chapter three is divided into two sections. The first part of the chapter includes sample inventory, general description and inspection of the samples. Characterization of materials on the basis of density and mineralogical analysis is also shown. The second part described research methodologies and testing protocols of Brazilian and UCS (Unconfined Compressive Strength) tests.

Chapter four covers the tensile strength analysis based on Brazilian test and divided into two major sections. The first section consists of all the results that presented in tables, plots and images. The second section is highlighted all results are their interpretation and detail discussion along with few comparisons made with previous works.

Chapter five focuses results and analysis of geomechanical (e.g. uniaxial compressive strength, Young's modulus) and acoustic parameters acquired by UCS test. The analysis is divided further into two major sections; first part consists of results in form of tables and plots along with main observations and second part focuses interpretation of data in more details.

Chapter six gives a brief summary of the thesis where most important points are discussed. Overall conclusions of important findings of the thesis are highlighted at the end.

Chapter 2: Geology of the study area

This chapter presents general geology of the study area by revising the published literatures. It is divided into three sections: 1) regional geologic setting, 2) structure and tectonic and 3) stratigraphy.

2.1 Regional geologic setting

The study area is located on the margin of the Barents shelf, on the northwestern edge of the Eurasian plate known as the Svalbard Archipelago. This subaerially exposed and uplifted area yield comprehensive geological record. Svalbard is covering an area of approximately 63000 km² (<5% of the total area of the Barents Sea) (Worsley, 2008). The uplifted portion comprises of a chain of islands considered to be the equivalent to the subsurface geology of the Barents Sea. North and west part encountered the strongest uplift and resulted in the exposer of progressively older rocks in this direction (Fig. 2.1). The Central Spitsbergen Basin which is very prominent synclinal feature covering almost all the central Spitsbergen. The West Spitsbergen Orogenic Belt and the Billefjorden (BFZ pointing by red arrow in the figure) and Lomfjorden Fault Zones are bounding the west (LFZ pointing by red arrow in the figure) and east margins of the basin respectively (Nøttvedt et al., 1993).

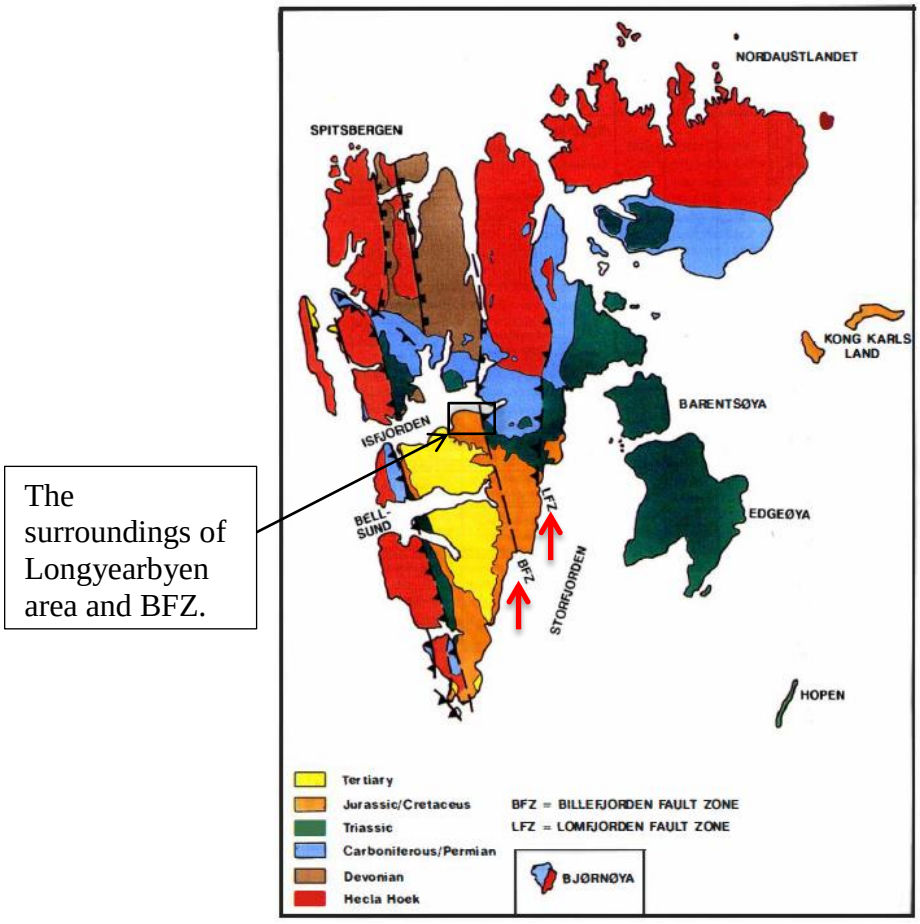

Fig. 2.1 Geological Map of Svalbard showing BFZ and LFZ bounding Central Spitsbergen basin. The LYB CO2 Filed Pilot is marked by black square (modified from Nøttvedt et al. (1993).

For simple and brief understanding of geology of the Svalbard, it can be divided into three main categories: i) basement rocks consisting of igneous and metamorphic rocks that have been through several episodes of alteration and folding. These rocks were formed during Precambrian to Silurian ages , ii) trough shaped unaltered sedimentary rocks of late Palaeozic to Cenozoic ages and iii) the Quaternary unconsolidated surficial deposits (Dallmann, 2007). Geological evolution of Svalbard described here is mostly based on (Worsley, 2008). The whole succession is about 20 km thick and consists of 20 different lithostratigraphical groups. These groups collectively called "Hecla Hoek". The geology of these groups are complex and consists of a large variety of rocks categorized into three terranes; (i) the north-eastern terrane consists of Precambrian igneous and prominently sedimentary rocks also glacial clastic and carbonates, (ii) the north-western province comprises of deep crustal metamorphic and (iii) the south-western part is a mix of metasediments typically subduction zone environment (Worsley, 2008). Several other authors such as Harland and Wright (1979) had explained the structural evolution of Svalbard's basement and Svalbardian movements during Devonian/Paleozoic period.

Evolution of post-Svalbardian succession and southwestern part of the Barent Sea during the age of the late Devonian/Paleozoic to the Eocene, has been explained by Worsley (2008), Larssen et al. (2002) and Dallmann (1999). All the depositions during this age are described in terms of five main stages. Also these depositional stages somewhat showed some evidence of the movement of this part of Eurasian plate. It is also believed that Svalbard has moved from the equatorial zone during mid Devonian-early Carboniferous until the present time and this high artic latitude position has caused the major climatic changes through the time.

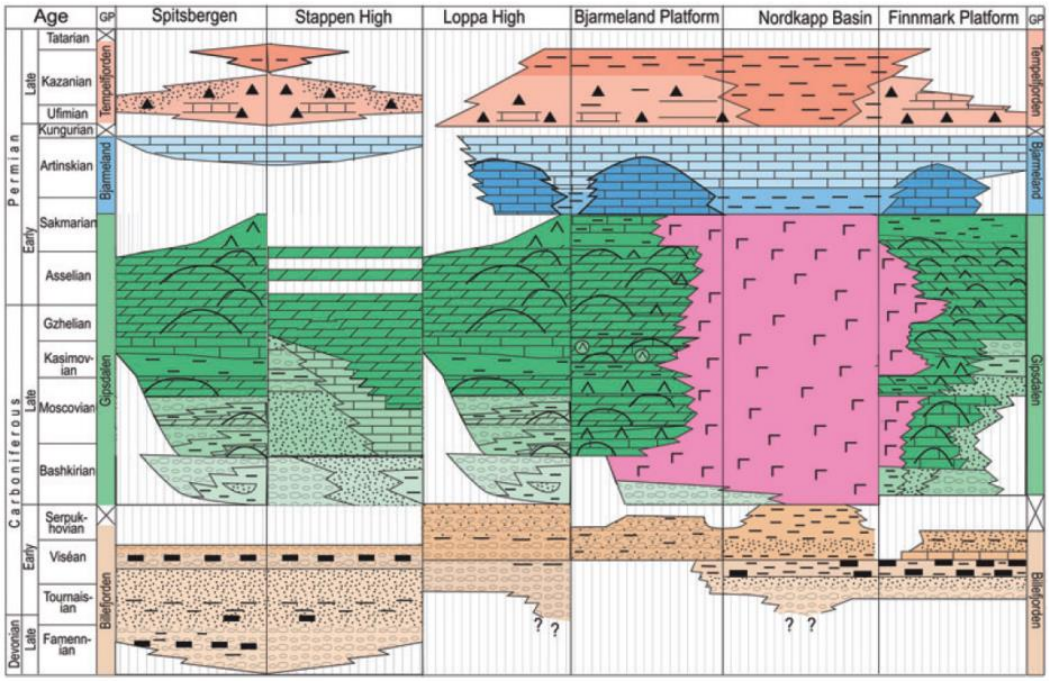

Fig. 2.2: Stage 1: Stratigraphy of Upper Paleozoic sequences of the Barents Shelf (Worsley, 2008).

The first depositional stage was started during late Devonian and continued till the mid of Permian. It mainly consists of development of a carbonate platform which is divided into several groups as the Billefjorden group (Late Devonian-early carboniferous), the Gipsdalen and Bjarmeland groups (Mid-Carboniferous to Mid-Permian) consist mainly of organic build-ups, evaporates, siliceous shales, sandstone and conglomerates (Fig. 2.2). This stage involves

major and abrupt changes in tectonic and climate which caused Gondwana glaciation and development of Uralide orogeny and host and graben development (Stemmerik and Worsley, 1995).

The 2nd stage was developed in Late Permian to mid Triassic age. It was a transition from carbonates to clastic deposition. This stage involves the development of the Tempelfjorden Group during late Permian age and the Sassendalen Group from early to middle Triassic. Main lithologies are non-siliceous and organic-rich shales, sandstone, mudstone, limestone and these shales are considered to be very vital hydrocarbon source rocks (Worsley, 2008).

The third stage of deposition is mainly the development of the polar Euramerican basin during Late Triassic-Late Cretaceous times. This stage involves crucial development of many sandstone units which are promising hydrocarbon reservoirs in the area, specifically the lower part of the section (Sassendalen and Kapp Toscana groups). Later in the succession it becomes more shale dominated (Adventdalen group) to upward direction. More importantly the Adventdalen group of mid-Jurassic–mid-Cretaceous ages (main part of study area) was developed during this stage.

The fourth stage during Paleogene time involves intense tectonic activity consists uplifting, subsidence and volcanism along the south-western and north-western shelf margins (Steel, 1985), later caused the ultimate opening of the Norwegian-Greenland Sea in Eocene time. Groups belong to this stage are the Van Mijenfjorden and Sotbakken groups of Paleocene–Oligocene times.

The fifth stage involves glaciation, reactivation of volcanism and uplifting during Neogene period. Glaciation played major role in the development of gigantic wedge deposits over and off the western shelf edges (Faleide et al., 1996). The Nordland Group of Miocene–Pleistocene times is also major development during this stage (Worsley, 2008).

2.2 Structure and tectonic

The Svalbard's archipelago is uplifted portion on the northwestern edge of the Barents Sea shelf and this uplift occurred due to crustal movements during late Mesozoic and Cenozoic times. Dimakis et al. (1998) proposed that tectonic movement during Tertiary time lead to uplifting in the western and northern margins of the Barents Sea as shown in Fig. 2.3. This uplift was linked to rifting, break-up and consequent opening of the Norwegian-Greenland Sea (started approximately 50 m.y. ago) gave rise to western margin and Eurasia basin gave rise to the northern margin of the Barents Sea (Dimakis et al., 1998).

Dallmann (2007) described the tectonic history and development of the major mountain belts and other structural elements in the Svalbard area. He suggested that present day area had been a segment for a long time span (from Devonian to the Cretaceous) of the giant Old Red continent which consisted of North America, Greenland and Eurasia. In-between Cretaceous and Tertiary time two major plates (the North American and Eurasian) were started drifting apart and lead to rifting in the area. In the meanwhile Svalbard and the Barents shelf slide past each other during the 1st episode of rifting. One side of the Svalbard was pressed by the oblique movement of the Greenland continental plate. These tectonically driven movements arose excessive folding and thrusting in the area and lead to Tertiary fold-and-thrust belt which is appeared as jagged and sharp peaks on the west coast of Spitsbergen.

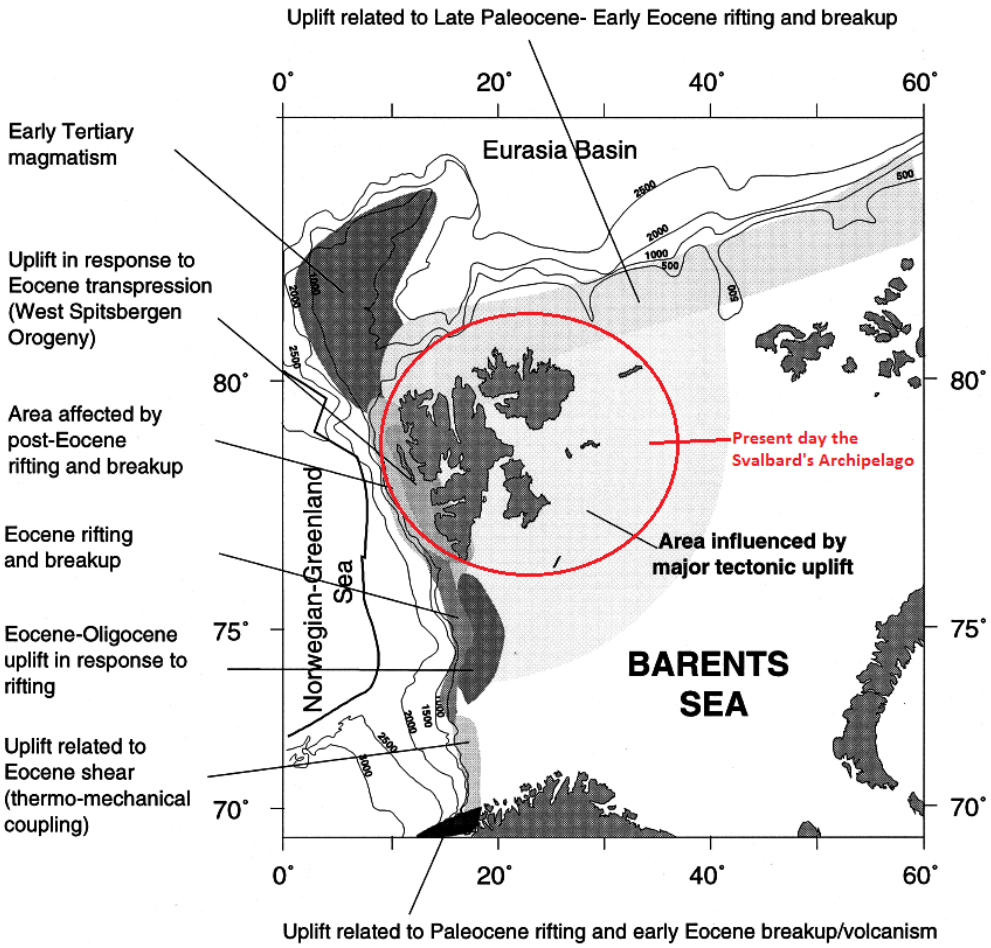

Fig. 2.3: Tectonic activity and uplift in the Barents Sea (modified from Dimakis et al. (1998)).

The collision of North American plate (Laurentia) against the North European plate (Baltica) during the late Cambrian and mid Devonian times gave rise to Caledonian orogenic belt (Dallmann, 2007). Fig. 2.4 shows structural elements of the Barents Sea where the study area on the northwestern corner is marked by red circle. During Paleogene opening of the North Atlantic Ocean gave rise to De Geer Zone which is a dextral transform fault zone splitting Svalbard from East Greenland (Braathen and Bergh, 1995; Eldholm et al., 1987; Ogata et al., 2014a). This transpression caused the evolution of a fold and thrust belt known as the West Spitsbergen Fold and thrust Belt (WSFB) and the Central Spitsbergen Basin (CSB) (Braathen and Bergh, 1995; Helland‐Hansen, 2010; Ogata et al., 2014a; Steel, 1985).

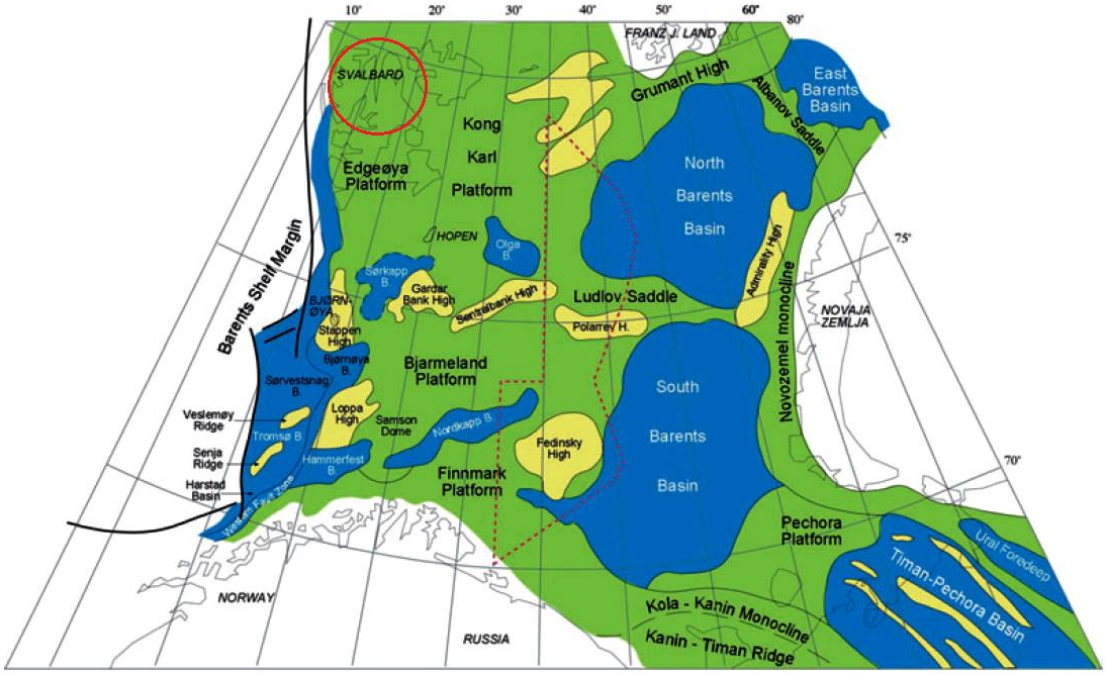

Fig. 2.4: Map showing major structural elements of the Barents Sea with location of Svalbard (modified from (Worsley, 2008)

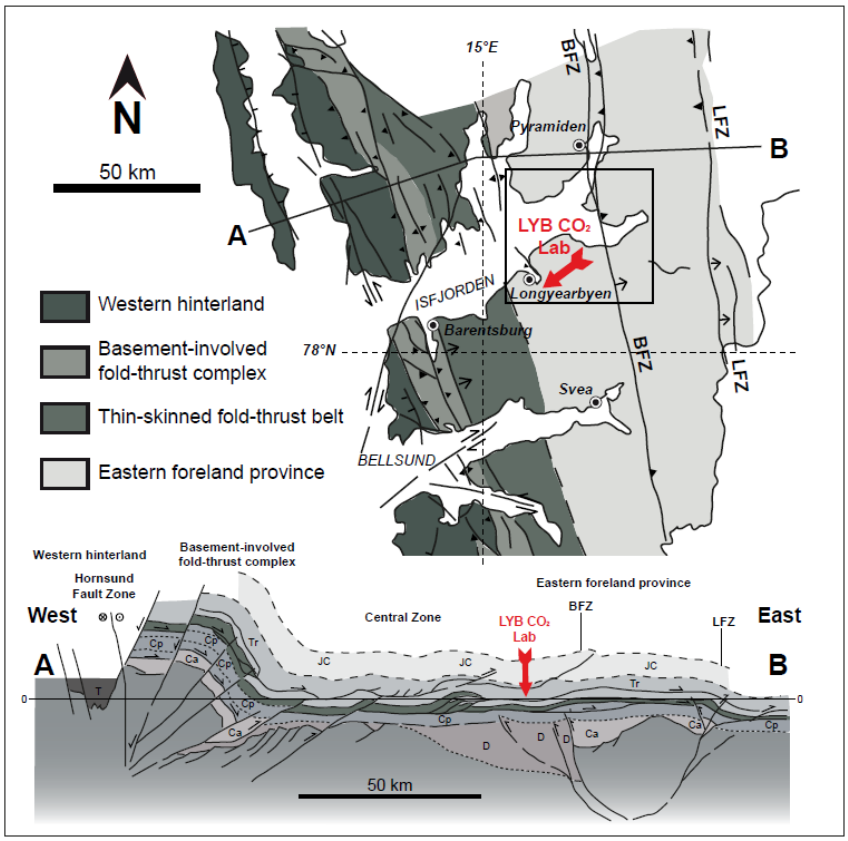

Fig. 2.5: Map showing major structural elements of central Spitsbergen including location of study area. Abbreviations: BFZ-Billeforden Fault Zone; LFZ- Lomfjorden Fault Zone (Ogata et al., 2014b).

.

Structure elements of Svalbard's archipelago can be categorized in six groups such as 1) Fault zones, 2) Post-Caledonian granite intrusions, 3) Devonian major fault blocks, 4) Bashkirian-Moscovian troughs and highs, 5) Tertiary basins and grabens and 6) Basement provinces. The major structural elements in the study area are Western hinterland, Basement involved fold-thrust complex, Thin-skinned fold-thrust belt, Eastern foreland province including Billefjorden and Lomfjorden fault zones (Fig. 2.5).

2.3 Stratigraphy

Stratigraphy of the study area is belong to Mesozoic Era and can be divided into Adventdalen and Kapp Toscana groups. Stratigraphy of the entire Svalbard is shown in Fig. 2.6. A brief description of these groups is given in the following sections.

2.3.1 Adventdalen Group

The Adventdalen Group of the Central Spitsbergen area and the depositional age varies from late Jurassic to early Cretaceous. This group comprises of Carolinefjellet and Helvetiafjellet and Janusfjellet subgroup (Rurikfjellet and Agardhfjellet formations). The thickness ranges from 750 to1600 meters at Svalbard. It comprises mainly of shale, siltstone and sandstone. Overlaid by Van Mijenfjorden Group (Svalbard) and Nygrunnen Group (Barents Sea Shelf) and underlying unit is Kapp Toscana Group. Succession of Upper Jurassic age, mainly Agardhafjellet, Fuglen and Hekkingen formations were reported as important hydrocarbon source rocks in the area (UiO Natrual history museum, 2015).

Carolinefjellet Formation

The Carolinefjellet Formation is of early Cretaceous (Aptian) age. The thickness varies from 120 to 1200 meters. Main lithologies are shale, siltstone and sandstone. It is divided into two members on the basis of shale or sandstone predominance in the Spitsbergen area. In the study area, this formation is a part of the overburden units (UiO Natrual history museum, 2015).

Helvetiafjellet Formation

The Helvetiafjellet Formation belongs to early Cretaceous age (Barremian). Thickness range of this formation is 40-155 meters. Major lithologies are sandstone, shale, coal and conglomerate. It is also part of the overburden in the study area (UiO Natrual history museum, 2015).

Janusfjellet subgroup

The Janusfjellet subgroup mainly consists of Agardhfjellet and Rurikfjellet formations. Mainly comprises black shale with intercalations of siltstone and sandstone in Svalbard area.

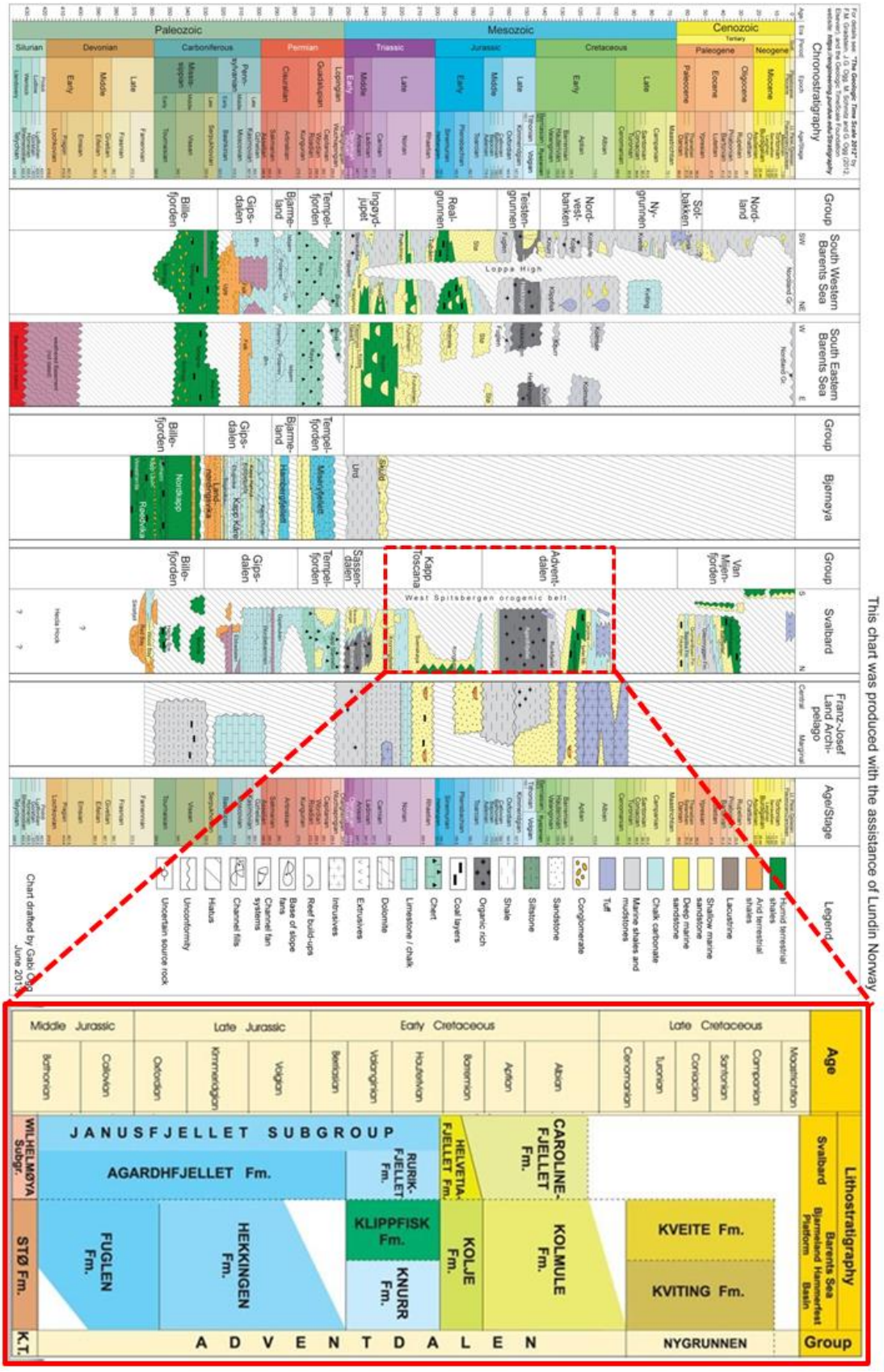

Fig. 2.6: Lithostratigraphic chart showing the stratigraphy of Svalbard and Barents Sea.The study area, is marked by red square (modified from UiO Natrual history museum (2015)).

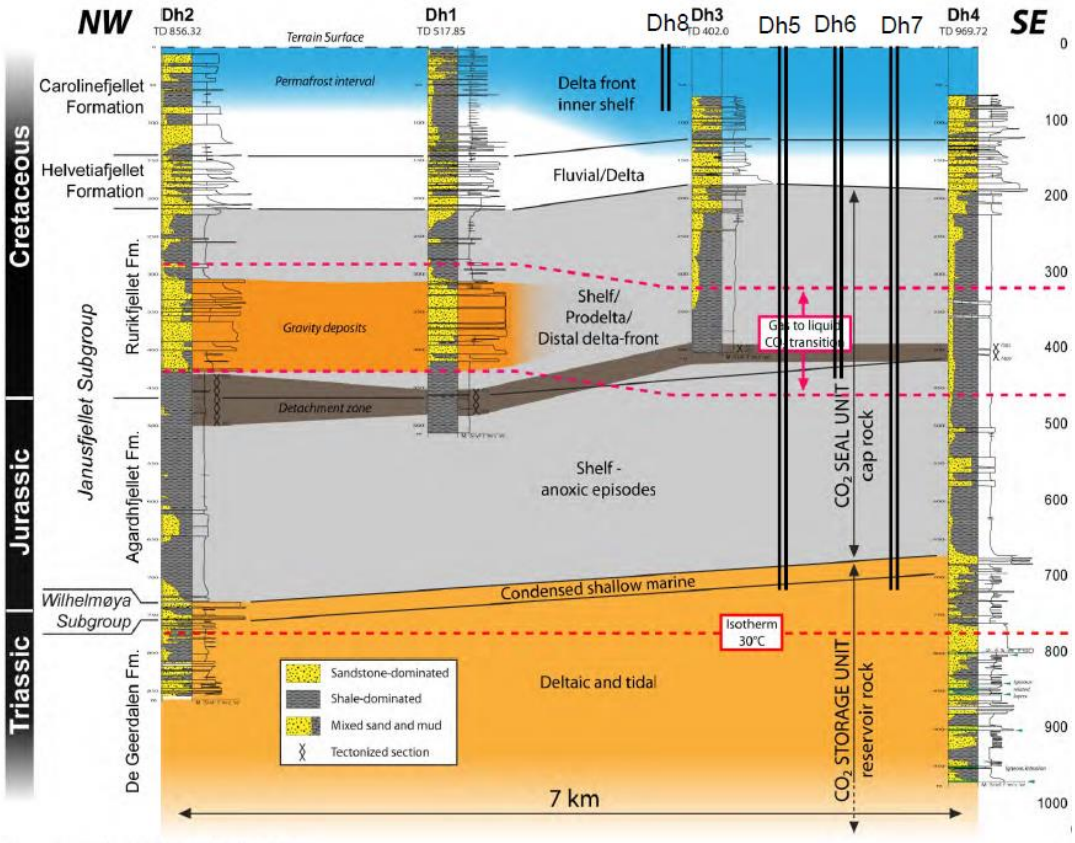

Fig. 2.7: Well log correlation with stratigraphy, depositional environment, ages. Figure shows all the wells and CO2 sealing and storage units (modified from Braathen et al. (2012a).

Rurikfjellet Formation

Rurikfjellet formation is partly with in Janusfjellet Subgroup. It varies from 110 to 400 meters in thickness. It's overlain by Helvetiafjellet Formation and underlain by Agardhfjellet Formation. It's part of a primary cap rock in the study as shown in Fig. 2.7 (Braathen et al., 2012b). Main lithologies are dark shale, siltstone and sandstone. Shale represents an open marine envirnoment and intercalations of tempestite sandstone show an offshore transition environment with sand derived from prodelta advances (UiO: The Natural History Museum?). As overall this formation has been deposited in a regressive succession under oxic conditions (Braathen et al., 2012b). Distinctive features sideritic nodules and shale thin beds are commonly cemented by siderite. From wells Dh1 and Dh2 as shown in Fig. 2.7 at a certain depth between 270-410 meters slump beds, conglomerates, massive to medium coarse grained muddy sandstone covered by palaeosol and thin coal layer (Braathen et al., 2012b).

Agardhfjellet Formation

Agardhfjellet Formation is partly within Janusfjellet Subgroup of late Jurassic age. Thickness varies from 90 to 350 meters. Overlain by Wilhelmøya Subgroup and underlain by Janusfjellet Subgroup. It mainly consists of black shale and siltstone. The shaly succession is organic rich and fossiliferous, deposition environment is offshore shelf. It is divided into four further members in Spitsbergen's nordenskiöld Land area. Upper most is the Slottøya member consists of dark grey shale interlayered with dolomite and siderite. Oppdalsåta member composed of siltstone and sandstone. Below this member is Lardyfjellet member and mainly

contain dark grey shale. The fourth member is Oppdalen consists of strongly bioturbated, structureless silty to sandy mudstone (Braathen et al., 2012b).Overall, this formation represents a fining upward succession of poorly sorted, clay rich fine grained sandstone (UiO Natrual history museum, 2015).

2.3.2 Kapp Toscana group

The Kapp Toscana group has different subgroups (total three) and formations (more than thirteen formations and their members) in the area. According to the study area we are only interested in De Geerdalen formation and Wilhelmøya Subgroup because both of these successions are major parts of CO2 storage unit. Reported thickness of this unit is over 475 meters in Svalbard area. This group contains mainly sandstone, shale and siltstone successions of Late Triassic to mid Jurassic age (UiO Natrual history museum, 2015).

Wilhelmøya Subgroup

The Wilhelmøya Subgroup contains various formations and members. Our interest is only in Knorringfjellet formation. This group overall composes of Sandstone, shale, mudstone and conglomerate successions of late Triassic to middle Jurassic. Reported thickness of the subgroup fluctuates throughout its entire distribution and ranges from 3 to 230 meters (UiO Natrual history museum, 2015).

Knorringfjellet formation.

The Knorringfjellet formation is the upper most part of CO2 storage unit (reservoir). This formation mainly composed of sandstone and shale with intercalations of conglomerates of Late Triassic to mid Jurassic age and thickness varies from 3 to 75 meters. Theses thin successions are reported from the entire Central Spitsbergen basin (UiO Natrual history museum, 2015).

De Geerdalen formation

De Geerdalen formation is the main reservoir unit in the study area and mainly composed of sandstone and shale of late Triassic age. Its thickness varies throughout the Spitsbergen area and overall range of thickness is 28-400 meters. Sandstones in this unit are reported as immature as both minerlogically and texturally and separated by shale. Carbonate beds with a minor thickness up to few decimeters are also encountered repeatedly and often capping the sandstones (UiO Natrual history museum, 2015).

Chapter 3: Materials and research methodology

This chapter consists of three sections; first section gives a brief description of available material and plug preparation, second section describes laboratory methods for this study and the third section presents characterization of material.

3.1 Available materials

All the core samples are selected for this study from well Dh-6 targeting Rurikfjellet and Agardhfjellet formations (depth range 308.00-428.28m). The main reason for selecting these samples is to evaluate integrity of upper part of the primary caprock of LYB CO2 storage site. There are limited data on the mechanical and physical properties of shale samples in this particular depth range of well Dh-6. These samples are summarized in Table 3.1.

Table 3.1: List of studied core samples from well Dh-6.

Core sample No.	Formation	Depth (m)	Length (cm)	Diameter (mm)
8	Rurikfjellet	308.00-308.26	26	38
17	Rurikfjellet	369.07-369.21	14	38
18	Rurikfjellet	369.21-369.35	14	38
19	Rurikfjellet	369.41-369.53	12	38
25	Rurikfjellet	386.74-386.89	15	38
32	Agardhfjellet	425.28-425.43	15	28
33	Agardhfjellet	428.15-428.28	13	28

3.1.1 Core sample inventory

All the samples were very well preserved in paraffin sealing and kept in the controlled temperature room. Samples were unsealed and inspected for any pre-existing defects e.g. fractures or any damage, etc. Pictures of the entire selected sample are shown in Table 3.2. We can clearly see some important features such as splitting along the bedding planes and fracture traces in few samples. All the material is inhomogeneous as we can see splitting along the bedding planes and more likely these samples consist of clay with minor amount of silt/sand. If we look at the fresh surface the color of the rock is very dark. The marked arrows on the core samples are pointing the top of the cores.

Table 3.2: Pictures of selected sample with their IDs and description of the cores.

Formation	Core sample	Picture	Description
Rurikfjellet (308.00-386.89 m)	8		Inhomogeneous dark shale, top edge surface look like a fracture surface.
	18		Inhomogeneous dark shale
	19	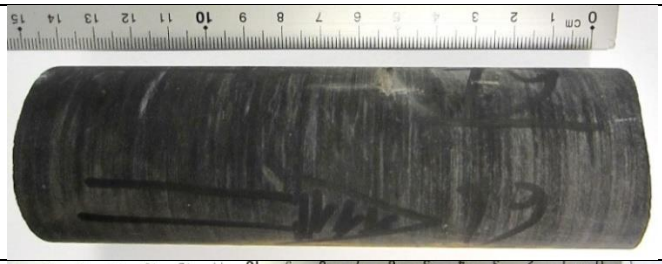	Inhomogeneous dark shale
	25	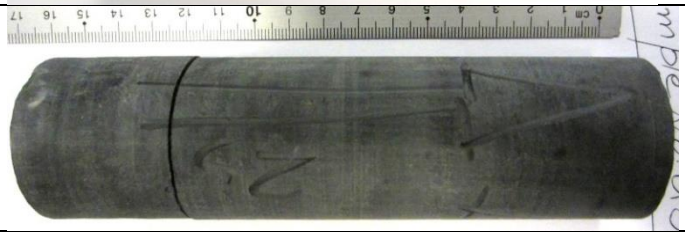	Inhomogeneous dark shale, splitting along the bedding plan in the bottom part.
Agardhfjellet (425.28-428.28 m)	32	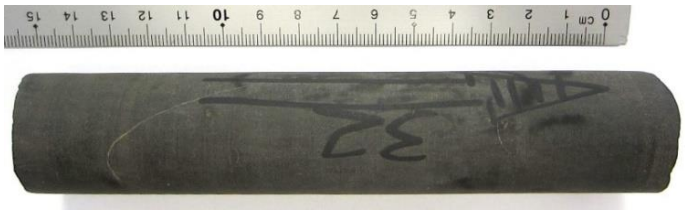	Inhomogeneous dark shale, fracture trace and filled with white colored material probably Siderite?
	33	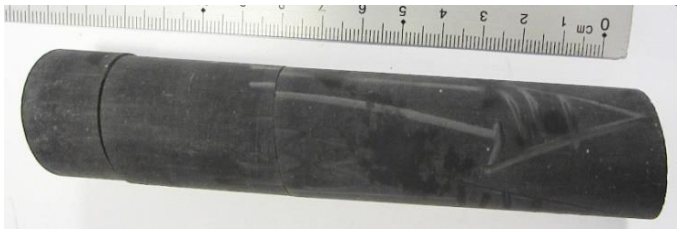	Inhomogeneous dark shale, significant splitting along the bedding plane in the middle and bottom parts.

3.1.2 Sample preparation

These cores were cut to make plugs according to the ASTM standard for Brazilian and UCS tests. The diameter and thickness of disc shaped plugs for Brazilian test were 40-40.5 mm and 19-21mm respectively. The diameters of cylindrical plugs for UCS tests were 40.4 and 28 mm and the heights were 82 and 60 mm. Due to the limited dimensions of available core samples, it was not very easy and possible to prepare plugs for both mechanical tests and characterization study from each core. Few examples of these cores and plugs are shown in

Fig. 3.1 and a brief summary of entire set of plugs and thin sections prepared from these cores is given in Table 3.3.

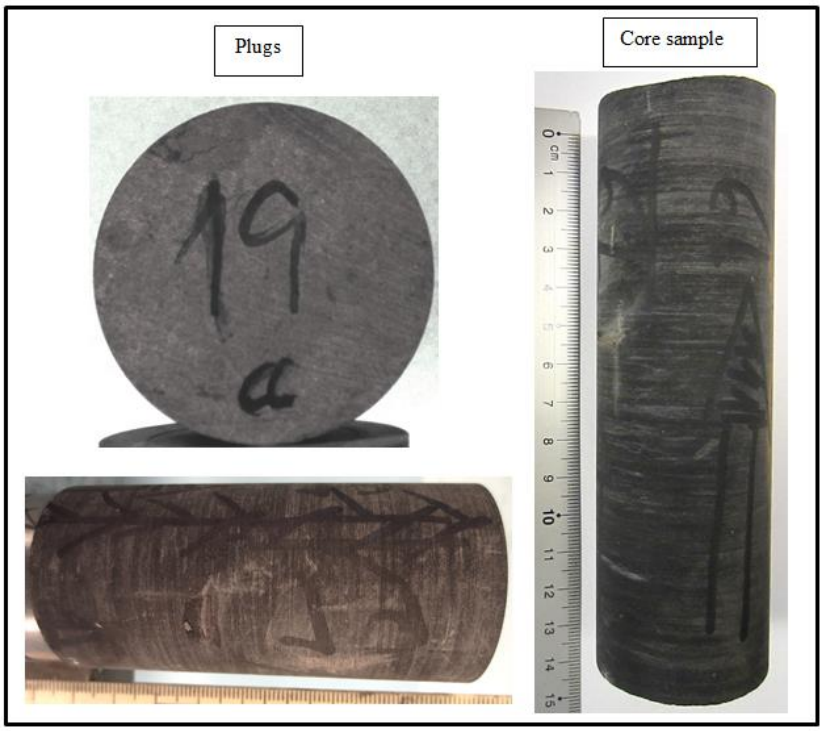

Fig. 3.1: Image on the upper left side is a plug for Brazilian test and down left side is a plug for UCS test. Image on the right side is the core sample.

Table 3.3: Summary of prepared plugs for mechanical thin section and XRD study.

Formation	Depth (m)	Core sample	Plug (IDs)	Test type	Number of plugs	
					Thin section	XRD
Rurikfjellet	308.00-308.26	8	RFF-8A-BR	Brazilian test	1	1
			RFF-8B-BR			
			RFF-8C-BR			
			RFF-8A-UCS	UCS test		
			RFF-8B-UCS			
	369.21-369.35	18	RFF-18-BR	Brazilian test	1	1
			RFF-18-UCS	UCS test		
	369.41-369.53	19	RFF-19A-BR	Brazilian test	-	1
			RFF-19-UCS	UCS test		
	386.74-386.89	25	RFF-25A-BR	Brazilian test	-	1
			RFF-25B-BR			
			RFF-25C-BR			
Agardhfjellet	425.28-425.43	32	AFF-32A-BR	Brazilian test	1	1
			AFF-32B-BR			
			AFF-32-UCS	UCS test		
	428.15-428.28	33	AFF-33-BR	Brazilian test	-	1
			AFF-33-UCS	UCS test		

3.2 Characterization of material

Write an introduction here and say which type of tests will appear next. You may give a short explanation on why you do different tests in your work. For example:

The main objective of the study is to determine mechanical properties of shale samples. However, we need to characterize the material before doing mechanical tests. The reason for measuring density, doing XRD and SEM analyses is to characterize mineralogical composition of the material. This is very useful to understand mechanical behavior of material as well as to compare results of strength tests with similar rocks from other locations.

Characterization of material is determined by direct observation and measurements in the laboratory. The material used for this study is characterized by determining the defects (fractures, splitting along bedding plane, etc.) by direct observation of core samples (as described before under section 3.1.1 Table 3.2) Core sample inventory, density, microstructures and mineral identification by using SEM and mineral quantification by XRD analysis.

3.2.1 Density

Density of rock is a basic property that affects its physical and mechanical behavior. A material with higher density might have higher mechanical strength, lower porosity and higher content of heavy minerals, so we can have some predictions for the results. For example sample AFF-32 has very high density as shale so it is investigated in details and mentioned in upcoming chapters. The density of the material is determined by measuring the diameter, mass and volume of the plugs drilled out from the core samples. Equation 3.1 is used to calculate the density (ρ, g/cm³). Final density values are listed in Table 3.4

Table 3.4: Calculated densities of selected samples.

Formation	Depth (m)	Sample ID	Diameter D(mm)	Density, ρ (g/cm³)
Rurikfjellet	308.00-308.26	RFF-8	40.4	2.58
	386.57-386.74	RFF-17	38	2.62
	369.21-369.35	RFF-18	40.4	2.60
	369.41-369.53	RFF-19	40.3	2.54
	386.57-386.74	RFF-24	38	2.61
	386.74-386.89	RFF-25	40	2.63
Agardhfjellet	425.28-425.43	AFF-32	28.5	3.15
	428.15-428.28	AFF-33	28.5	2.51

$$\rho = \frac{\text{mass}}{\text{volume}} \qquad 3.1$$

Where ρ is the density and g/cm² is the unit used for the values.

Density range for shale is 2.4-2.8 g/cm³ (geology.about.com). As we can see in Table 2.3, density range of samples from Rurikfjellet Formation is 2.54-2.63 g/cm³ and it fits within the normal range of shale density. On other hand samples from Agardhfjellet Formation such as sample AFF-33 has normal density but sample AFF-32 has density up to 3.15 g/cm³. This

value is very high for a shale sample and reason for this has been investigated in Sections (3.2.3 and 3.2.4).

3.2.2 Mineralogical analysis

Mineralogical testing or analysis is conducted to determine mineral quantification and microstructures of the mineral in a rock sample. For this study two methods that are X-ray diffraction (XRD) and Scanning electron microscopy (SEM) are used for mineralogical analysis.

3.2.2.1 X-ray diffraction (XRD)

XRD is a modern technique that is used to identify and quantify the mineralogy of rock and soils specimens. This technique is a set of various equipment, machines and software to analyse the final results (British Geological Survey BGS, 2015).Six core samples were used to determine their bulk mineralogy from Rurikfjellet and Agardhfjellet formations. Small pieces from these core samples were crushed in grinding/crushing mill to make powder. To get best results this powder should be 5 grams and mixed properly, so that it can represent the whole sample. This powder was not fine to use for XRD, because to make a perfect XRD sample the particle size should be 5 to 10 microns. Then a portion of this powder was grinded by mixing a certain quantity of Alcohol in Micronizing mill. This liquid was placed in the dryer at 60 degrees for 12 hours. After drying up this very fine powder was placed in special type of sample holder and these samples were placed in the Philips X'Pert MPD X-ray diffractometer at University of Oslo lab and supervised by Maarten Aerts. A diffractogram is shown in Fig. 3.2. A diffractogram was produced for each sample. Later, these diffractograms were interpreted by using different software and data bases to determine the bulk mineralogy.

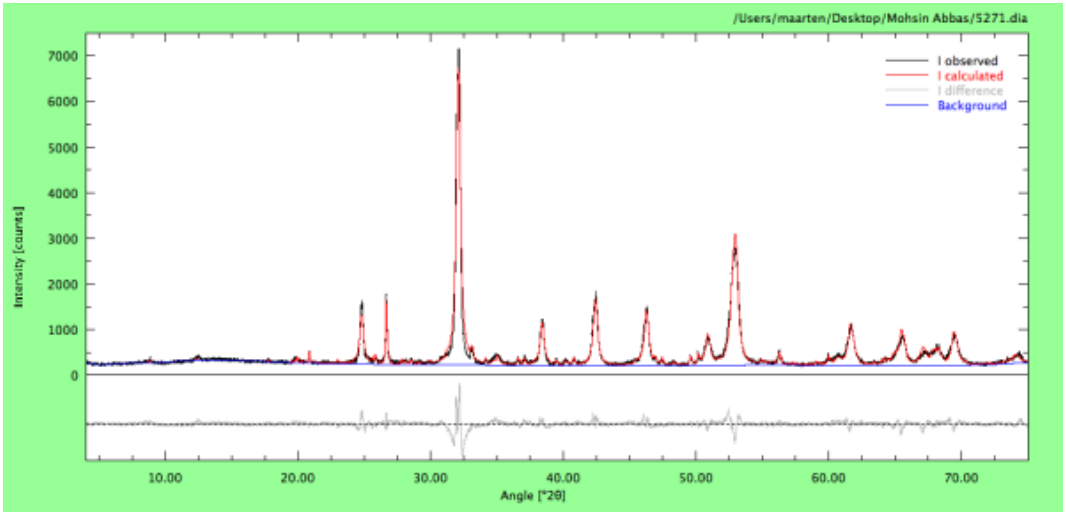

Fig. 3.2: Diffractogram of sample RFF-32.

3.2.2.2 Scanning electron microscopy (SEM)

Shales are very fine grain, heterogeneous and have very complex microstructures.These properties are very challenging when we need to visualize and quantify their microstructures and minerals. Scanning electron microscopy (SEM) is one of the best techniques to analyses microstructures and mineralogy of shale samples.

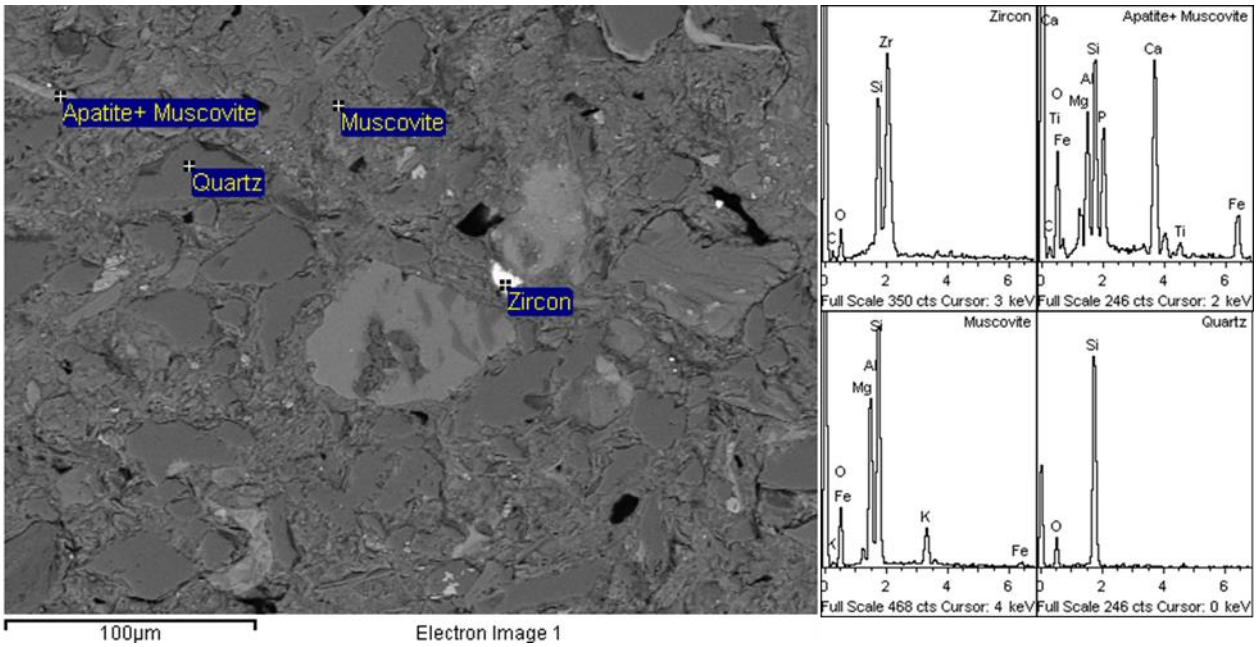

Fig. 3.3: Scanned and zoomed area of thin section RFF-8 with spectrums is shown.

Three thin sections were used to analyze the microstructure and mineralogy of the shale samples from Rurikfjellet and Agardhfjellet formations. Thin sections were prepared from different samples according to the requirement and availability of material and lab at the University of Oslo.

All these thin sections and rock fragments were carbon coated by using Carbon Coater Cressington 208C according to the SEM method standards before analyzing them. Later these thin sections were mounted on a sample holder and placed in the SEM machine (type JEOL JSM 6460LV scanning electron microscope, with LINK INCA EDS Energy Dispersive X-ray System from Oxford Instruments) and analyzed one by one. All the procedures and work was supervised by Berit Løken Berg at SEM lab, University of Oslo.

A procedure was followed; by observing different areas of thin section which were scanned and zoomed at different scales (600-40 µm) and interesting grains were inspected for identification by just clicking on the scanned images in the software of mentioned SEM machine before. An example is shown in Fig. 3.3 in which we can see that different minerals are identified by their spectrums during the SEM analysis in a thin section.

3.2.3 Mineral quantification

Mineral quantification is the main and very useful method to characterize the rock samples in term of total number of minerals present and their percentage. This information is determined by X-ray Diffraction (XRD) from bulk rock samples. Quartz, Muscovite, Pyrite, kaolinite, Chlorite and Siderite are most common minerals in all the specimens (Table 3.5). Approximately 40 to 55 % of the shale from both formations is made up of Quartz. Except sample 32 from Agardhfjellet Formation at the depth range of 425.28-425.43 meters, that has 80.19 % Siderite ($FeCO_3$).

Table 3.5: Summary of bulk mineralogy of the selected samples.

	Formation					
	Rurikfjellet				Agardhfjellet	
Sample ID Mineral (%)	8	18	19	25	32	33
Quartz	55.57	40.19	45.54	41.12	06.16	39.03
Pyrite	16.75	0.81	0.78	09.56	01.38	06.36
Chlorite	05.64	09.70	0.85	13.75	-	08.70
kaolinite	09.12	12.56	13.95	16.58	01.91	10.15
Albite	05.66	06.92	07.07	-	-	06.25
Muscovite	18.58	21.57	20.72	25.79	05.80	23.51
Dolomite	-	-	01.62	01.18	-	05.85
Siderite	-	8.24	0.92	-	80.19	0.153
Diopside	03.75	-	-	-	-	-

3.2.4 Microstructure analysis and mineral identification

Microstructure analysis and mineral identification have been done by scanning electron microscopy (SEM) technique. Area measurement is also a very useful parameter of this technique which gives an idea of porosity, heavy minerals and rest of the matrix in a rock sample. Three thin sections were prepared for SEM analysis as shown in Table 3.3.

Thin section from sample RFF-8

The thin section was prepared from sample RFF-8 and analysed with SEM. Eleven minerals were identified and mentioned in Table 3.6 from this thin section by scanning different sites of interest (Fig. 3.4).

Table 3.6: List of identified minerals for sample RFF-8.

Identified minerals	
Quartz	Albite
Muscovite	Siderite
Pyrite	Zircon
Chlorite	Apatite
Kaolinite	Rutile
Calcite	

Zircon and Rutile are the heavy minerals present in this sample. These minerals were identified by matching the spectrums with the data base (automatically by the software) and shown SEM images at different scales in Fig. 3.4.

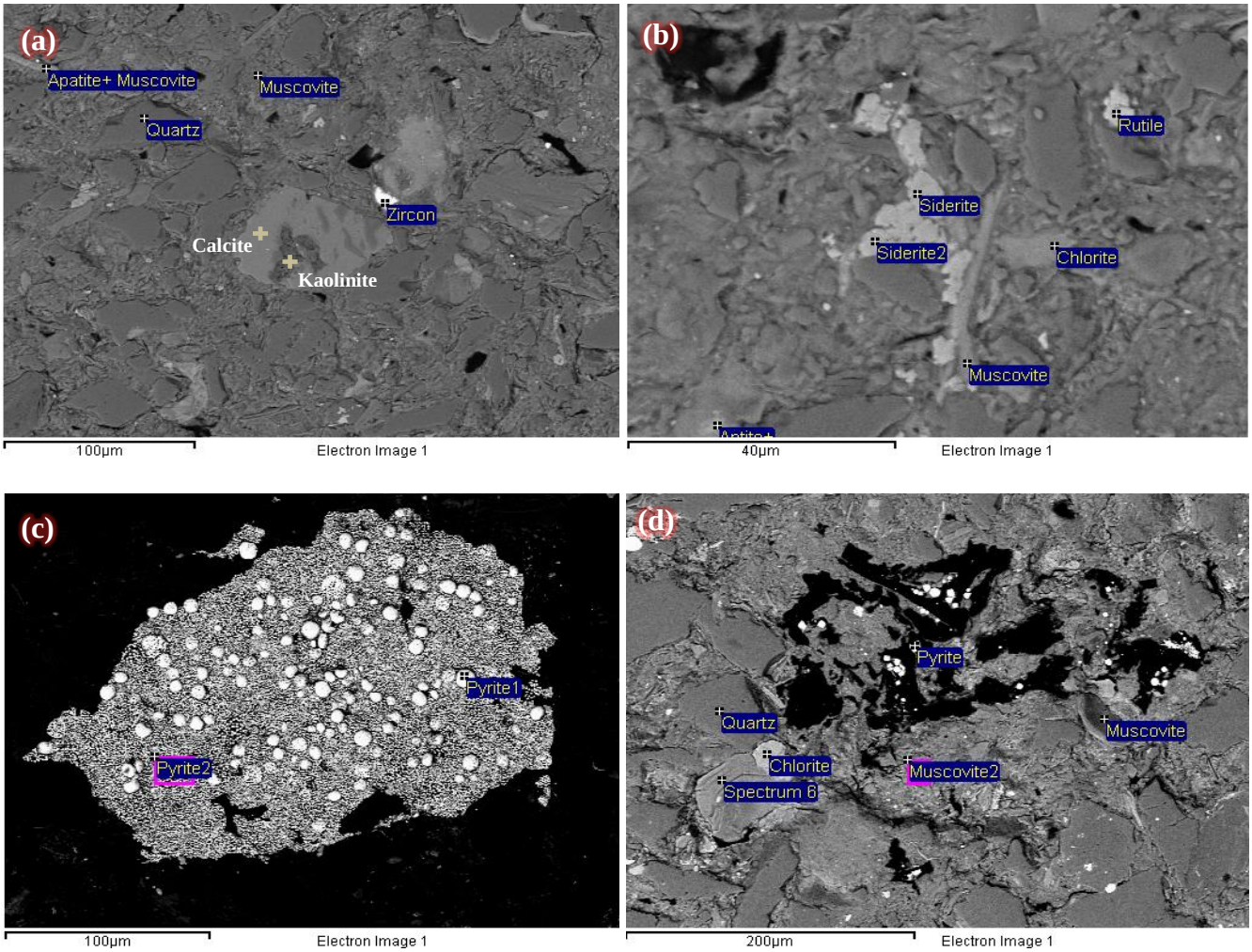

Fig. 3.4: SEM images at various scales: (a) Identified minerals are shown at 100 µm scale, (b) identified minerals at 40 µm scale, (c) very clear identification of pyrite minerals at 100 µm and (d) identified minerals and porosity (black color) at 200 µm scale

All the identified minerals during SEM analysis can be clearly seen in Fig. 3.4. The thin section prepared from the sample (RFF-8) may not be a representative of the whole core sample and on the basis of SEM analysis of this thin section we can see that Quartz and Muscovite are very prominent throughout the section. Few heavy minerals such as Zircon, Apatite, Siderite, Rutile and Pyrite are also identified.

Microstructure of the sample is very complex because of its various varieties of grains and matrix. As we can see in these electron images from SEM, Mostly Quartz grains are irregular flake and elongated in shape and there are also some micro-fractures produced between grains and matrix. In Fig. 3.4a, we can see a fusion of Kaolinite minerals into a Calcite particle and it might be an indication of higher compaction at that depth in Rurikfjellet formation.

Rough calculation of porosity, heavy minerals and rest of the minerals is made by area measurements as shown in Fig. 3.5. Where we can see that porosity (Red) is 3.0 % which is

below average for shale, heavy minerals (Blue) are 4.5% also not very high and rest of the (Green) 92.5% rock is different minerals such as Quartz, Muscovite and Kaolinite, etc.

(Area) (Measurements)

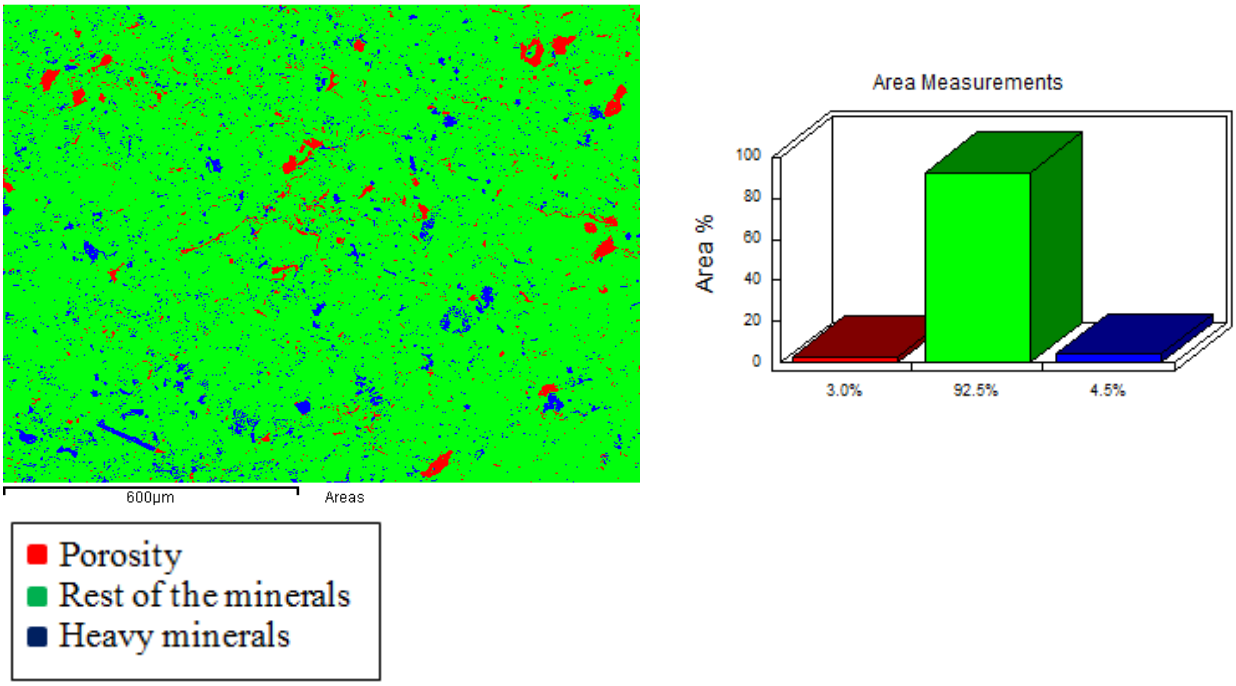

Fig. 3.5: Area measurements of thin section from sample RFF-8; Red: porosity, Blue: heavy minerals and Green: rest of the minerals.

Very low porosity, high matrix content and presence of significant amount of heavy minerals can be interpreted as very compact and mechanically strong sample. Also the calculated value of density for this sample is quite high (2.58 g/cm3) as a verification for this argument.

Thin section from sample RFF-18

Thin section from sample RFF-18 has been analysed by using SEM. Ten minerals are identified during the analysis as mentioned inTable 3.7. Most of these minerals are commonly found in a shale sample. Few heavy minerals such as Siderite, Rutile and Monazite (Known as rare earth metals) are also spotted.

Table 3.7: Identified minerals in RFF-18 during SEM.

Identified minerals	
Quartz	Albite
Muscovite	Siderite
Illite	Dolomite
Chlorite	Monazite
Kaolinite	Rutile

Observations from these selected sites of interest during SEM are clearly showing all the identified minerals in the sample as we can see in Fig. 3.6. Flake shaped Quartz grains are more prominent than the other minerals as shown in Fig. 3.6 (a and c).

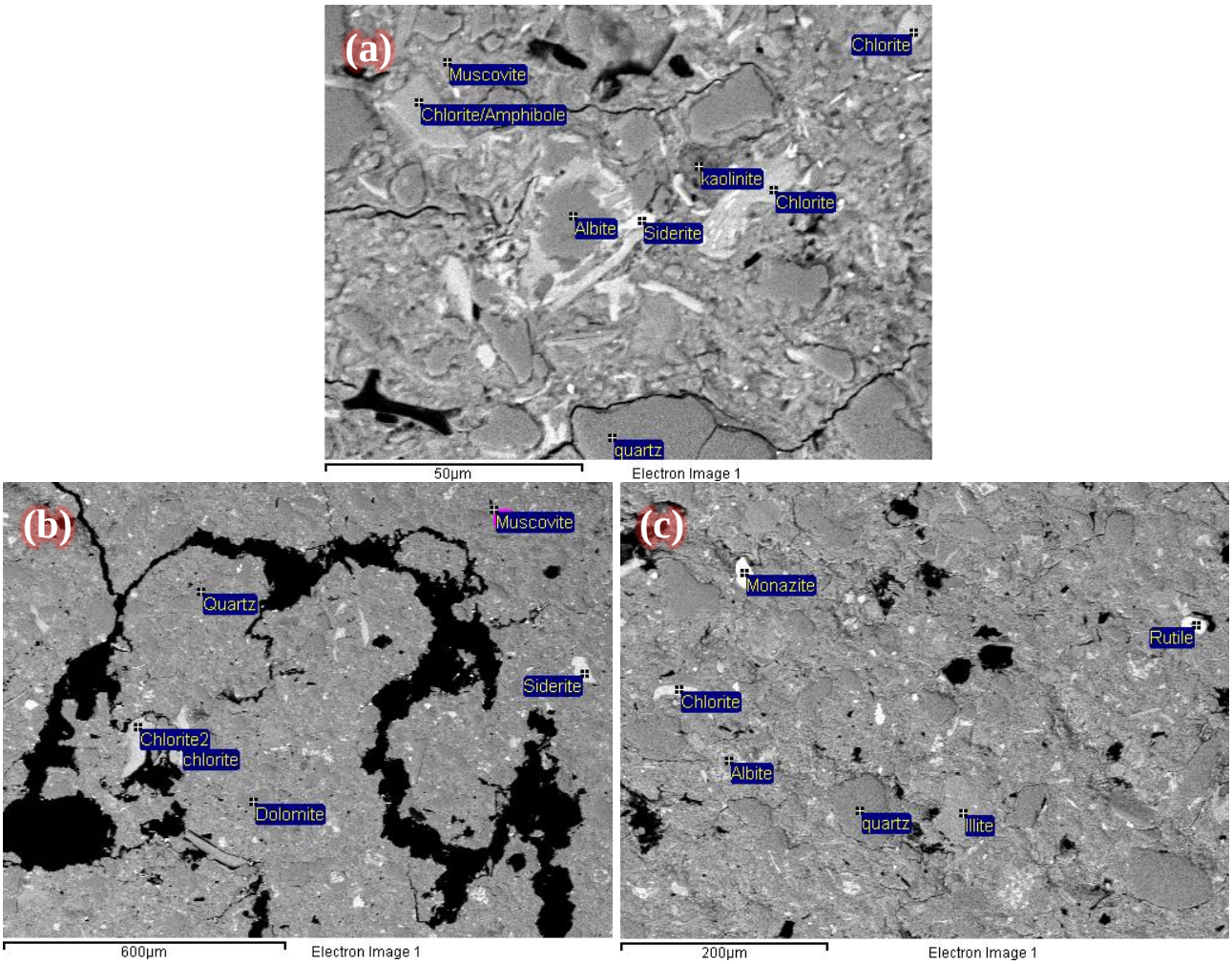

Fig. 3.6: SEM images: (a) Site of interest at 50 um scale showing most of the identified minerals, (b) Image at 600 um is not a clear picture to see the various grains but blank spaces are very visible and (c) Image at 200 um scale where particles are more visible with few blank spaces and very tiny fractures.

There are few microfractures visible at 50 µm and 200 µm scale in Fig. 3.6(a and c). The three heavy minerals spotted from these sites of interest, look very similar in color and shape of the grain. There are also many blank spaces (black color) in these images; most of them look like missing particles during thin section preparation.

Microstructure of sample RFF-18 is more complex than RFF-18 because of the large variety of grains such as chlorite (greyish to off-white), siderite (bright white). There are few very visible micro-cracks in this sample as we can see in Fig. 3.6 (a, b & c) but these cracks could have been produced during preparation of thin section.

Two sites of interest were selected for area measurements for this sample due to the uncertainty of these blank spaces in the thin section as shown in Fig. 3.7. The information of the porosity, heavy minerals and rest of the matrix is uncertain or rough estimate and cannot be applied to the whole sample. Anyhow according to these measurements in Area-1 and Area-2, the porosity (6.1% and 4.2% respectively) is quite high and uncertain but there is not big difference between heavy minerals and rest of the matrix.

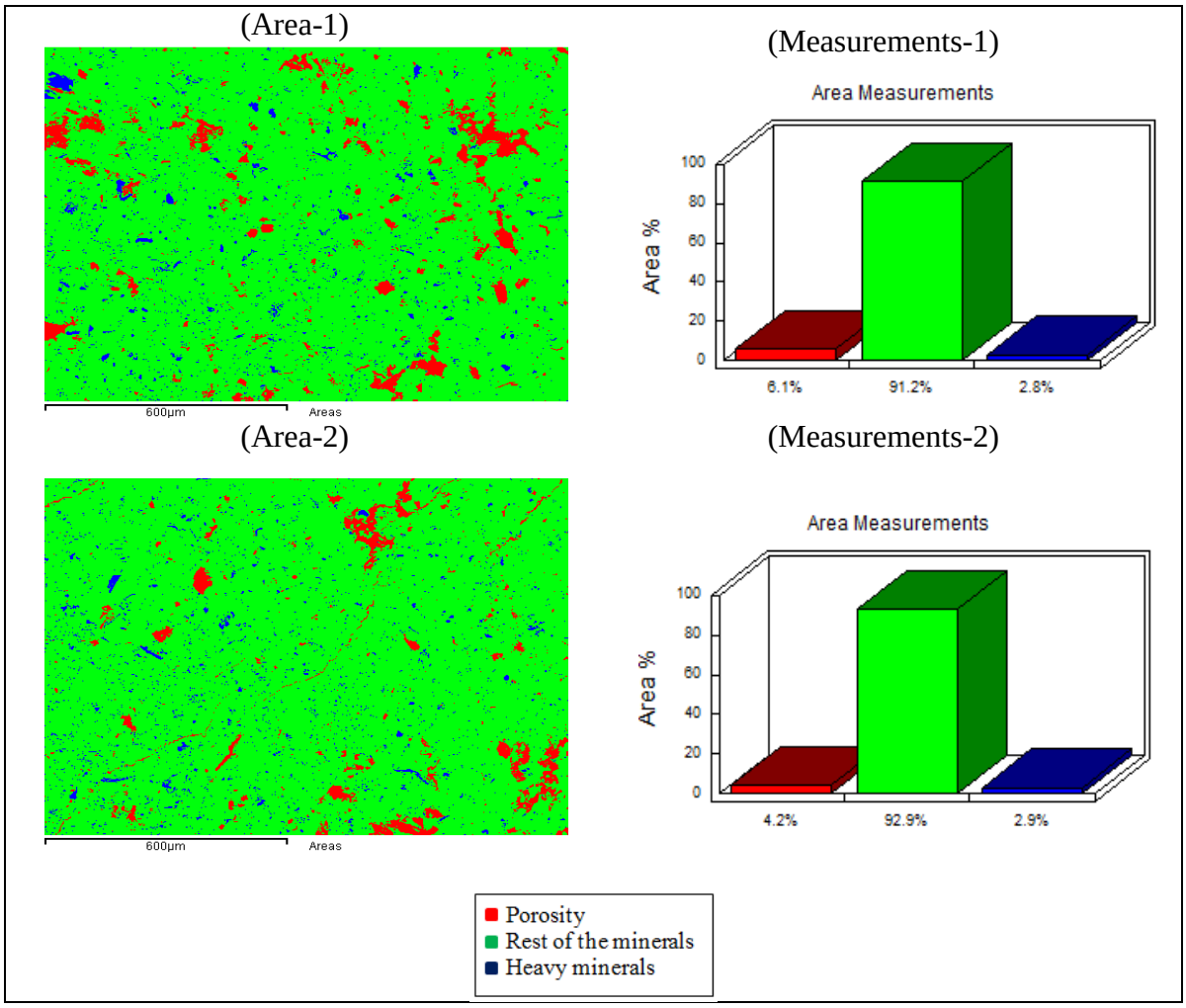

Fig. 3.7: Area measurements from two selected sites on thin section from sample RFF-18

Thin section from sample AFF-32

Thin section was prepared from sample AFF-32 and analysed under SEM. Total six minerals are identified during SEM analysis and show in Table 3.8.

Table 3.8: list of identified minerals from thin section (sample AFF-32).

Identified minerals	
Siderite	Kaolinite
Quartz	
Muscovite	
Pyrite	
Dolomite	

Siderite (covers most of the area in this thin section light grey in color) and Pyrite are very prominent throughout the entire thin section as shown in Fig. 3.8. Pyrite grains are white and round shape, Quartz grains are irregular and flake shaped with variable size and Dolomite grains are prominent block or square shape in this sample as shown in Fig. 3.8 (c & d).

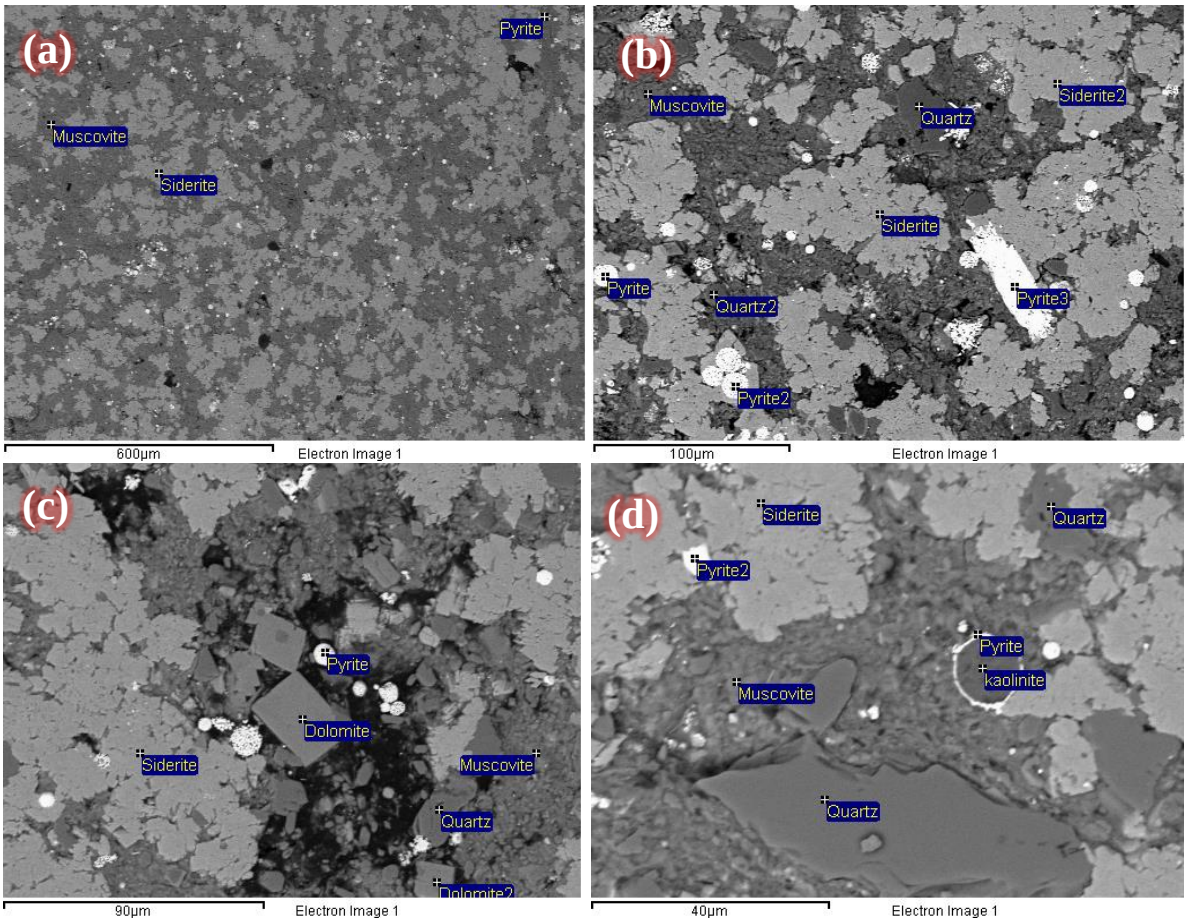

Fig. 3.8: SEM images of sample AFF-32: (a) Electron image at 600µm scale showing prominent distribution of Siderite, Muscovite and Pyrite, (b) Electron image at 100µm scale showing most of the identified minerals and there grain shapes are also visible, (c) Electron image at 90 µm scale showing very prominent Dolomite and Pyrite grains with few other minerals and (d) SEM image at 40 µm scale showing Kaolinite surrounded by Pyrite ring and clearly visible Quartz grains.

As we see images from SEM analysis of thin section from sample AFF-32 Fig. 3.8a shows a quite regular distribution of light and dark grey color material with many white spots at 600 µm scale and after zoom about 100, 90 and 40 µm, microstructure and grain pattern and shape is clearly visible. There are not any microfractures spotted in this thin section. Overall structure looks more compact and dense without any defects as compared to other two thin sections from samples RFF-8 and 18 (Rurikfjellet formation).

As we can see in Fig. 3.9 area measurements from a selected site of interest of sample AFF-32, porosity is only, Siderite, rest of the minerals and heavy minerals are 0.8%, 41.6%, 55.7% and 1.8 respectively for this sample.

(Area) (Measurements)

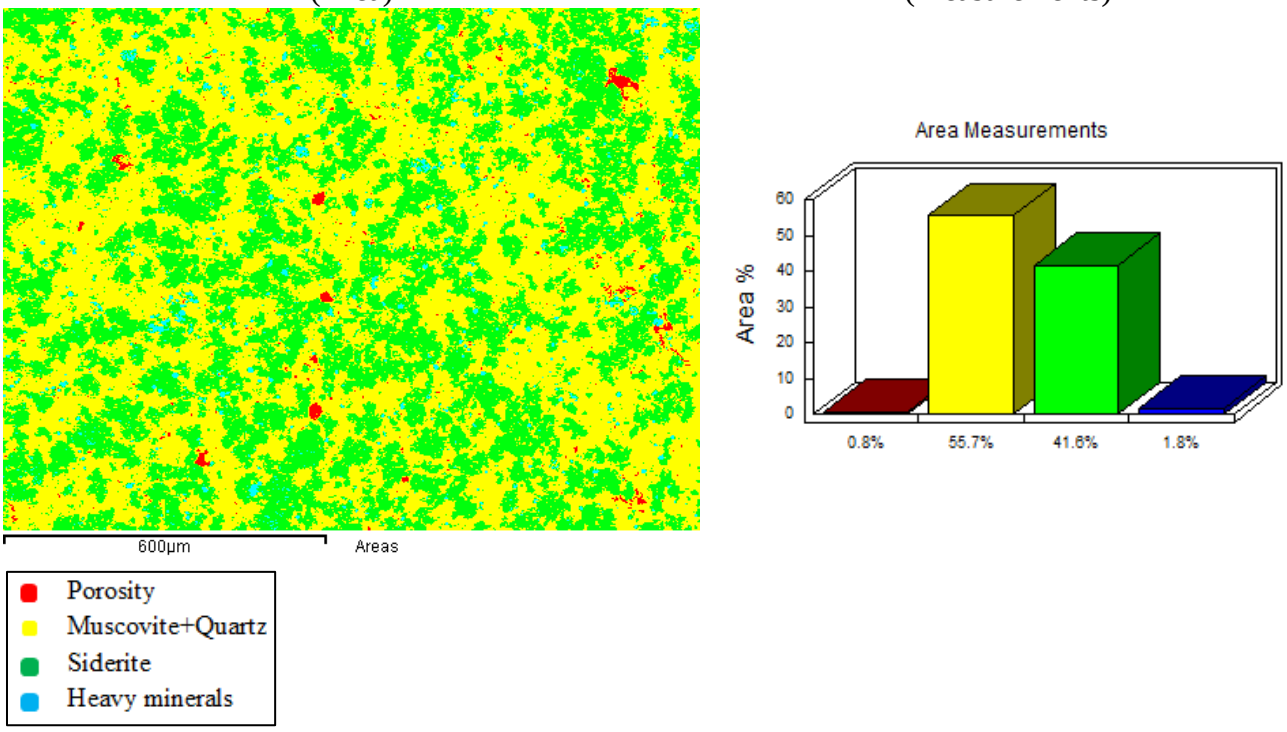

Fig. 3.9: Area measurements from a selected site of interest (sample AFF-32).

3.3 Mechanical testing

Mechanical testing is carried to determine the Geomechanical properties of the selected core samples. This mechanical testing program consists of two standard tests; uniaxial compressive strength test where strength of rock is determined under unconfined compression conditions and the tensile strength (Brazilian) test which measures tensile strength of plugs indirectly. These tests methodologies are presented in the following sections.

3.3.1 Brazilian Test

Brazilian test is also known as indirect tensile strength test. In this method one principal stress is tensile and the other finite principal stress is compressive and tension is the failure mechanism as shown in Fig. 3.10. Add some text from ASTM standard on Brazilian test.

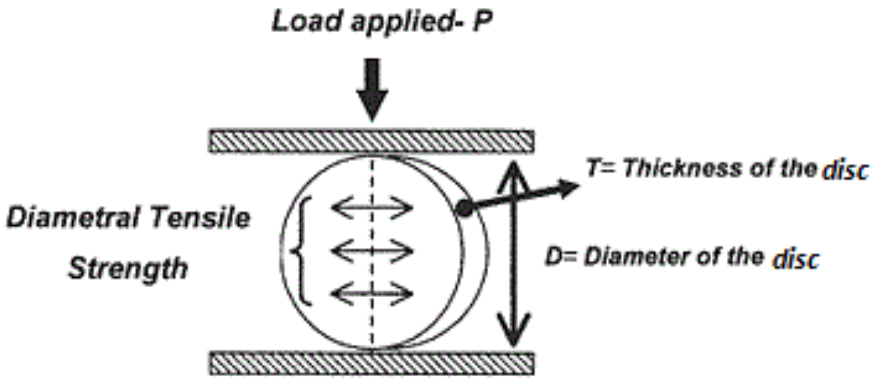

Fig. 3.10: Schematic illustration of Brazilian test (modified from Bresciani et al. (2004)).

Test Procedure

Brazilian test is conducted according to ISRM standard (ISRM, 1978). A disc shaped plug is wrapped by a tape to reduce friction at the contact points. Curved jaws are used to hold the plug as shown in Fig. 3.11. Following steps are made for this test: plug was placed between the jaws and apparatus was adjusted by moving the upper jaw down close to the plug surface. Then some parameters (Load recording sensors type; 25 and100KN, Zero readings and path of file to save logging of measurements) were selected in the software of attached computed to the machine. In next step, load was applied at constant rate to get the failure within 15 to 30 seconds. After the failure applied load was stopped and results recording file was saved for further work. These steps were repeated for all plugs.

A total of ten disc shaped plugs of two sizes of diameters (40 mm and 28 mm) were used for Brazilian test. Logging file was saved and copied in the user defined data folder. Plug was removed and this procedure was repeated for the all samples. The setup is supervised by lab engineer at NGI lab.

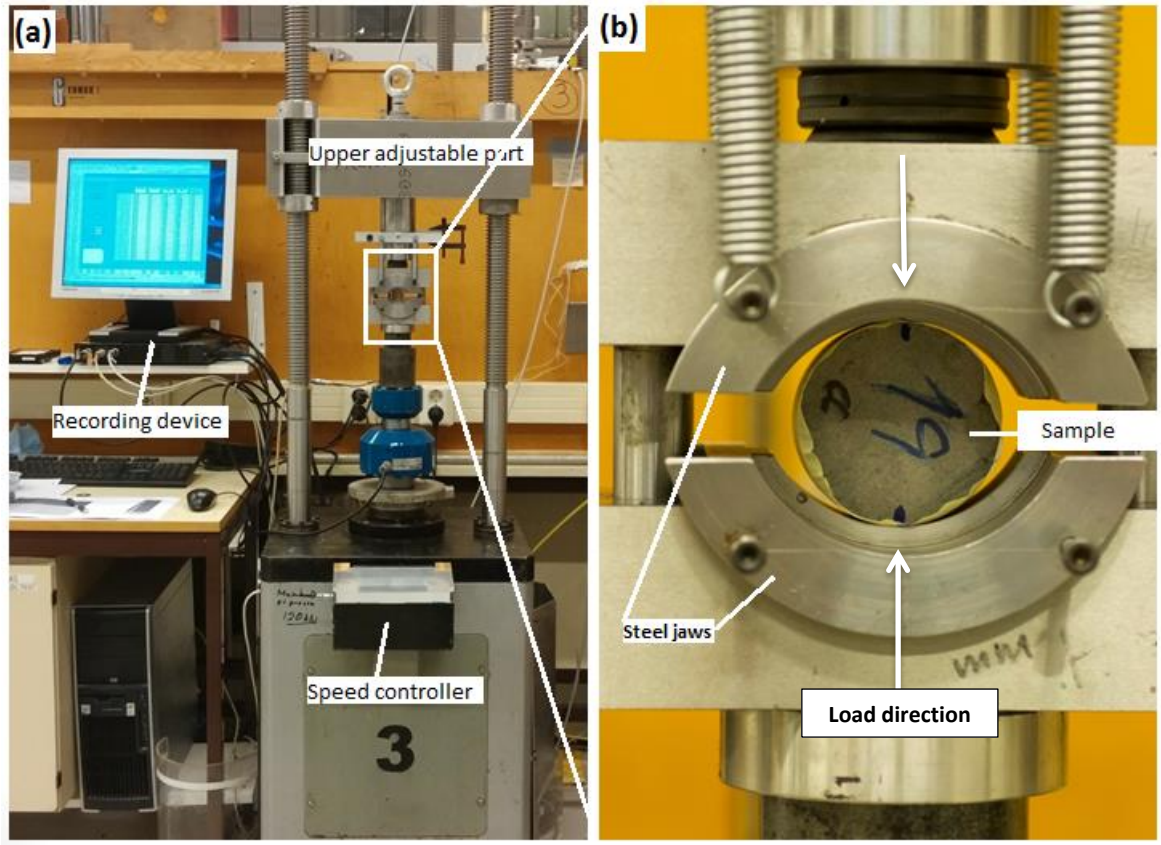

Fig. 3.11: (a) Apparatus for Brazilian test at NGI lab and (b) Steel jaws for holding a sample.

These samples were loaded in perpendicular direction to the bedding for the Brazilian tests. A schematic illustration shown in Fig. 3.12 describes the logic of loading sample perpendicular or parallel to the bedding planes. In this illustration, direction of drilled or cut plugs with reference to core axis are shown and three different simple cases (a, b & c) in Fig. 3.11 for loading directions; (a) perpendicular loading direction because applied load and failure planes are perpendicular to the bedding planes, also measured tensile strength in this case will be vertical strength of the rock, (b) parallel loading direction because applied load and failure plane are parallel to the bedding planes of the rock and (c) in this case (used in this study) we call the loading direction perpendicular to the bedding because failure plane is perpendicular and the fracture is cutting across the whole beddings as in case (a). If we analyse the direction of applied load that looks like parallel to the bedding plane but it is not a point load so that is why we can consider this case as perpendicular loading direction to the bedding plane.

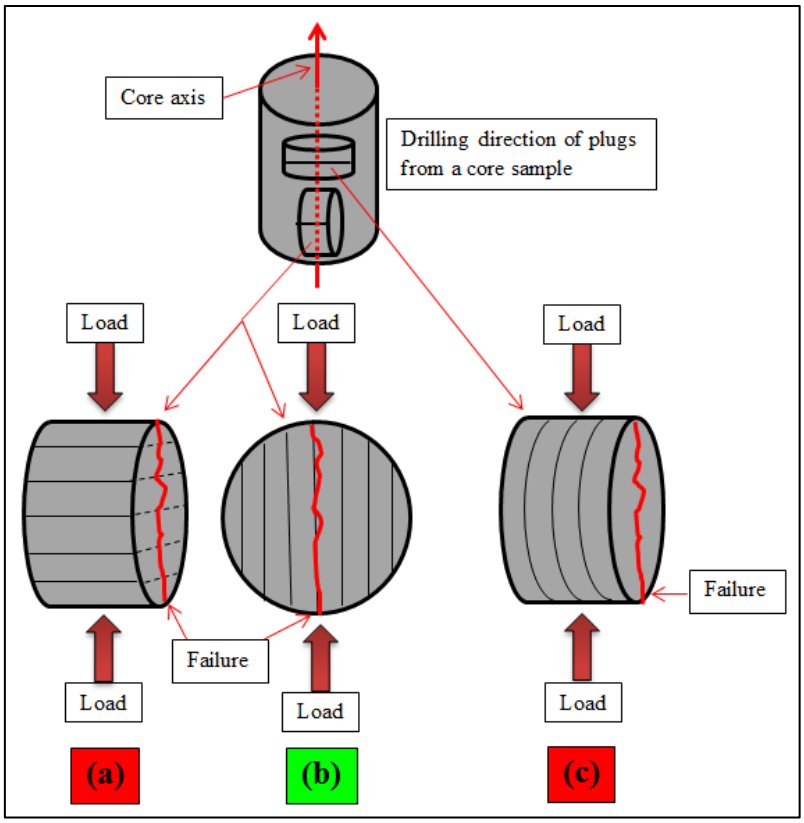

Fig. 3.12: Schematic diagram of load application to measure Brazilian tensile strength of the plugs loaded in perpendicular and parallel directions to the bedding planes.

Measurements

To determine the tensile strength of these tested samples, peak load was picked from the load vs time graph. This peak load is a maximum load at the first break or fracture produced in the sample during the test under the applied axial load. An example of the graph is shown in Fig. 3.13. Later this information is used in the following formula 3.2 to calculate the tensile strength, σt, (ISRM, 1978):

$$\sigma t = \frac{0.636 \cdot P}{Dt} \qquad 3.2$$

where σt is tensile strength (MPa), P is peak load at failure (N), D is the diameter of plug (mm) and t is average specimen thickness (mm).

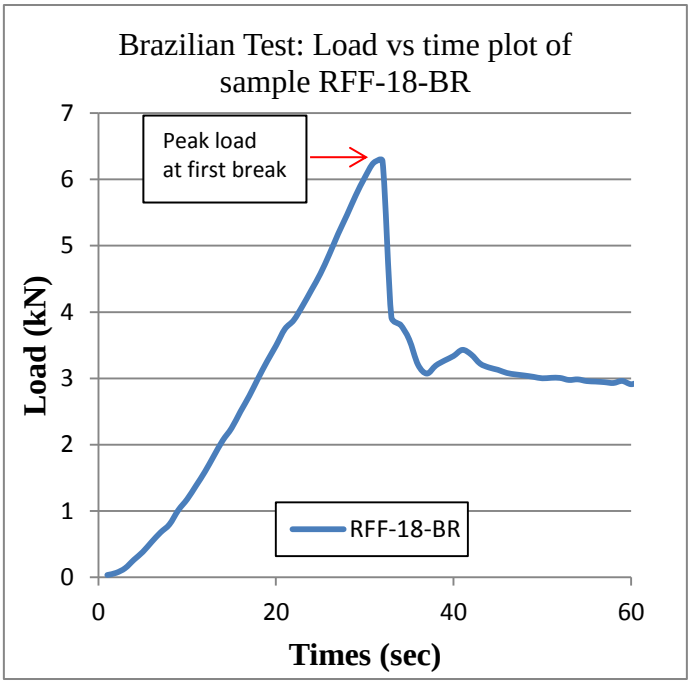

Fig. 3.13: Graph showing the load vs time plot and peak load at the first break.

3.3.2 Uniaxial compressive strength test

Uniaxial Compressive Strength test (UCS) belongs to destructive strength test category. Principal force is compression and failure mechanism is shear for UCS. Fig. 3.14 shows simple parameters of a test sample.

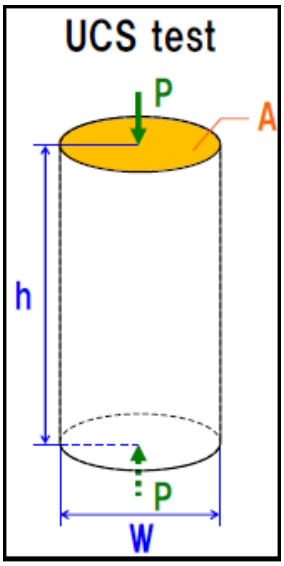

Fig. 3.14: Uniaxial compressive strength test conditions (JCRM, 2011).

In Fig. 3.14, A is initial cross-sectional area of the sample, P is peak load (at failure load), H is sample height and W is sample width.

Test Procedure

Test is conducted according to the ASTM standard D2938 for determination of Geomechanical parameters (uniaxial compressive strength (σ) and Young' modulus) and P and S-waves velocities. Six cylindrical shaped plugs of two sizes of diameters 40 mm and 28 mm were used for UCS test. All the cylindrical shaped plugs were wrapped in thin plastic transparent sheet for safety and sample preservation, so that pieces from sample during testing and break do not fall apart.

Pre-defined parameters are used for logging the results in the programme of the machine. Apparatus was set according to the ASTM standard as shown in Fig. 3.15a and supervised by lab engineer at NGI. Disc shaped steel platens were used between test plugs and the loading pistons (Fig. 3.15b). Test plug was placed between the platens and then load was applied at a constant rate to reach failure within 2 to15 minutes. Logging file consists of load and time values was saved and copied in the user defined data folder. Plug was removed and this procedure was repeated for all the samples.

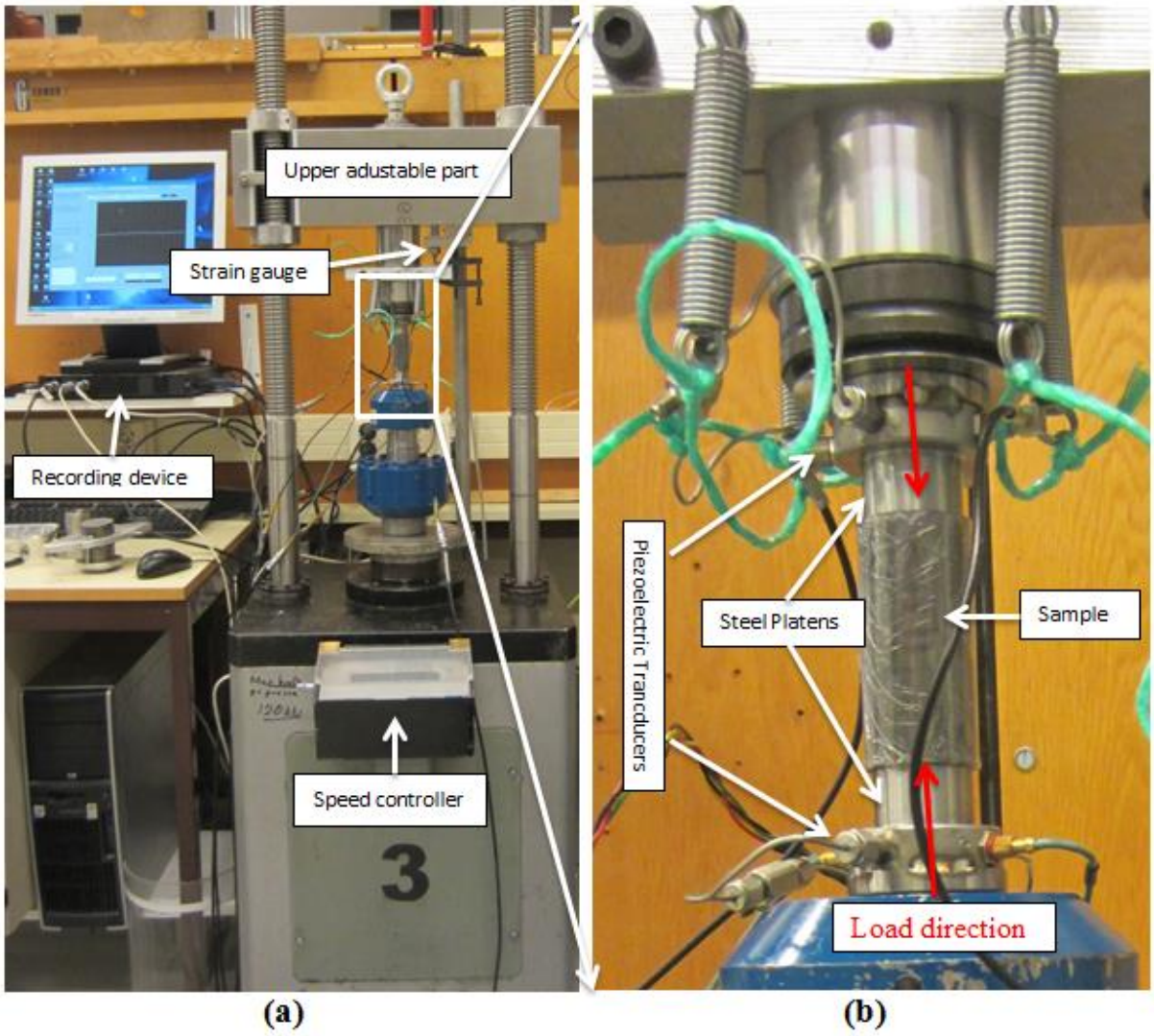

Fig. 3.15: (a) Apparatus for UCS test at NGI lab, (b) Steel platens while holding a plug during test.

Measurements

To determine uniaxial compressive strength of these tested samples, peak load was picked from the load vs time graph. This peak load is a maximum load at the first break or fracture produced in the sample during the test under the applied axial load. An example of the graph is shown in Fig. 3.16a. Following calculation method is used to determine UCS as shown in equation 3.3.

$$\sigma = P/A \qquad 3.3$$

where σ is uniaxial compressive strength (MPa), P is maximum load (KN), A is cross-sectional area (mm^2) of the plug.

To determine the cross-sectional area (A) of the specimen, equation 3.4 is used:

$$A = (\pi D^2)/4 \qquad 3.4$$

where A is the cross-sectional area (mm^2) and D is diameter (mm) of the plug.

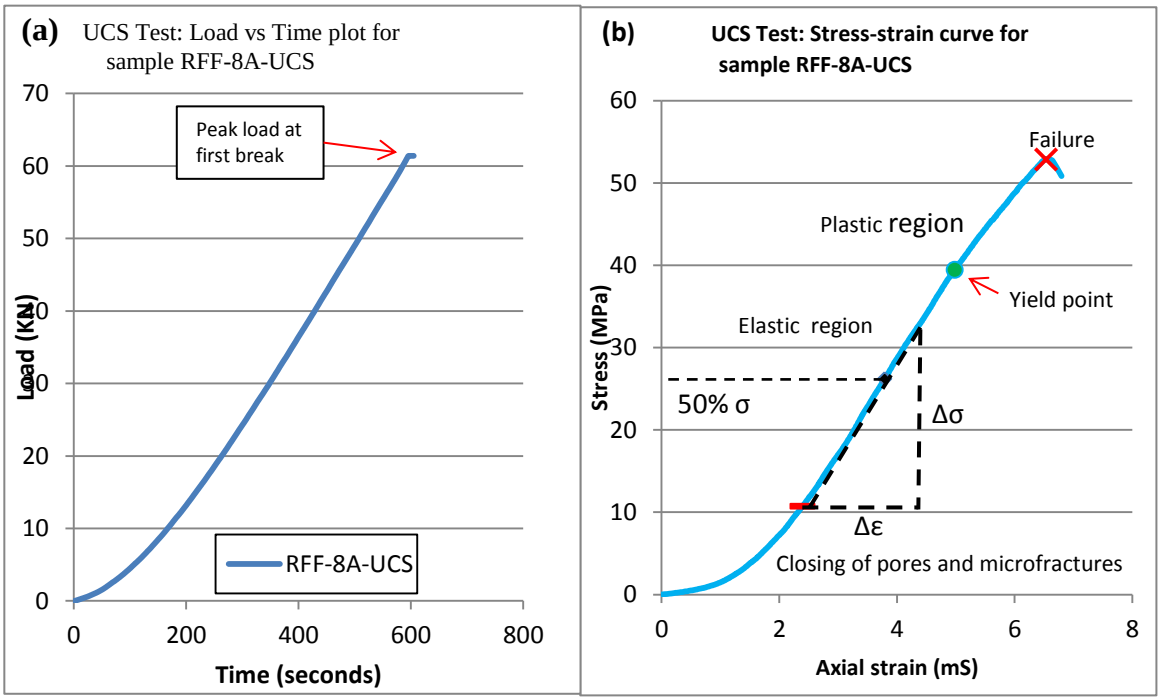

Fig. 3.16: (a) Graph showing the Load vs time plot and peak load at 1st break and (b) Graph showing stress-curve of sample RFF-8A-UCS.

Young' modulus (E) is also calculated by tangent young's modulus method (Fig. 3.16b)as described by ISRM et al. (2007), formula is given in 3.5 for the entire set of tested plugs.

$$E_t = \frac{\Delta\sigma}{\Delta\varepsilon} \qquad 3.5$$

Where Et is tangent Young's modulus.

Axial deformation (displacement in mm) was recorded by axial strain gauge that was attached to the apparatus as shown in Fig.3.17.

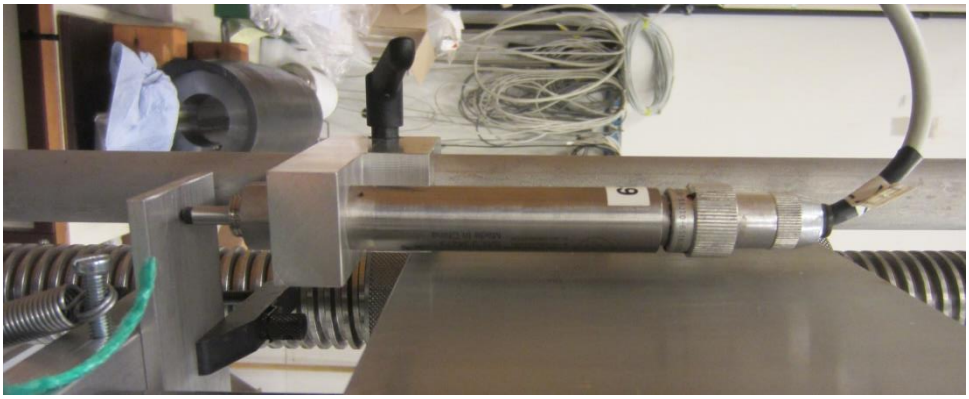

Fig.3.17: Axial strain gauge (NGI lab)

By using axial deformation values for samples, their axial strain was calculated by the following method: first, the recorded axial deformation was zeroed (means the first contact between loading platens and plug from where load-time curve starts rising as marked by red circle at (0.0) in Fig. 3.16(a) and then this values was subtracted from the entire set of axial deformation values). Secondly, a correction was applied to plot accurate stress-strain curve. This correction was determined by plotting false deformation (mm) as a function of applied load (kN) as shown in Fig. 3.18. And then the value of this curve was calculated by using Eq. 3.6 and subtracted from the recorded deformation of the sample during test.

$$\boldsymbol{Y = 0.0057X} \qquad 3.6$$

where Y is the value of false deformation curve and X is false load (KN).

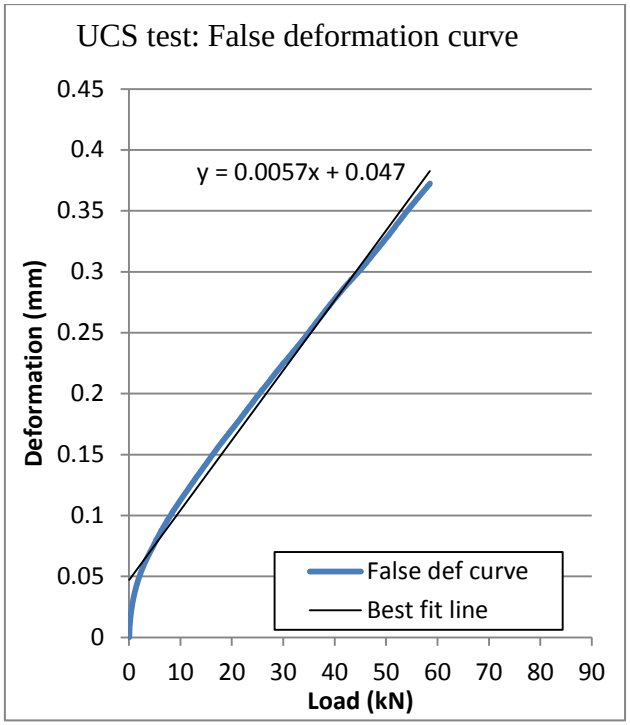

Fig. 3.18: False deformation curve

The equation 3. 7 is used to calculate the axial strain after applying corrections on the data.

$$\textbf{Axial strain} = \frac{\boldsymbol{Corrected\ deformation}}{\boldsymbol{Height\ of\ plug}} \qquad 3.7$$

Also P and S wave velocities are measured during UCS test for the whole set of plugs. The pulse transmission technique as described by Birch (1961) was used to measure these velocities. Piezoelectric ceramic elements were mounted inside the top cap and the bottom pedestal of the steel platens (where we put plug for UCS test) as shown in Fig. 3.15b. These elements work as both receiver and transmitter as the electrical potential applied to them causes a mechanical vibration. The mechanical impact on receiver causes recordable electrical potential. The wave that has travelled through the sample is recorded at the receiver with a given sample interval. We utilized only the first arrival in order to determine the velocity. The input signal is a 500 kHz sinusoidal signal (ultrasonic).

All the velocity measurements were recorded in .sg2 file format. The Matlab script "time_picker" was used to open these files for further analysis. This script helped to pick first arrival time for P- and S-waves by giving a visual presentation of traces in 2 different windows as shown in Fig. 3.19. After time picking and applying available corrections in the script, the data was saved into a text file for further velocity calculations.

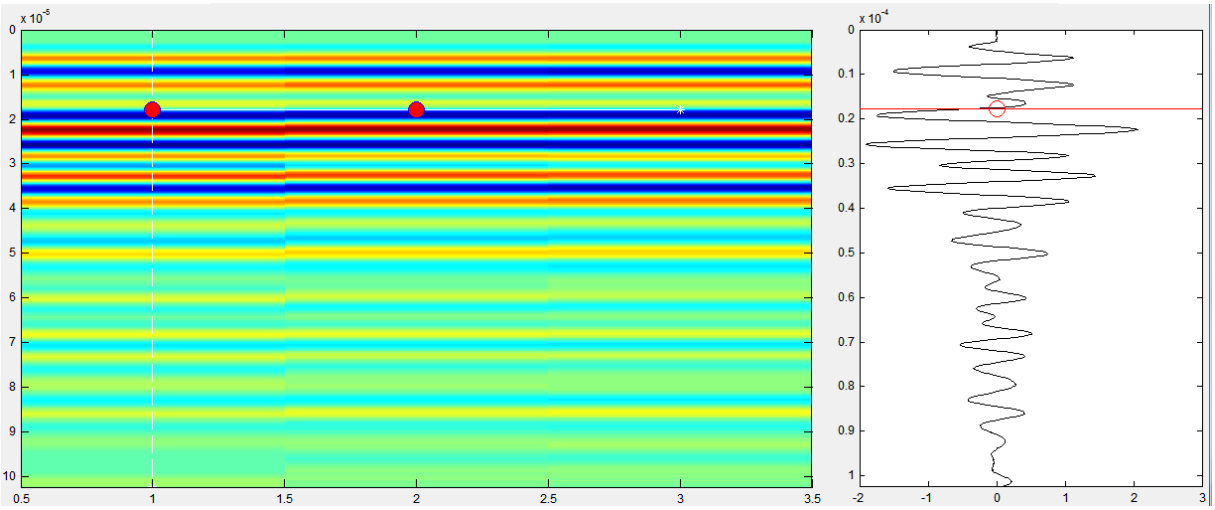

Fig. 3.19: An example of time picking for velocity measurements using the NGI's time pick script.

Zero correction (time required for an ultrasonic wave to pass through transducers) was applied to get the accurate travel time for velocity measurements for the actual length of plugs as shown in Fig. 3.20.

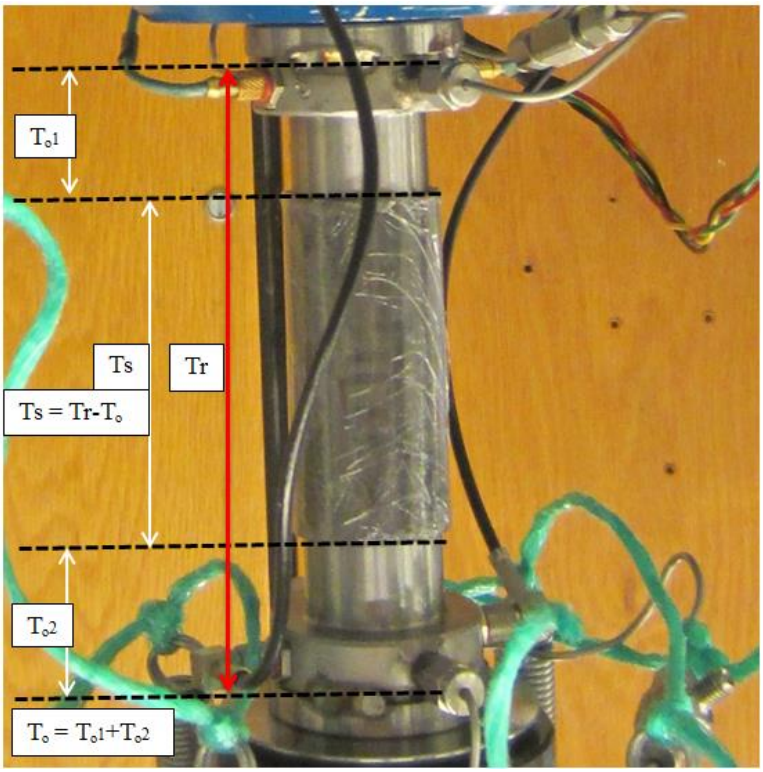

Fig. 3.20: Visual explanation of zero correction to get the actual travel time through a sample (T_o = travel time in the steel platens, Tr = total travel time from one transducer to another and Ts = travel time of signal in the length of sample).

After correcting the travel time, following equation 3. 8 is used to calculate velocity:

$$\boldsymbol{V = \frac{L}{Ts}} \qquad 3.\ 8$$

Where V is P-or S-wave velocity, L is the length of plug and Ts is the corrected travel time according to plug's height.

3.4 Work flow

A detail work flow used for this study is shown in Fig. 3.21. All the main steps to achieve maximum objectives for this study are mention in this chart.

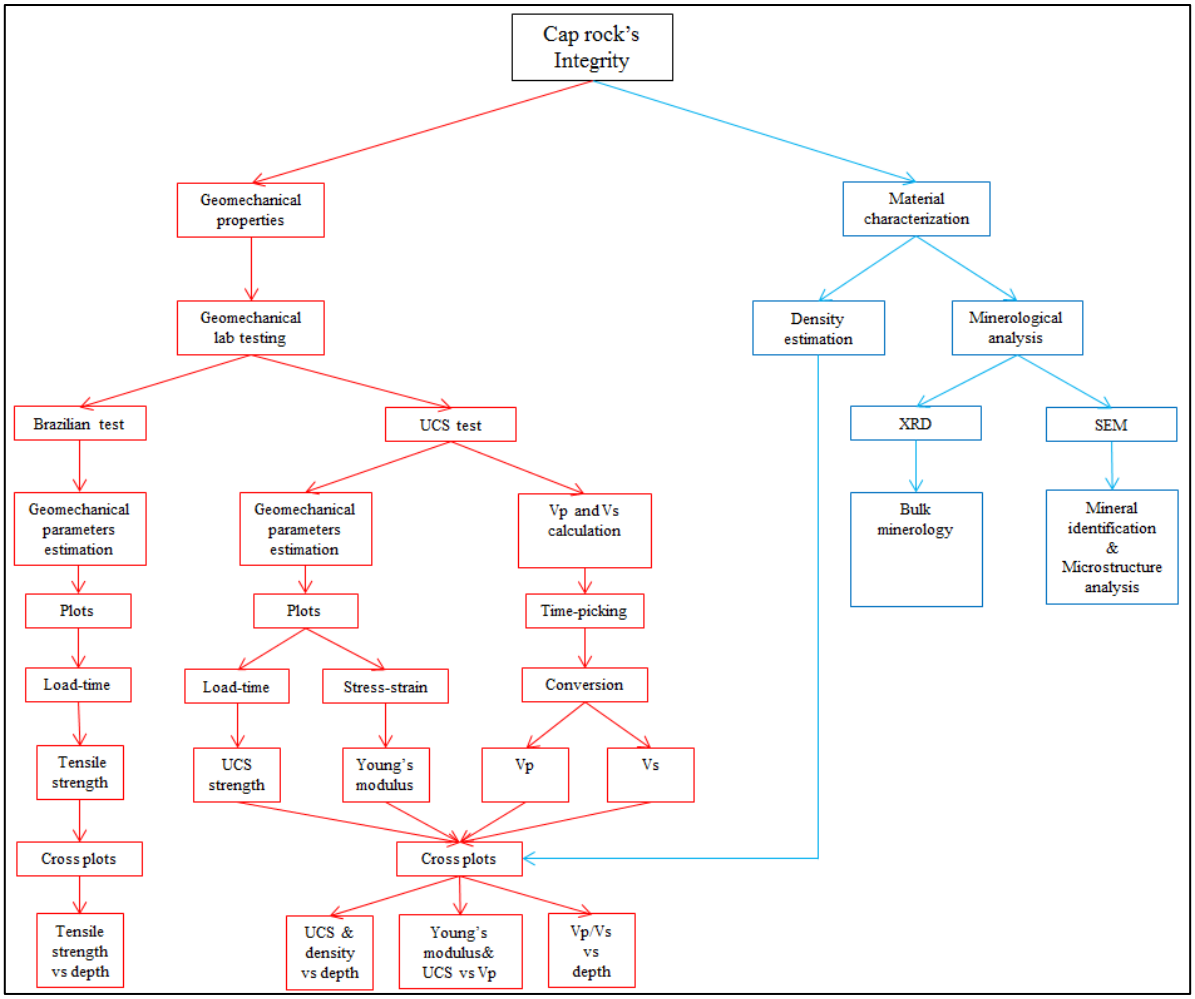

Fig. 3.21: Work flow for this study.

Chapter 4: Tensile strength Analysis

This chapter focused on tensile strength analysis and this strength is determined by Brazilian test in the laboratory. It is divided into three major sections; results, discussion and comparison of results with previous research. Tested samples are caprock shales from Agardhfjellet and Rurikfjellet formations. These results are presented combine and separately for both formations in form of tables, plots and pre- and post-test photos. The discussion part includes interpretation of these results in details and the comparison section includes comparison of these results with previous research.

4.1 Results

Total ten plugs were prepared from six selected core samples for Brazilian tensile strength tests from well Dh-6 from two formations; Rurikfjellet (depth range 308.00-386.89 m) and Agardhfjellet (depth range 425.28-428.28 m). All results are summarized in Table 4.1. The plug ID for exam RFF-8A-BR represents Rurikfjellet Formation (RFF), the original number of core samples from well (8A) and the Brazilian test (BR). Similarly the plugs ID in other form such as AFF-33A-BR represents Agardhfjellet Formation (AFF), the original number of core samples from well (33A) and the Brazilian test (BR).

Table 4.1: Summary of results from Brazilian tests and parameters of all the plugs used for testing.

Formation	Depth, (m)	Plug ID	Diameter, D (mm)	Thickness, t (mm)	Density, ρ (g/cm3)	Load at failure, P (N)	Tensile strength, σ_t (MPa)	Time to break, (sec)
Rurikfjellet	308.00-308.26	RFF-8A-BR	40.4	21	2.58	7376	5.53	30
	308.00-308.26	RFF-8B-BR	40.5	21	2.57	6492	4.85	31
	308.00-308.26	RFF-8C-BR	40.4	21	2.58	7198	5.40	31
	369.21-369.35	RFF-18-BR	40.4	20.75	2.60	6278	4.76	30
	369.41-369.53	RFF-19A-BR	40.3	19	2.54	5297	4.40	33
	386.74-386.89	RFF-25B-BR	40	20	2.60	4977	3.96	28
	386.74-386.89	RFF-25C-BR	40	20	2.56	4977	3.96	25
Agardhfjellet	425.28-425.43	AFF-32A-BR	28.5	15	2.85-3.15	6957	10.35	31
	425.28-425.43	AFF-32B-BR	28.5	15	2.85-3.15	5381	8.01	25
	428.15-428.28	AFF-33-BR	28.5	15	2.51	1543	2.29	17

Results presented in Table 4.1 are produced from actual laboratory experiments and some direct measurements using small lab tools such as digital vernier caliper and digital weight scale. Diameter and thickness of the plugs are measured by using digital vernier caliper and mass is measured by using digital weight scale. Later this information is used to calculate the density of all these plugs for Brazilian tensile strength tests. The calculation method and

formulas to calculate tensile strength from peak load is described in chapter 3 under section 3.3.1 that explain Brazilian Test.

4.1.1 Rurikfjellet formation

Seven of the total ten plugs are selected from Rurikfjellet formation as mentioned in Table 4.1. A brief overview of Rurikfjellet formation on the basis of this study and depth of the formation in the Dh-6 is from Ogata et al. (2014a) are summarized in Table 4.2. The diameter of these plugs is from 40 to 40.5 mm and thickness is from 19 to 21 mm. The tensile strength range of these samples is 3.96 to 5.53 MPa and the time of first break also matches the ISRM standard. Sample RFF-8A-BR from a depth range of 308.00-308.26 m has highest tensile strength about 5.53 MPa, its 1st break time is about 30 seconds and has maximum load of 7376 N. Sample RFF-25B-BR from depth range of 386.74-386.89 has the lowest tensile strength about 3.96 MPa in this formation.

Table 4.2: Overview of Brazilian test plugs from Rurikfjellet formation.

Rurikfjellet Formation	
Lithology	Shale
Well	Dh-6
Total number of tested plugs	7
Range of density	2.54-2.60 g/cm^3
Vertical tensile strength	3.96-5.53 MPa

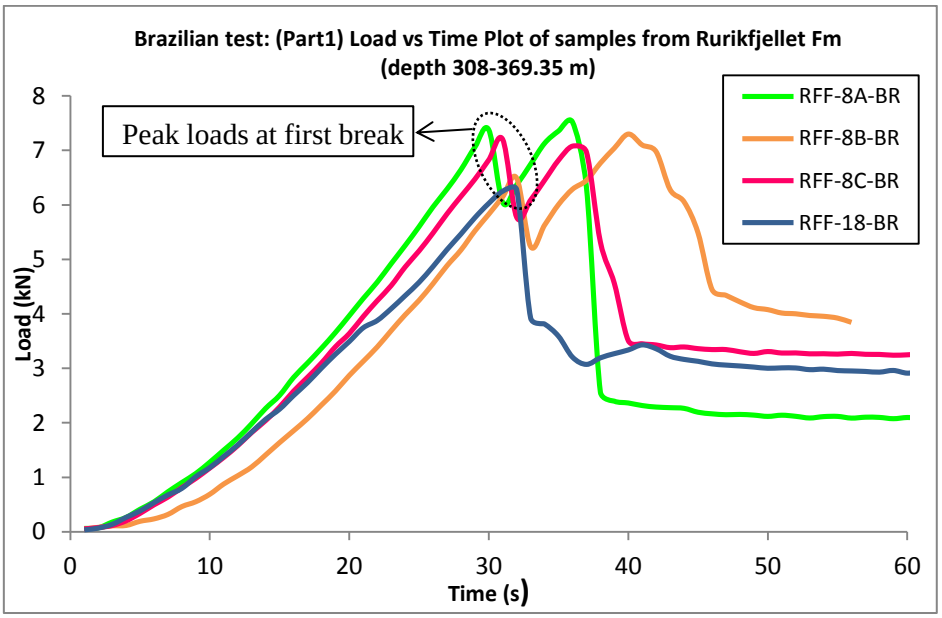

Fig. 4.1: Load-time plot (part1) of samples from Rurikfjellet Formation.

The peak load is identified as described in methodology under section 3.3.1 (Fig. 3.13). As we can see in Fig. 4.1, three curves for sample RFF-8(A, B and C)-BR have very similar pattern, almost same time of first break and peak loads of RFF-8(A & C)-BR is also close but RFF-8C-BR has lower peak load compared to other two plugs. Sample RFF-8A-BR has highest peak and Sample RFF-18-BR has lowest peak and a different curve than others.

On the basis of shape or trend observations of these load-time plots, we can see that curves of plugs (RFF-8A, 8B & 8C-BR) have roughly linear trend (except the beginning of the curves) until they reach the maximum (peak load) point and then a sudden drop as we can see in Fig. 4.1 marked by an oval shape. Also the load-time curves for these three plugs from core sample 8 have second peaks, slightly higher, slightly lower and higher than the peak at first break respectively for RFF-8A-BR, RFF-8B-BR and RFF-8C-BR. But curve of RFF-18-BR is different as compared to other three curves in this plot and it is linear to the point (load: 3.74 KN and time: 21 sec) and then it deviates and again linear until the maximum point (peak load).

Another interesting observation is that plugs prepared from a single core sample have very similar behavior in these time-load plots. As we can see in Fig. 4.1 three plugs (RFF-8A-BR, RFF-8B-BR & RFF-8C-BR) prepared from core sample 8, have very similar and linear trends till the maximum point (peak load) and almost same time of first break as compare to a plug prepared from different core and even though these cores are from same formation. Another example is two plugs (RFF-25B-BR and RFF-25C-BR) prepared from core sample 25. If we compare it with RFF-19A-BR we can see that they are very different in trends as shown in Fig. 4.2 represents load versus time plots of last three samples (RFF-19A, 25B & 25C-BR) from same formation.

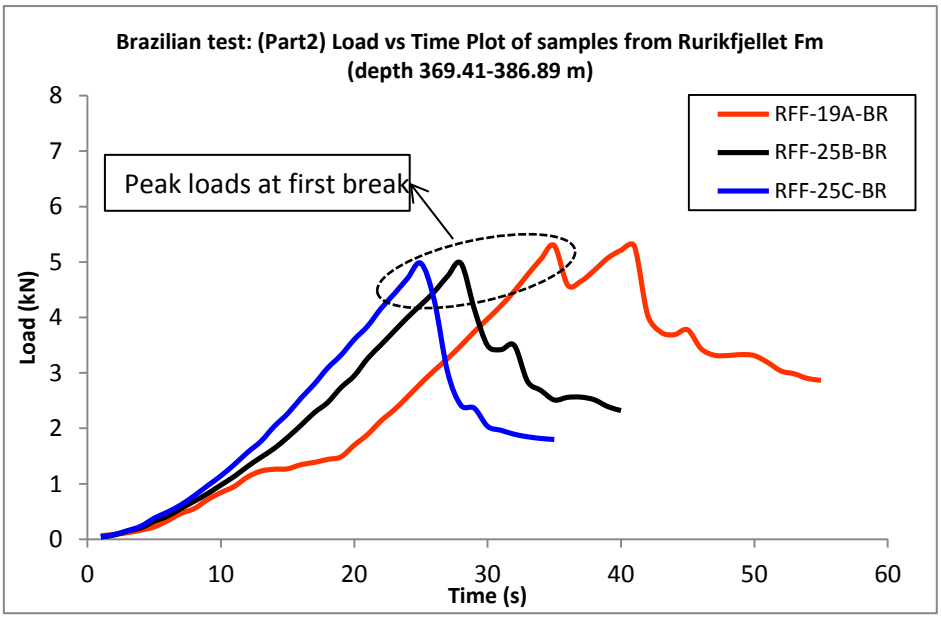

Fig. 4.2: Load-time plot (Part 2) of samples from Rurikfjellet Formation.

We can see from Fig. 4.2 two plugs RFF-25B-BR and RFF-25C-BR have very similar shaped and linear curves up to the maximum point (peak load) and have almost same peak loads but has a small difference in the first break times of 3 seconds. Load-time curve of RFF-19A-BR is irregular from starting point to the point reflects the load: 1.22 KN and time: 13 seconds is roughly shown linear trend and then it deviates till another point (load: 1.485 KN & time: 19 seconds) and very linear rise up till the maximum point (peak load) followed by sudden drop. Also RFF-19A-BR has a second peak after first break with almost the same load value.

The fracture pattern recorded at initial stages of failure during test were captured and shown in Fig. 4.3 and Fig. 4.4. These images were captured sometime after the first break and may

not indicate the first peak failure. On the basis of available images which are shown in Fig. 4.3 and the observation during test performance, the following can be stated:

- A diametral fracture connects the loading zones in sample RFF-8A-BR.
- For sample RFF-8B-BR the fracture is more prominent in the lower half and terminating towards the upper loading point. This may show that fracture started from the middle or lower part propagating outwards or upwards.
- For sample RFF-8C-BR the fracture is diametral in the central part of the specimen (similar to 8a) but is diverting away from lower loading area at the bottom. There are also few very small fractures besides loading area and this fracture is different from 8b and 8c because it is not connecting upper and lower loading points like in first two plugs.
- Fracture in RFF-18-BR has a rough pattern, continues with almost equal intensity throughout the plug and diverting from lower middle part towards the lower loading point.

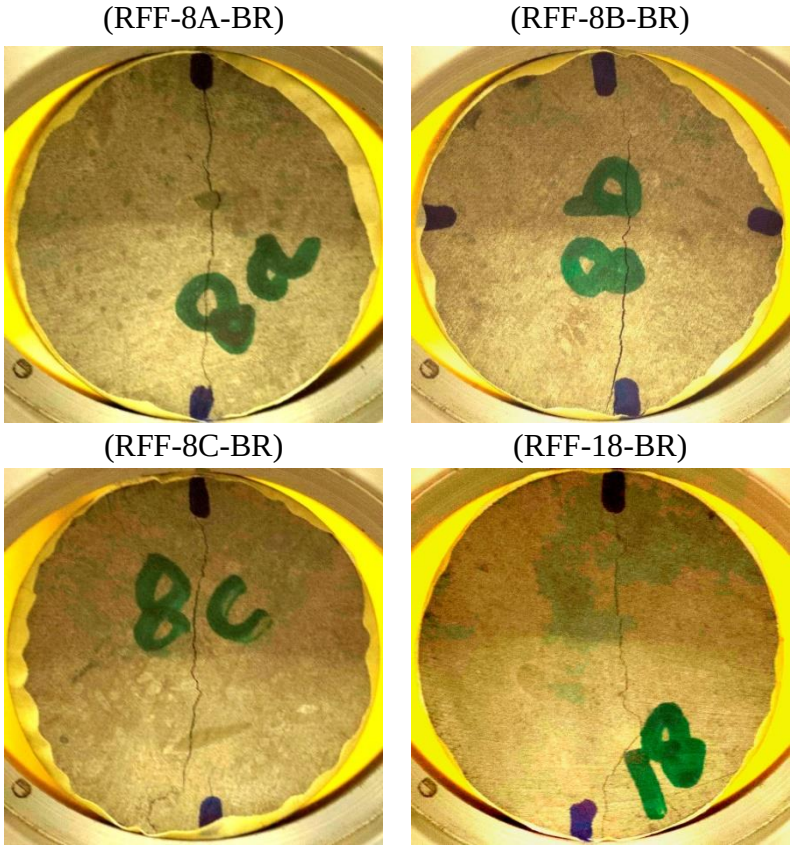

Fig. 4.3: Fracture pattern recorded for four different test plugs (part 1) from Rurikfjellet Formation.

The patterns of fractures for three other samples were recorded at initial stage of failure are and on the basis of available images shown in Fig. 4.4 and the observation during test performance, the following can be stated:

- As we can see the first break in plug RFF-19A-BR (upper image in the figure), is more prominent from the upper loading point to the middle of

the sample and then gradually becoming thinner towards the lower loading point. But this fracture is not connecting the both loading areas and is quite away from the upper loading area and also splitting in the top edge.

- Initial fracture in the plug RFF-25B-BR is more prominent in the middle part and propagatting towards the loading points and also connecting the both loading zones.
- The fracture in RFF-25C-BR is very pominent and is probably not a first break, but it is connecting the both loading zones and also splitting at the lower loading area.

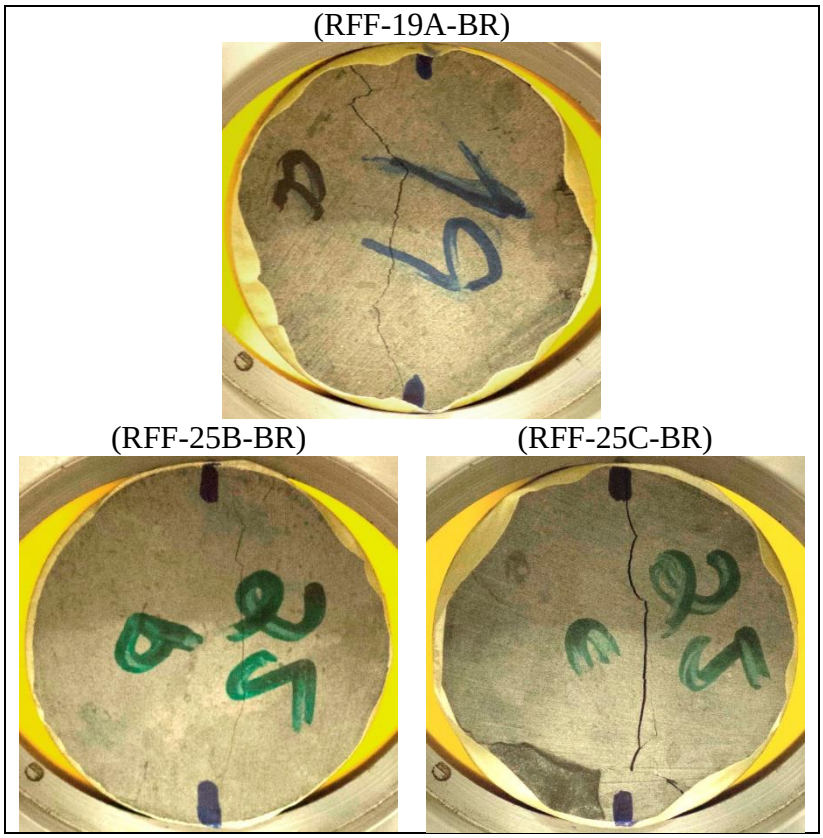

Fig. 4.4: Fracture pattern recorded for three different test plugs (part 2) from Rurikfjellet Formation.

Tensile strength versus depth is shown in Fig. 4.5 for entire set of tested plugs from Rurikfjellet formation. As we can see from figure that variations with increasing depth in the upper part of curve is quite noticeable. Overall trend of the curve is showing slight linear decrease in tensile strength with increasing depth in the middle and quite sudden drop in tensile strength at the lower part.

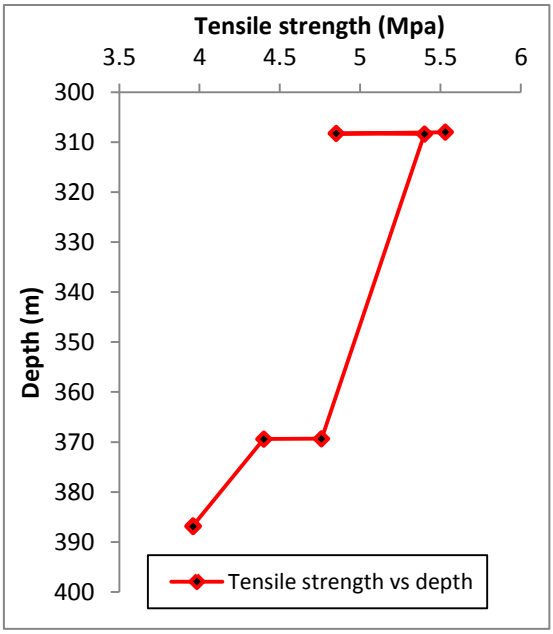

Fig. 4.5: Tensile strength versus depth of entire set of plugs from Rurikfjellet Formation.

4.1.2 Agardhfjellet formation

Three out of ten total plugs for Brazilian tensile strength test were selected from Agardhfjellet Formation as mentioned in Table 4.1. The depth of these samples varies from 425.28 to 428.28 m in bore hole Dh6. These plugs had a diameter of 28.5 mm and a thickness of about 15 mm. A brief overview of test plugs from Agardhfjellet formation is given in Table 4.3.

Table 4.3: Brief overview of test plugs from Agardhfjellet Formation.

Agardhfjellet Formation	
Lithology	Shale
Core sample source Well	Dh-6
Total number of tested plugs	3
Range of density	2.51-3.15 g/cm³
Calculated vertical tensile strength	2.29-10.35 MPa

Calculated tensile strength for Agardhfjellet formation ranges from 2.29 MPa to 10.35 MPa and this range is lowest and highest amongst the entire set of tested plugs from the both formations. Because tensile strengths of the plugs AFF-32A-BR (depth 425.28-425.43 m) and AFF-32B-BR (425.28-425.43m) from core sample 32 is 10.35 and 8.01 MPa respectively and it is almost twice the strength of other samples. Also the calculated lowest tensile strength amongst the whole set of data belongs to this formation which is 2.29 MPa for AFF-33-BR (depth 428.15-428.28 m).

Load versus time for samples from Agardhfjellet Formation is shown in Fig. 4.6. The peak load value of plug AFF-32A-BR is the highest amongst the entire set of the tested samples from Rurikfjellet and Agardhfjellet formations. Also sample AFF-32B-BR has the second highest peak load value amongst the whole set of the tested plugs. But sample AFF-33-BR has completely different trend in this plot and it has lowest peak load value among all the tested plugs from both formations. Trend based observations show that the load-time plots for

both plugs (AFF-32A-BR and AFF-32B-BR) from same core sample 32 have quite similar shape and linear trend of curves, except one point (load: 1.89 KN and time: 15 sec) that has little variation in the trend. AFF-33-BR has very different shape of curve, not very linear and there is gradual drop in load after the first break.

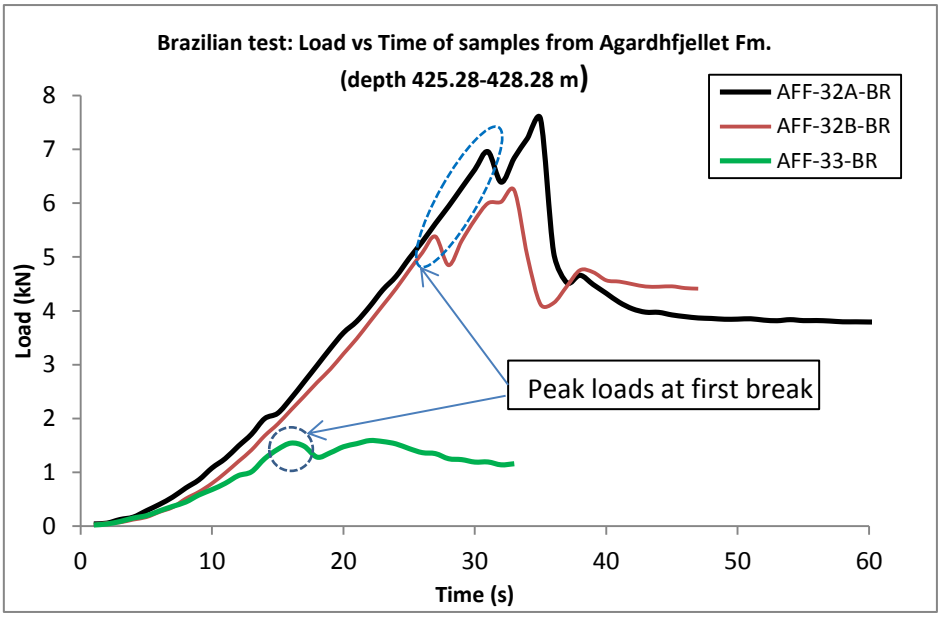

Fig. 4.6: Load-time plots of samples from Agardhfjellet Formation.

All the plugs from Agardhfjellet Formation have 2nd peaks in the load-time plots as we can see in Fig. 4.6. Plugs AFF-32A-BR and AFF-32B-BR have quite higher 2nd peaks after the first peaks at first break. Load-time curve of AFF-33-BR doesn't show any sharp peaks but also has 2nd peak and these peaks are smooth and gradual in trend and quite close in their peak values.

The fracture pattern is recorded at initial stage of failure in plugs from Agardhfjellet Formation during testing as shown Fig. 4.7 and the observation during test performance, the following can be stated:

- Fracture in plug AFF-32A-BR is straight and connecting both loading points and also have two minor fractures beside the upper loading point.
- Plug AFF-32B-BR has two side by side fractures from top to the bottom and curve shape fracture on the right of the upper loading point.
- Fracture is more prominent in the upper middle part of the plug AFF-33-BR and propagating towards both loading points from middle.

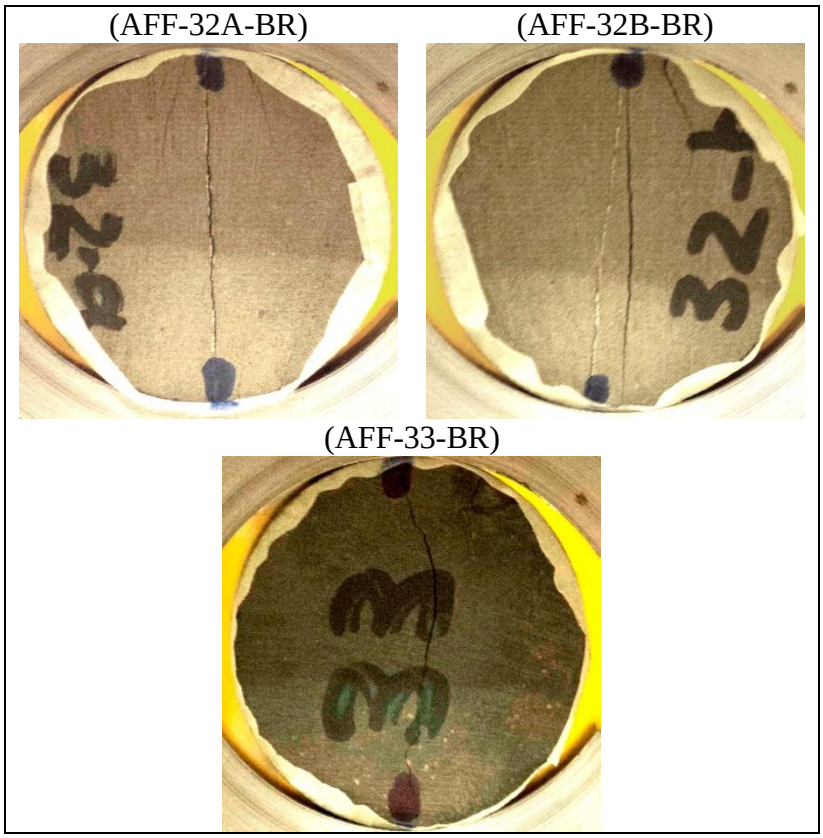

Fig. 4.7: Fracture pattern recorded for the different tests from Agardhfjellet Formation.

4.2 Discussion

This section focuses interpretation of the findings from the results based on the Brazilian tensile strength test. Discussion is divided into several subsections focuses pre- and post-test analysis, load-time curves corresponding to tensile strength analysis, tensile strength and density versus depth plot and a comparison of data acquired in this study and previous works.

4.2.1 Pre- and post-test analysis of tested plugs

Ten plugs were used to test tensile strength of the caprock units from two geological formations; Rurikfjellet and Agardhfjellet as mentioned in Table 3.3. Image based summaries are reported in Tables 4.4 and 4.5 where we see the comparison of pre- and post-test plugs. The description of pre- and post-test plugs, based on the pre-existing visible defects and the pattern of fractures produced after Brazilian testing for Rurikfjellet Formation are summarized in Table 4.4.

Table 4.4: Pre- and post-test pictures of tested plugs from Rurikfjellet Formation.

Sample ID	σt, (MPa)	Brief description	Pre-test	Post-test
RFF-8A-BR	5.53	A good sample with no pre-exiting defects. One clear fracture is produced between loading points following by two fractures after the test.	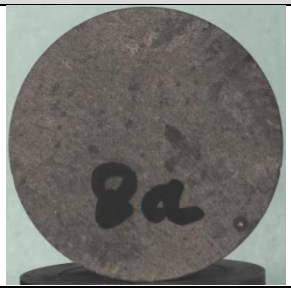	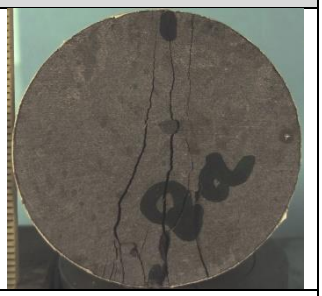
RFF-8B-BR	4.85	No pre-existing visible defects. A clear fracture between the loading points and splitting into many small fractures at the lower loading point. Also few small fractures are encountered in the upper part beside the loading point.	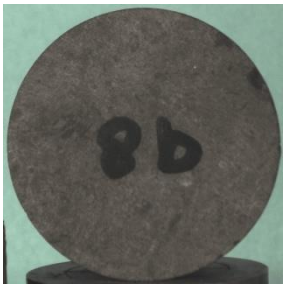	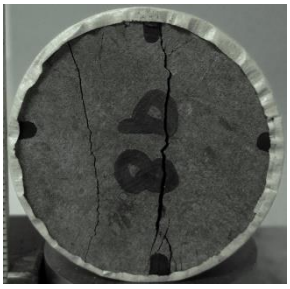
RFF-8C-BR	5.40	Inhomogeneous and strong sample. Prominent fracture that is splitting into two fractures in the middle and continuing to the lower loading point and also more than two fractures from the top and terminating in middle of the sample.		
RFF-18-BR	4.76	Medium quality sample with no visible pre-existing defects. An interesting fracture between the loading points and splitting into various fractures at the lower loading point. From this main fracture to the left side a portion is popped up due to closed shape fracture.		

Sample ID	σt, (MPa)	Brief description	Pre-test	Post-test
RFF-19A-BR	4.40	An inhomogeneous sample with a small pre-existing fracture. Prominent fracture that is making V shape at the lower loading point after splitting and small lift of left portion by opening of fracture.		
RFF-25B-BR	3.96	Comparatively weak and inhomogeneous sample. Visible fracture between loading points and two roughly curve shape fractures beside the lower loading point.		
RFF-25C-BR	3.96	Inhomogeneous and comparatively weak sample, edge at the lower loading point is broken,. Fracture between the loading points split into V shape at the both loading points.		

All the tested plugs were loaded perpendicular to the bedding planes from both formations. Three of the plugs RFF-8A, 8B & 8C-BR prepared from one core sample 8, the material is inhomogeneous but there are no visible defects and the fractures produced in these discs are mostly in the middle parts with some major and minor fractures besides them. As we can see they have shown higher tensile strength compared to other tested plugs prepared from other core samples (18, 19 and 25). Plugs RFF-18 and 19-BR has medium tensile strength and the fractures are cutting across the whole discs. Two plugs RFF-25B & 25 C prepared from core sample 25, showed low tensile strength compared to the rest of the plugs tested from Rurikfjellet Formation. The discs of these samples have weak edges and fracture patterns are also different.

Three plugs were tested from Agardhfjellet formation. Pre- and post-test summary is given in Table 4.5. Plugs AFF-32A and 32B show the highest tensile strength in the entire set of tested plugs. The patterns of fractures in both plugs are quite similar. Most of the fractures are in the middle parts and main fractures are very straight from upper loading points to lower loading points. If we look at the pre-test plugs, there is a white line in the middle and the main fractures are produced along this line in both plugs. This line looks like a fracture filled with light-colored minerals which was also very visible in the core sample 32 before the preparation of the plugs (Table 3.2).

The 3rd plug tested from this formation is AFF-33-BR which shows very low tensile strength compared to any other tested plug in this work. The fracture pattern of plug AFF-33-BR is also totally different from other tested plugs from this formation. It has a curve shaped fracture that is connecting upper and lower loading points with a small fracture beside. The reason could be weak edges and pre-existing fractures but they were not clearly visible before test.

Table 4.5: Pre- and post-test summary of plugs from Agardhfjellet Formation.

Sample ID	σt, (MPa)	Brief description	Pre-test	Post-test
AFF-32A-BR	10.35	A very sound sample with no visible pre-existing defects. There is a white colored vein in the middle of the sample. Three fractures cut across the whole sample.		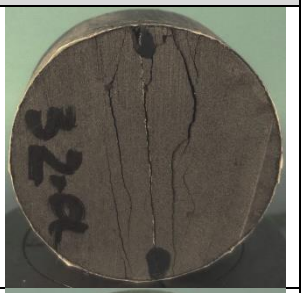
AFF-32B-BR	8.01	Strong sample, there are no visible defects observed. Two very clear fractures are produced in the middle of the plug connecting upper and lower loading zones.	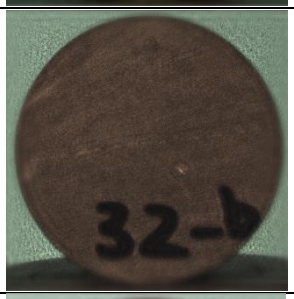	
AFF-33-BR	2.29	Edges of the disc were little weak, a weak plug. There is curve shaped fracture going through the whole disc with a small fracture beside in the upper part.		

4.2.2 Load-time curves and corresponding tensile strength analysis

Further analysis of tested plugs under Brazilian test from Rurikfjellet and Agardhfjellet formations has been done by plotting load-times curves. Peak load was picked from these curves to calculate their corresponding tensile strength for each plug as described in Chapter 3 under section 3.2.1.2. The peak loads and calculated tensile strengths are reported in Table 4.1 in the result section. This analysis is further explained for each formation.

4.2.2.1 Rurikfjellet Formation

Load-time curves of plugs from Rurikfjellet Formation are plotted in Fig. 4.1 and Fig. 4.2. On the basis of these curves we can analyze the time based load bearing of these rock specimens. We can also see from the calculated tensile strengths of these plugs from Table 4.1, three prepared plugs from same core sample 8 has highest tensile strengths in this formation as compare to all other tested plugs from this formation. The average measured density of this formation is 2.59 g/cm3 and it is almost the same for all these samples, so it cannot be the

reason for such difference in strength and failure behavior. Based on bulk mineralogy of these samples is mentioned in Table 3.5 we can see that core sample 8 has higher content of Pyrite (16.75%) than other core samples. Pyrite is a heavy mineral compared to common minerals found in a shale rock. Another interesting difference is Kaolinite content; it is less in core sample 8 (9.12%) and more in other core samples (12.56 to 16.58%). As we know that kaolinite is very common clay mineral and most of the clay minerals are considered mechanically weak.

SEM analysis was also done on two thin sections for two core samples; 8 and 18 from this formation. We can see the difference between microstructures, porosity and content of heavy minerals in these core samples (sample 8: Fig. 3.4 & Fig. 3.5 and sample 18: Fig. 3.6 & Fig. 3.7). Core sample 8 seems to have 3 % porosity based on the SEM and 4.5 % of heavy minerals. Core number 18 has 6% porosity and 2.9% of heavy minerals. This composition of minerals and the porosity can indicate that sample 8 may be stronger than 18.

4.2.2.1 Agardhfjellet formation

Load versus time curves are shown in Fig. 4.6 for three tested plugs from Agardhfjellet formation. Two of the plugs AFF-32A and 32B-BR have quite similar load-time curve in trend but the load bearing capacity is a bit different although both plugs were prepared from one core sample; 32. If we compare these two plugs with AFF-33-BR in terms of trend, loading capacity and post-failure load bearing, then AFF-33-BR is completely different in curve shape, has much less loading capacity and has very different and flat post-failure part.

If we compare the load bearing capacity and tensile strength of AFF-32A&32B-Br with AFF-33-BR, we can see that the difference is significantly high if we just look at the load-time curves and see the tensile strength values are 10.35, 8.01 and 2.29 MPa for AFF-32A-BR, AFF-32B and AFF-33-BR respectively. These three samples are from same formation and AFF-33-BR is just 3 m deeper than other two samples but the difference in their strength is big. The reasons of this anomaly in the entire data set are tried to be find out by doing XRD for bulk mineralogy and SEM, even at initial stage of this study when density was estimated for these plugs from core sample 32 which was very high (3.15 g/cm3) for one shale sample. We found that sample 32 from Agardhfjellet formation has 80.19% of Siderite content. Siderite is a ferrous carbonate mineral with high density (3.7-3.9 g/cm3).

SEM analysis of a thin section from this sample 32 is shown in Fig. 3.8, where we can observe its microstructure with no visible microfractures even at 40 to 600 µm scale. Another observation made on this sample by using SEM is the area measurements as shown in Fig. 3.9 where we can see that porosity is just 0.8 % and siderite plus other heavy minerals are more than 42%. On the basis of all these facts we can say that rock specimen from Agardhfjellet formation at depth from 425.25 to 425.43 m is mechanically very strong as it has the highest recorded tensile strength (8.01- 10.35 MPa).

Another reason for this highly dense and high content of Siderite can be detachment or tenctonized zone that is reported by Ogata et al. (2014b) and also shown in Fig. 2.7, reported depth range of this detachment zone in well Dh-2, Dh-4 and Dh-6 is 385-409m, 430-502m and approximately 385-409 m respectively. The depth range of these plugs from this formation is 425.25-428.28m, which is very close to the detachment zone. There is possibility that this material has gone through fracturing, compaction and filling of fractures with mineral veins. Also if look at the Fig. 2.5 in chapter two under section 2.2 Structural elements and

tectonics, we can see that Billeforden Fault Zone (BFZ) is present in this area (Ogata et al., 2014b).

4.2.3 Tensile strength and density versus depth analysis

Tensile strength and density values are plotted versus full depth range for the whole set of tested samples from Rurikfjellet and Agardhfjellet formations (Fig. 4.8). The important point of this profile is to see and compare the variations in tensile strength with reference to increasing depth for both of these formations. As we can see the overall trend of tensile strength has some significant variations, especially in the upper and lower parts and these variations with reference to depth are quite sudden. As whole profile for both formations of density versus depth, the tensile strength is slightly increased followed by a sharp rise and fall in the lower part as a function of depth.

Rurikfjellet formation is marked with light green color in this profile (Fig. 4.8). If we compare variations in tensile strength and density with depth, we noticed that both curves are quite similar in overall trend. Tensile strength is decreasing and density is slightly increasing with increasing depth. Agardhfjellet Formation is marked by light blue color in the lower part of the profile, where we can see that both tensile strength and density values increase abruptly till depth 425 m and then there is a sudden drop with increasing depth.

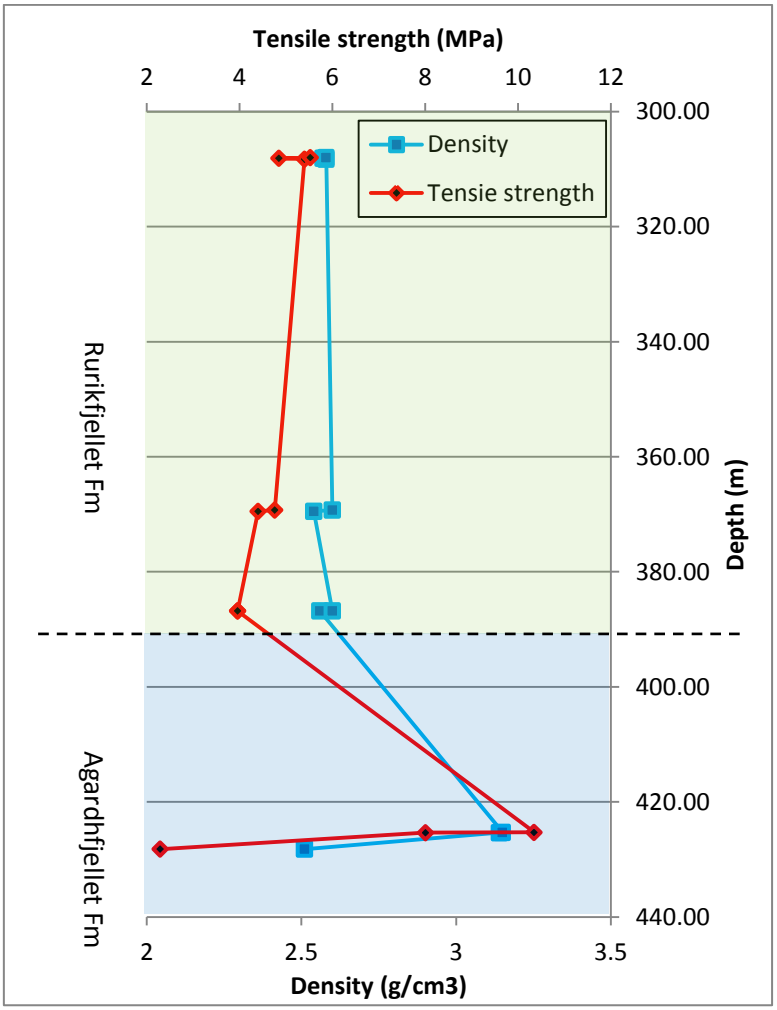

Fig. 4.8: Tensile strength and density are plotted versus depth for Rurikfjellet and Agardhfjellet formations.

From these observations, we can clearly see that density and tensile strength is not very much dependent on depth. For example in Rurikfjellet formation, the density is in-between 2.57 and 2.60 g/cm^3 and it's not changing with increasing depth. Lin (1983) also proposed that tensile strength of shale is not very much depth dependent as compare to other rocks (e.g. sandstone) and tensile strength of shallower origin can be higher compare to deeper origin of shale rock. But it might not be true because in this case the total tested depth is just 120.28 m (depth range 308-428.28m) and it is not enough to make a general conclusion. The tensile strength decreased/increased with increased depth, it might be dependent on some other factors such as mineral composition, microstructure and physical conditions of the core sample from a certain depth at the time of testing. But if we compare depth versus tensile strength and density of plugs tested from Agardhfjellet Formation, one of the tested plug (AFF-32-BR) that is just 40 m deeper than the tested plugs from Rurikfjellet Formation and it has 3.15 g/cm3 of density and 8.01-10.35 MPa of tensile strength that is way higher than all the tested material from less deeper depth and then just 3 m below from the same formation, the density and tensile strength (2.51 g/cm3 and 2.29 MPa) is the lowest in the whole profile.

The possible reasons for this sudden decrease or variations could be; material is affected (inner fractures) by detachment zone and these produced fractures that haven't filled with mineral veins and subjected to compaction like in AFF-32-BR. One reason can be significant upliftment of deep burial rocks can also altered the geomechanical properties such as fracture patterns, intrusions and cementation (Senger et al., 2014; Throndsen, 1982).

4.2.4 Comparison with previous studies

Previously geomechanical studies have been done for LYB CO2 Storage at NGI for caprock and reservoir units (NGI, 2010, 2012, 2014). Reference numbers of these reports from NGI are mention in Table 1.1 (Chapter 1; section 1.4). This study is also a part of geomechanical studies of same caprock samples but different bore-holes. That is why it is more appropriate to compare the results of this study to the previous studies performed at NGI. Comparison of tensile strength with previous work performed at NGI is shown in Fig. 4.9.

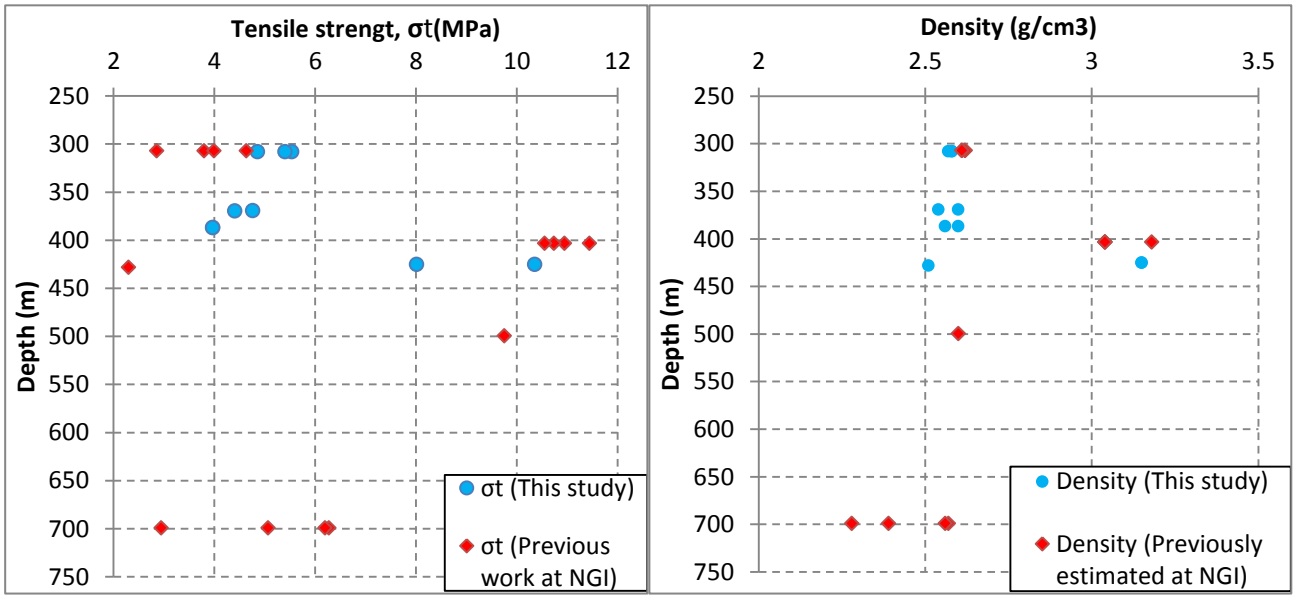

Fig. 4.9: Comparison of tensile strength and density of this study with previous work performed at NGI. Plot on the left side is tensile strength versus depth and on the right side is density versus depth

As we can in Fig. 4.9 (left plot) estimated tensile strength from Rurikfjellet formation (Well: Dh-6, depth: 300-308.26m) is little bit higher than previously estimated at NGI (Document no: 20120649-02-R) but densities are quite similar. Tensile strengths and densities from Agardhfjellet formation (depth 400-428.28 m, material used by NGI is from well Dh-4) are matching quite well (NGI, 2010).

Another interesting observation is found out by comparing the results of this work with previous work of Bohloli B. et al. (2014) that if plugs are loaded in different directions, the values of tensile strength and post-failure behavior in their load-time curves would be different. For this study, all the plugs are loaded perpendicular to the bedding.

Two plots are shown in Fig. 4.10 in which we can see that load versus time curves of plugs loaded parallel to the bedding planes, there are higher peaks than first break and a prominent post-failure behavior trend as compare to the plugs are loaded perpendicular to the bedding planes. It means parallel loaded plugs can bear higher load than the peak load at first break but their capacity of maximum load is quite lower as compare to plugs loaded perpendicular to the bedding planes. On other hand perpendicular loaded plugs after their first break at peak load they will never reaches the same level as first peak again and then there will be sudden drop in load but their time dependent load bearing capacity is a lot more than the other case. In terms of tensile strength, perpendicular loaded plugs have higher strength than the parallel loaded plugs (Bohloli B. et al., 2014).

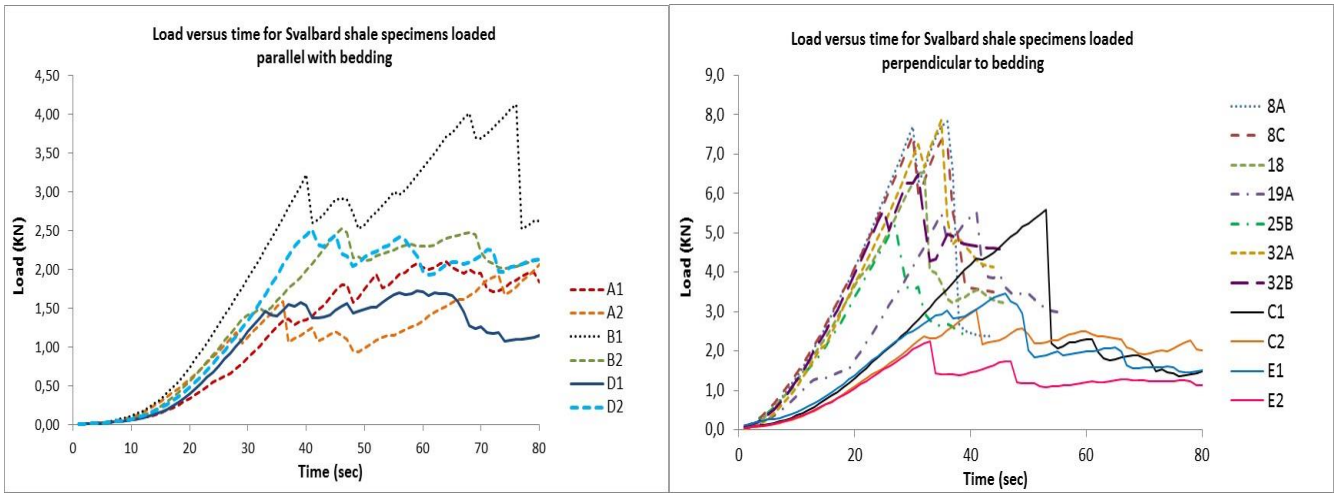

Fig. 4.10: Load-time plots of plugs loaded parallel (left side) and perpendicular (right side) to the bedding planes (data from Bohloli B. et al. (2014)).

Since mechanical failure of rock can be monitored by acoustic or microseismic measurements, the findings of this comparison may be useful to understand fracture propagation relative to bedding. If a fracture propagates perpendicular to bedding, it may produce one or two big acoustic events followed by much smaller events. If a fracture propagates parallel with bedding it may create a main event followed by several equally or slightly higher acoustic events.

Apart from all the factors which are analyzed and discussed before for tensile strength of a caprock on the basis of this study, there are many other important factors to be considered for

a better understanding. For instance, Hangx et al. (2010) has described that strength of caprock is affected by temperature and confining pressure, with rise in temperature can decreased the strength due to temperature driven chemical changes in the mineralogy of the rock and with increasing confining pressure will increase the strength and stability of the rock.

Another comparison is shown in Fig. 4.11, where we can see the previously calculated tensile strength at NGI for Svalbard shale and sandstone with calculated tensile strength for this study. Tensile strength of deeper rock samples is higher than shallower samples (tested plugs for this study are shallower and from bore hole Dh6). The reason for this difference is might because deeper buried rocks are more compacted and cemented (NGI, 2012).

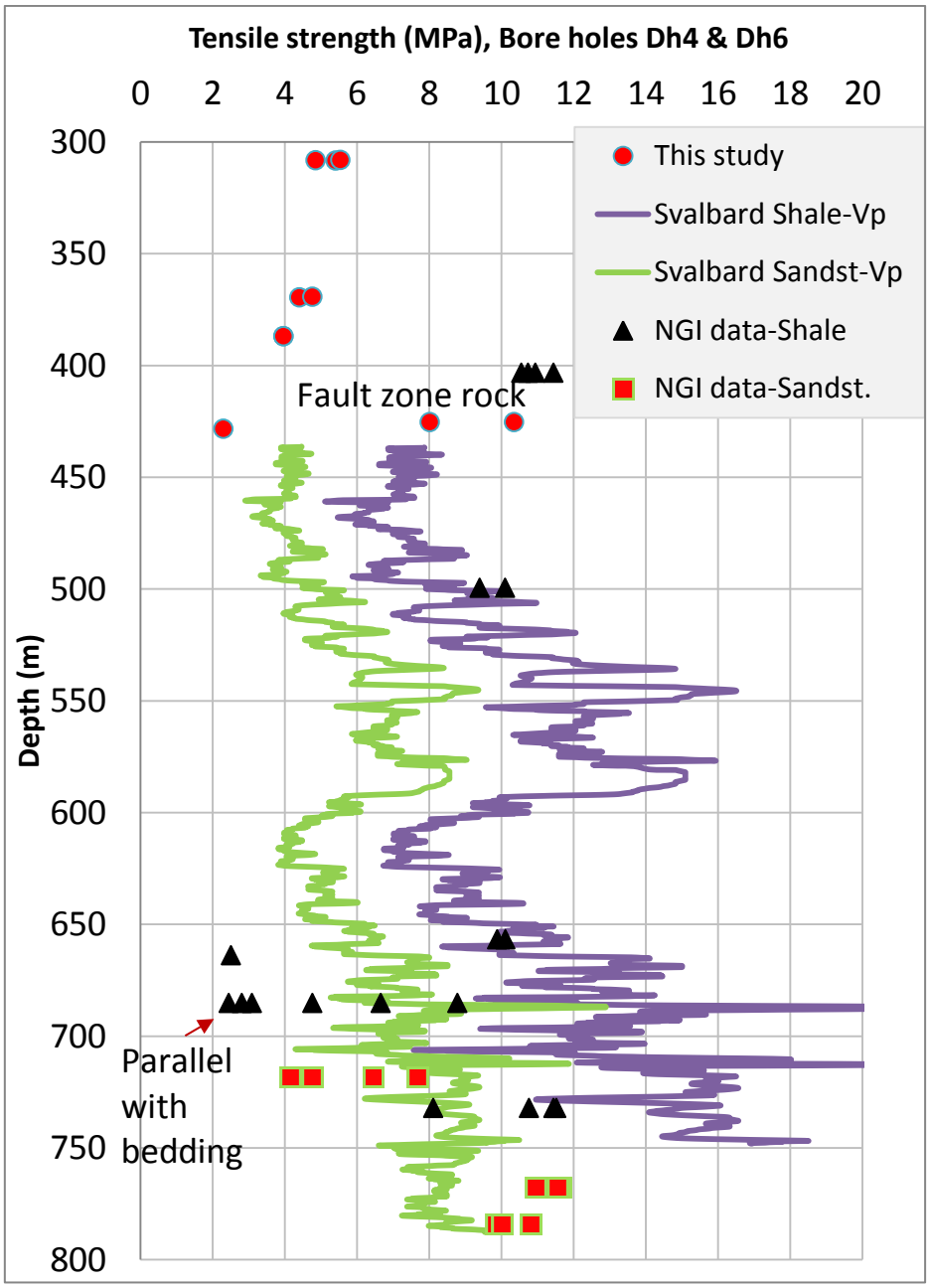

Fig. 4.11: Comparison of tensile strength of this study with previously measured data at NGI for different rocks from different depths (modified from NGI (2012))

Chapter 5: Uniaxial compressive strength and velocity analyses

This chapter focuses uniaxial compressive strength (UCS) test and velocity analysis. It is organized in two sections (results and discussion). The results section is further organized into UCS test and velocity analysis for Rurikfjellet and Agardhfjellet formations. All the measured and estimated outcomes of the research are presented in form of tables, plots and figures. The discussion part is based on interpretation of all the results in details and comparison with previous works.

5.1 Results

5.1.1 Uniaxial compressive strength test

Six plugs were prepared for UCS tests from five core samples with diameters of 28.5 to 40.5 mm and height of 60 to 82 mm. All the core samples are selected from well Dh6 (Longyearbyen CO2 storage lab, Svalbard) and from two geological formations; Rurikfjellet and Agardhfjellet with a depth range of 308.00-369.53 m and 425.28-428.28 m respectively. Explanation for plugs ID used: RFF (Rurikfjellet formation), AFF (Agardhfjellet formation)—plug number (original number of core sample)—UCS (Uniaxial Compressive Strength test). Results from uniaxial compressive strength tests and calculated parameters of entire set of plugs used in this study are listed in Table 5.1.

Table 5.1: Results of entire dataset from UCS test and parameters of plugs are listed.

FM	Depth, (m)	Plug ID	Diameter, D(mm)	Cross-sectional area, A(mm2)	Thickness, t(mm)	Density, ρ (g/cm3)	Load at failure, P(KN)	Axial Strain, ε_α	UCS, σ (MPa)	Young's Modulus E (GPa)	Time to break, (sec)
Rurikfjellet	308.00-308.26	RFF-8A-UCS	40.4	1281.25	82	2.61	67.85	05.79	52.93	11.41	634
	308.00-308.26	RFF-8B-UCS	40.5	1287.60	82	2.60	52.55	03.25	40.79	13.20	507
	369.21-369.35	RFF-18-UCS	40.4	1281.25	82	2.59	44.33	10.60	34.58	5.17	555
	369.41-369.53	RFF-19-UCS	40.4	1281.24	82	2.59	46.72	08.28	36.44	5.95	565
Agardhfjellet	425.28-425.43	AFF-32-UCS	28.5	637.62	60	2.85-3.15	55.73	03.59	87.37	44.34	474
	428.15-428.28	AFF-33-UCS	28.5	637.61	60	2.51	23.02	06.12	36.09	7.47	315

The overall ranges of peak loads, uniaxial compressive strength and axial strain are 23.02 to 67.85 KN, 34.58 to 87.37 MPa and 3.25 to 10.60 mS respectively for the entire set of tested plugs. The estimated densities of these plugs are in the normal range (2.51-2.61 g/cm3) for shale except for the plug AFF-32-UCS with density of 3.15 g/cm3. The failure of all the plugs is also with in a time limit (2-15 min) according to the ASTM standard for UCS test. For better understanding and to see the variations within the formation and then comparison with each other, these results are further categorized in term of two formations, Rurikfjellet and Agardhfjellet in the upcoming part.

5.1.1.1 Rurikfjellet formation

Four of the total plugs for UCS test are selected from Rurikfjellet formation from a depth range of 308.00 to 369.53 meters in well Dh-6. The diameter of these plugs is 40.4 to 40.5 mm and height is 82 mm as mentioned in Table 5.1. These samples are primarily dark shale (if we look at the fresh surface). Estimated densities for these plugs do not have any exceptional variations and just varies from 2.59 to 2.61 g/cm3. Uniaxial (unconfined) compressive strength varies from 34.58 to 52.93 MPa in this formation. A general overview of the formation is summarized in Table 5.2.

Table 5.2: A general overview of Rurikfjellet formation

Rurikfjellet Formation	
Observed lithology	Shale
Core sample source Well	Well Dh-6
Total number of tested plugs and dimensions	4 (Diameter: 40.4-40.5mm, height: 82 mm)
Range of density	2.59-2.61 g/cm^3
Calculated uniaxial (unconfined) compressive strength	34.58-52.93 MPa
Calculated axial strain	03.25-10.60
Young's Modulus	5.17-13.20 GPa

UCS strength is calculated from peak loads of the plugs as described in methodology under section 3.2.1.1 and shown in Fig. 3.16a. 1st breaks at peak loads are pointed by red arrows in Fig. 5.1. Load-time curves are plotted for entire set of tested plugs from Rurikfjellet Formation. As we can see load-time curves for plugs RFF-8A-UCS and RFF-8B-UCS are very similar in trend and overlapping each other. The noticeable difference they have is the time 627 and 508 seconds and peak loads 67.85 and 52.55 KN respectively. Both of these plugs are prepared from the same core sample 8. The peak load and unconfined compressive strength of the plug RFF-8A-UCS is highest amongst all the tested plugs from Rurikfjellet formation and 2nd highest in the entire set of tested plugs under uniaxial compressive strength test.

If we look at these load-time curves together, their overall trend is linear and very similar. Another noticeable observation is their grouping such as the load-time curves plugs RFF-8A-UCS and RFF-8b-UCS from same core sample are together and the other set of load-time curves for plugs RFF-18-UCS and RFF-19-UCS are also overlapping each other and they are in same group.

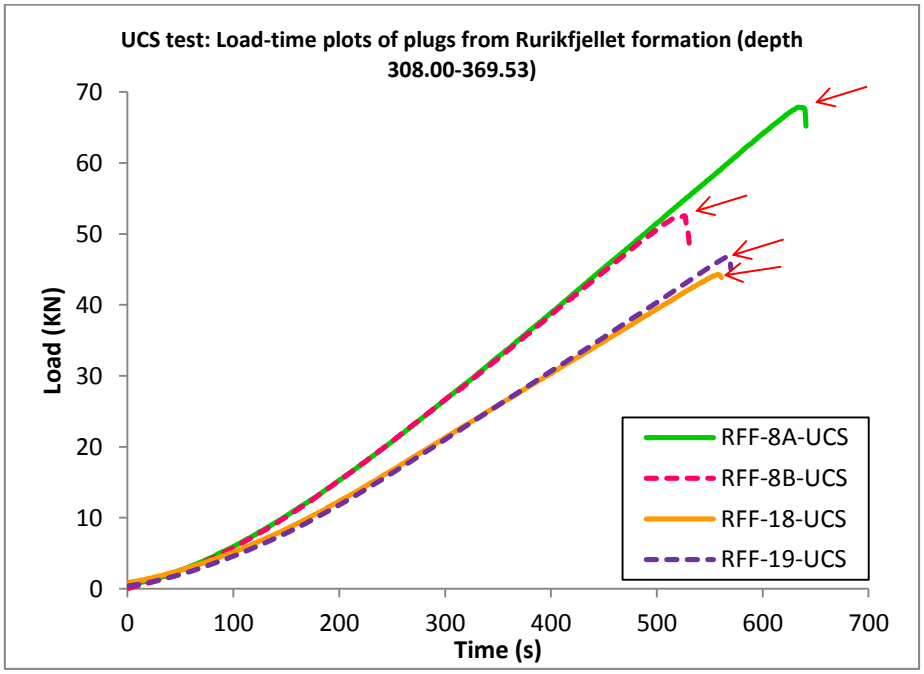

Fig. 5.1: Load-time plots of plugs from Rurikfjellet formation.

Stress versus axial strain is plotted for four tested plugs. The axial strain is calculated to follow the procedure that mentioned earlier in Chapter 3, Section 3.2.1.1. Stress-strain is also explained and labeled and shown in Fig. 3.16b. As we can see in Fig. 5.2 the overall trend of these curves for all four plugs is more likely linear and the shape of curves are showing mostly elastic deformation. The concave up parts of these curves represent the closing of pre-existing pores and microfractures in the samples (marked by red bars in the plot).

Stress-strain curve for RFF-8A-UCS shows very linear trend and we can claim that it is following an elastic deformation trend; also it is very steep curve with no plastic region and can be considered as brittle failure on the basis of the shape of the curve. Stress-strain plot of RFF-8B-UCS is different from rest of the curves. It has big elastic and a smaller plastic region, so we may consider it as brittle-ductile transition deformation. Both of the above mentioned plugs are from same core sample 8 and have quite similar behavior in closing of microfractures and pores and elastic deformation areas except that RFF-8A-UCS has plastic deformation area too.

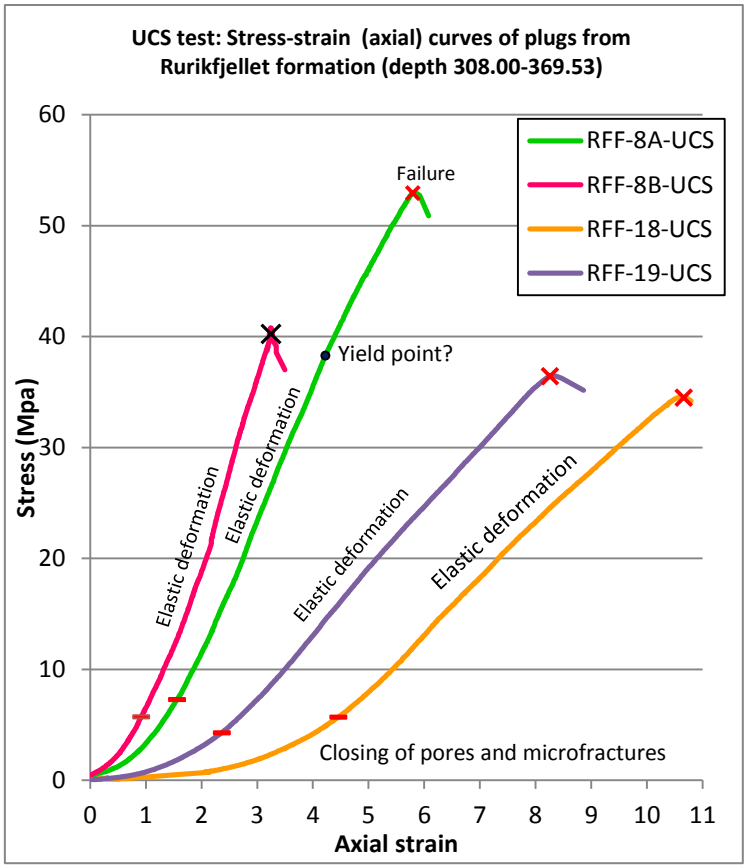

Fig. 5.2: Stress-axial strain plots of plugs from Rurikfjellet formation.

The trend of stress-strain curve of plug RFF-18-UCS is linear, less steep compare to 1st two curves in the plot and it also has quite big elastic deformation and the trend of the curve seems like brittle failure. Stress-strain plot of RFF-19-UCS is very similar to RFF-18-UCS with a bit more initial deformation

On the basis of stress and axial strain calculation (as plotted in stress-strain curves in Fig. 5.2), Young's modulus (*E*) is also estimated and presented in Table 5.1. It varies from 3.26 to 12.55 GPa in the Rurikfjellet formation and depth range from 308 to 369.53 m. E value (12.55 MPa) of plug RFF-8B-UCS is the highest in this formation and depth range and RFF-18-UCS has the lowest E value of 3.26 MPa.

5.1.1.2 Agardhfjellet formation

Only two plugs; AFF-32-UCS and AFF-33-UCS are tested for UCS test from Agardhfjellet formation that listed in Table 5.1. The dimensions of these plugs are the same; with diameter of 28.5 mm and the height or thickness is 60mm. The depth range for these samples varies from 425.28 to 428.28 m. The uniaxial (unconfined) strength varies from 36.09 to 87.37 MPa. The estimated values of Young's modulus for this formation at different depths vary from 7.47 to 44.34 MPa. Highlights of this formation based on this study are presented in Table 5.3.

Table 5.3: Highlights of Agardhfjellet formation

Agardhfjellet Formation	
Observed lithology	Shale
Core sample source Well	Well Dh-6
Total number of tested plugs and dimensions	2 (Diameter: 28.5mm, height: 60 mm)
Range of density	2.51-3.15 g/cm³
Calculated uniaxial (unconfined) compressive strength	36.09-87.37 MPa
Calculated axial strain	03.59-06.12
Young's Modulus	7.47-44.34 GPa

Load versus time curves are plotted for plugs AFF-32-UCS and AFF-32-UCS from Agardhfjellet formation, as shown in Fig. 5.3. The first breaks at peak load are indicated by red arrows. Overall trend of these plots is linear and somehow similar. Load-time curve of plug AFF-32-UCS is very linear in trend and there is a small deflection in the middle part (marked by black circle) and it can be an inner fracture produced while testing. This sample has the highest uniaxial unconfined strength amongst the entire set of tested plugs from both formations. The load-time has smaller concave up portion at initial stage and after approximately 9 KN load and 100 seconds, the trend become very linear and at peak load the 1st break is followed by sharp sudden drop.

Plug AFF-33-UCS has the lowest load bearing capacity (23.02 KN) in the whole set of plugs. Load-time curve of this plug has linear and less steep than AFF-32-UCS. At peak load the 1st break is followed by sharp and sudden drop. If we have an observation of the load-time curve of AFF-33-UCS at large size of plot area, there are also few points where we can see very minor deviations and it may be indication of inner fractures produced while compression the test before 1st break. There is no post-failure behaviour recorded in this plot.

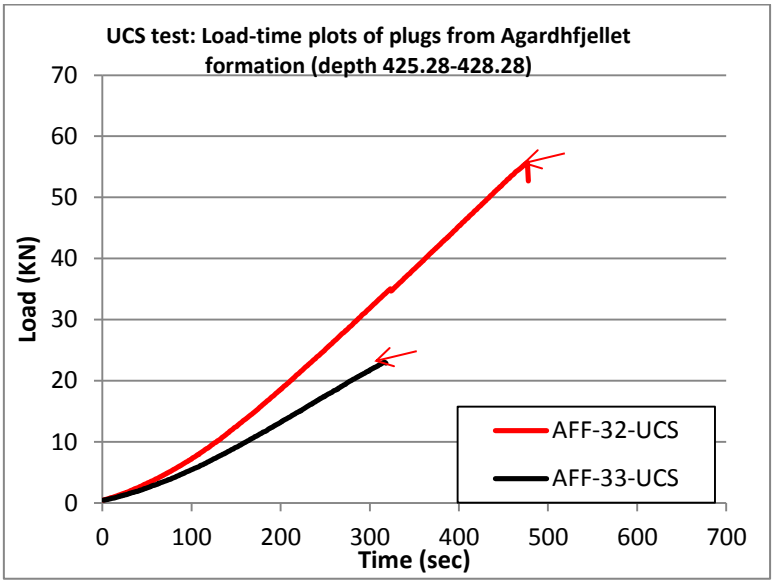

Fig. 5.3: Load-time plots of two plugs from Agardhfjellet formation (depth range 425.28-428.28m).

Stress and axial strain is calculated for the plugs from Agardhfjellet formation and calculation method is described in Chapter 3 under Section 3.2.1.1 (Fig. 3.16a). Stress-strain curves for the axial deformation of the plugs from this formation are plotted and shown in Fig. 5.4. As the first look at the trend of these curves, we can see that it is almost linear in most of the area of plot.

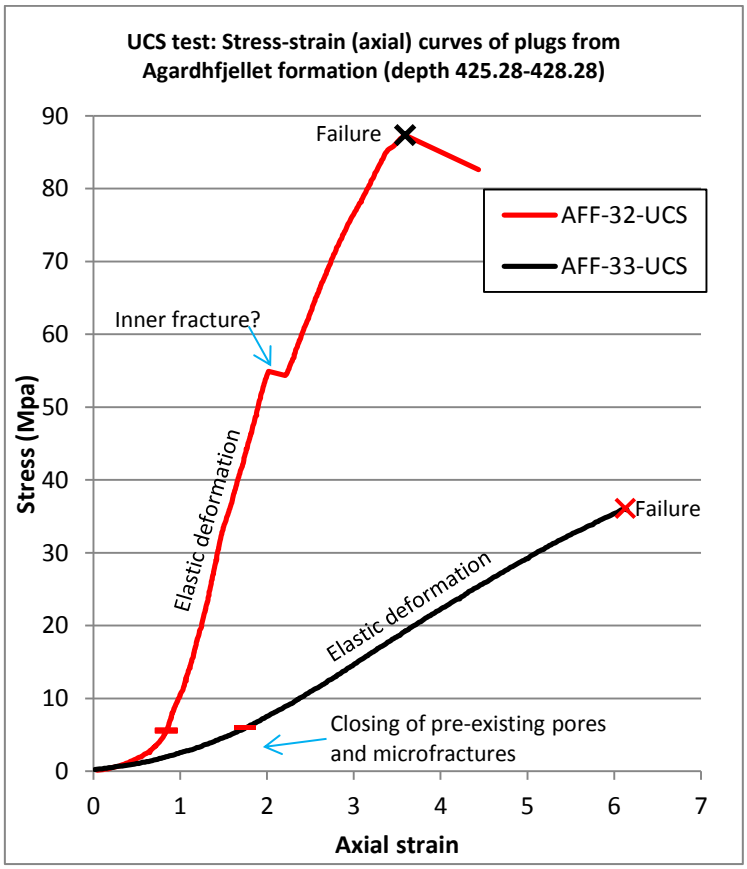

Fig. 5.4: Stress-strain (axial) curves of plugs from Agardhfjellet formation.

Stress-strain curve of plug AFF-32-UCS is showing linear trend and generally elastic deformation. But there is a sharp deviation in the curve in the upper middle part and then it becomes a bit less steep and a small bend like variation before failure point. Failure points in these curves are selected as 1st break at peak load.

Plug AFF-33-UCS has quite different trend and elastic behavior in the stress-strain curve than AFF-32-UCS. Pre-existing pores and microfractures closing part is larger than the other sample and after this closing part, its trend and deformation behavior becomes linear and elastic respectively until the failure point.

On the basis of these stress and axial strain calculations, Young's modulus (E) is also calculated (Table 5.1) for the tested plugs of Agardhfjellet formation from depth 425.28 to 428.28 m. The E values varies from 5.90 to 24.34 GPa and like other estimated parameters, the difference in E values is also enormous.

5.1.2 Velocity measurements

P- and S-wave velocities were measured for entire set of plugs from Rurikfjellet and Agardhfjellet formation during uniaxial compressive strength test and procedure is described in methodology section 3.2.1.1 (Fig. **3.19**). P- and S-wave velocities were recorded at different stress levels. The overall stress range for whole set is from 0.67 to 88.37 MPa and P- and S-wave velocities vary from 3300.65 to 5677.06 m/s and 1421.95-3686.10 m/s respectively as shown in Table 5.4.

Table 5.4: Summary of P- and S-wave velocity measurements

Formation	Depth (m)	Plug ID	Stress range (MPa)	Vp range (m/s)	Vs range (MPa)
Rurikfjellet	308.00-308.26	RFF-8A-UCS	2.53-52.93	3619.39-4119.10	2011.66-2063.20
	308.00-308.26	RFF-8B-UCS	6.92-40.70	4024.83-4120.75	2332.36-2303.84
	369.21-369.35	RFF-18-UCS	2.59-34.58	3300.65-3551.20	1507.92-1510.15
	369.41-369.53	RFF-19-UCS	0.58-36.23	3326.75-3658.66	1421.95-1567.51
Agardhfjellet	425.28-425.43	AFF-32-UCS	0.67-87.37	3930.51-5677.06	3686.10-4100.01
	428.15-428.28	AFF-33-UCS	9.22-36.00	3393.51-3628.82	1549.11-1625.55

These velocity measurements are divided into Rurikfjellet and Agardhfjellet formations and described in upcoming sections.

5.1.2.1 Rurikfjellet Formation

P- and S-wave velocities were measured at different stress levels for four plugs from this formation (depth range 308-369.53m). P- and S-wave velocities vary from 3300 to 4120.75 m/s and from 1421 to 2332.36 m/s respectively at various level of stresses (0.58 to 52.53 MPa) throughout the formation. This compressional and shear wave velocities are plotted versus stress to see the variations throughout the plug at different stress points as shown in Fig. 5.5.

As we can see in Fig. 5.5a, Vp versus stress plot for plug RFF-8A-UCS, there is prominent rise in the first part of the curve and then it becomes more stable with less variations in Vp compare to changing stress. The overall trend of curve for RFF-8B-UCS like a sinusoidal wave with many rises and falls in the compressional wave with changing stress and it is quite different from RFF-8A-UCS. Variations in plug RFF-18-UCS are not very sharp; the trend of the curve shows gentle rise and small variations. Plug RFF-19-UCS has very steep, almost vertical trend in curve up till 3600 m/s and within 0 to 5 MPa stress after that, it has smaller variation in Vp as compared to stress. Power line fits are also added for all curves and they matches quite good, so now we can have better idea to see Vp versus stress variations and overall trend of these plots.

Vs are plotted versus stress and shown in Fig. 5.5b. As we can see that overall trend of these curves is roughly flat with small variations. But Stress-Vs curve of RFF-19-UCS is slightly different from other plots; the curve is rising gradually and flattens out after some initial rise. The other common observation in all the curves is that the variations in their shear velocities

is in a range of 200 m/s, for example curve of RFF-8A-UCS is varying between 2200-2400 m/s interval in the plot.

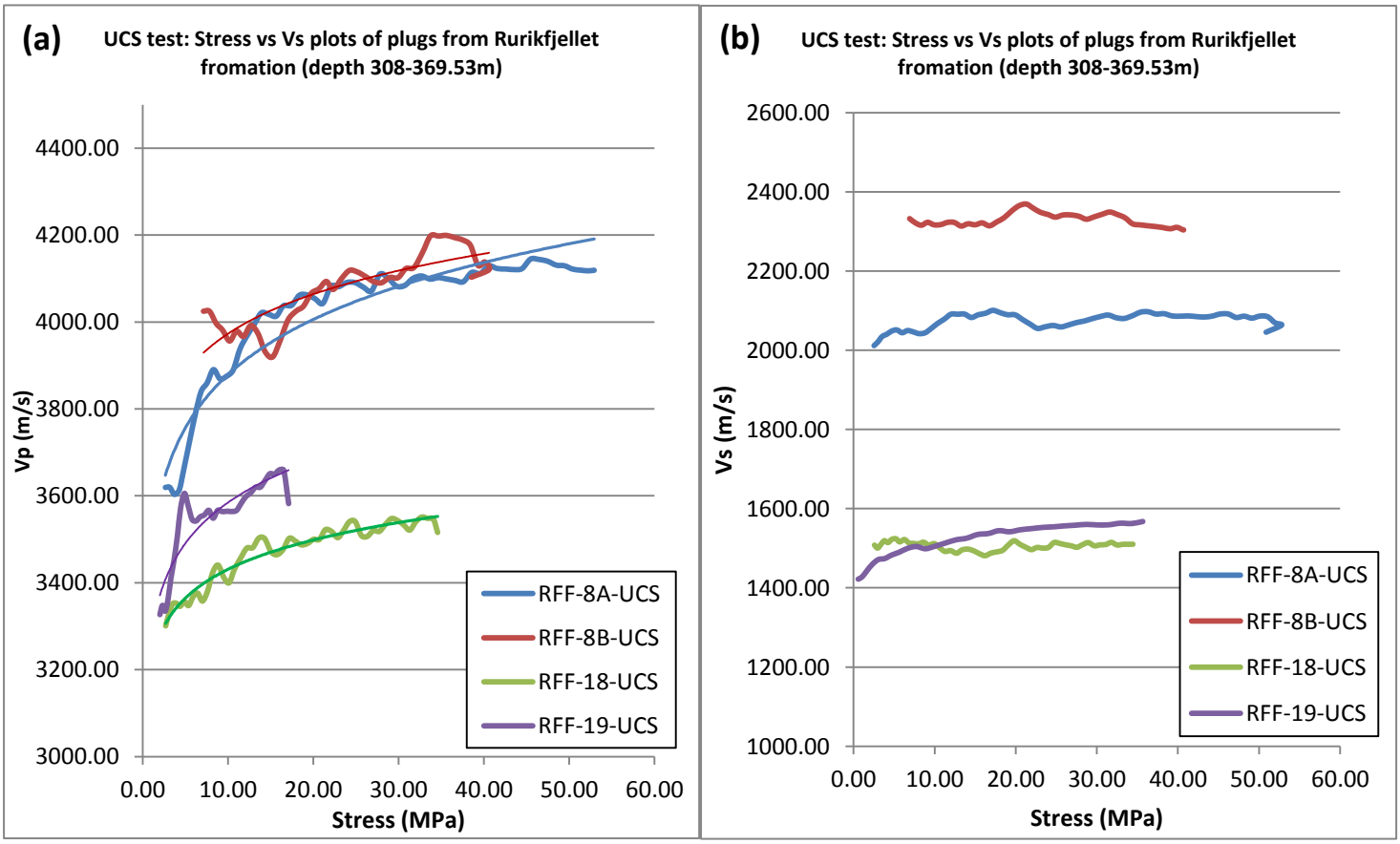

Fig. 5.5: Stress versus velocity: (a) stress versus Vp and (b) stress versus Vs of four plugs from Rurikfjellet formation (depth 308-369.53m).

5.1.2.2 Agardhfjellet Formation

Velocities of compressional and shear waves are measured for two plugs from Agardhfjellet formation as reported in Table 5.4. Compressional wave and shear wave velocities vary from 3393.51 to 5677.06 m/s and from 1549.11 to 3686.10 m/s respectively. The stress range for these velocity measurements is between 0.67 and 87.37 MPa.

Vp and Vs are plotted versus stress (Fig. 5.6). In Fig. 5.6a, compressional wave velocities versus stress for AFF-32-UCS and AFF-33-UCS are shown, curves of these plugs are very different in terms of trend and variations. Plot for plug AFF-32-UCS has very sudden rise and steep trend till point (stress 9.93 MPa, Vp 5166 m/s) and then it is becoming more flattened with few high and sharp peaks followed by a little steeper drop in the curve. Plug AFF-33-UCS has a gradually rising and flattening out trend with very small variations.

Shear wave velocity versus stress plots are shown in Fig. 5.6b. General trend of curves for AFF-32-UCS and AFF-33-UCS is roughly flat. Trend of AFF-32-UCS is quite different from the other sample AFF-33-UCS, it is rising in linear fashion and then the middle part is flattening out followed a slightly dropping at last portion.

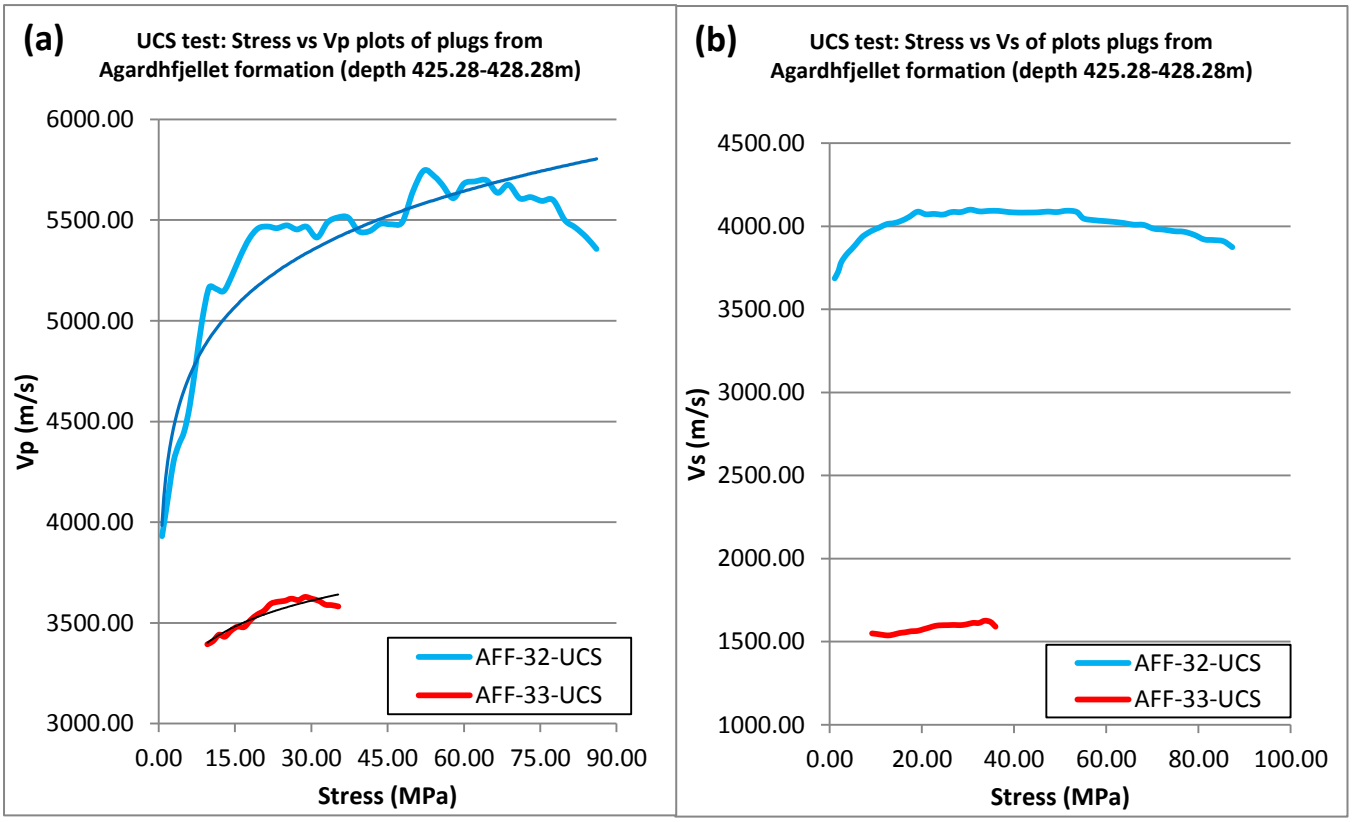

Fig. 5.6: Velocity versus stress: (a) Vp versus stress and (b) Vs versus stress plots of plugs from Agardhfjellet formation (depth 425.28-428.28m). Decrease of velocities at very high stresses may be related to initiation of fractures inside the sample.

5.2 Discussion

Here we present detail interpretation of our results from uniaxial (unconfined) compressive strength test. This part is divided into six sub headings; Pre- and post-test analysis of tested plugs, Load-time plots and featured UCS strength based analysis, UCS and density versus depth profile, Stress versus axial strain and Young's modulus analysis, Velocity analysis, Comparison with previous work and Importance of UCS test based findings to evaluate integrity of cap rock.

5.2.1 Pre- and post-test analysis

Images of pre- and post-test plugs based on uniaxial compressive strength test are summarized in tables 5.5 and 5.6 for visual analysis of fractures. Complete summary of results for entire set of seven tested plugs from two formations Rurikfjellet and Agardhfjellet is also shown in Table 5.1.

Four of the tested plugs from Rurikfjellet formation are shown in Table 5.5 for pre- and post-test comparison. Plugs RFF-8A-UCS, RFF-18-UCS and RFF-18-UCS are showing normal failure (shear failure) if we look at their fractures pattern. Two of plugs from core sample 8 are resulted into highest UCS strength for this formation because of the homogeneous material and no visible or prominent pre-existing defects. Plugs RFF-18 and 19 have quite similar but comparatively lower UCS strength in this formation. Possible reason could be pre-existing defect and in-homogeneity of the material; especially we look at the scattered fracture pattern of RFF-19-UCS.

Table 5.5: Visual summary of pre- and post-test plugs from Rurikfjellet formation.

Plug ID	UCS (MPa)	Brief description	Pre-test	Post-test
RFF-8A-UCS	52.93	A sound specimen with no pre-existing defects resulted into higher strength. Main fracture's pattern shows clear shear failure and there are small adjacent fractures in the middle and lower part of the plug.		
RFF-8B-UCS	40.79	Homogenous specimen with no visible defects. Failure does not show clear shear fractures. Upper and middle part is more fractured with some major and minor visible fractures.		
RFF-18-UCS	34.58	Inhomogeneous specimen with some visible filled fractures in the upper middle part and resulted into lower strength compared to other specimen from the same core. Failure shows a very clear shear pattern in the main fracture.		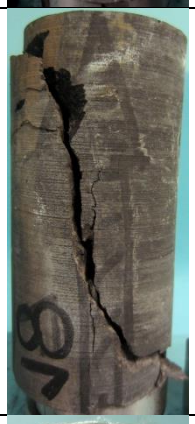
RFF-19-UCS	36.44	Inhomogeneous specimen with visible pre-existing fracture and small piece is missing in the middle part marked by red circle. Resulted into quite low strength comparatively. Failure shows somehow shear fractures with some other big and small fractures.		

Two of tested plugs from Agardhfjellet formation are summarized in Table 5.6. Plug AFF-32-UCS resulted into very high UCS strength because it is belonged to detachment zone that is subjected to high compaction and cementation as discussed in the geological evolution and stratigraphy sections in Chapter 2. Also filled fracture with mineral vein is visible (see image of core sample in Table 3.2) and its failure shows a clear curve shaped fracture. AFF-33-UCS failed in different pattern as we can see the propagation of fractures is prominent mostly in middle and lower parts and UCS strength is comparatively low. The reasons could be inhomogeneity and pre-existing defects such as weak beddings as we have observed in its core sample 33 (see image in Table 3.2).

Table 5.6: Visual summary of pre- and post-test images of plugs from Agardhfjellet formation.

Plug ID	UCS (MPa)	Brief description	Pre-test	Post-test
AFF-32-UCS	87.37	In-homogeneous with pre-existing filled fracture that is visible in the lower part but specimen showed highest UCS strength. Failure caused prominent curved fracture and is splitting further into few more fractures. Overall fracture trend shows somehow shear failure.		
AFF-33-UCS	36.09	In-homogenous weak specimen but there is no visible pre-existing defects. Failure caused various fractures mostly in middle and lower parts. UCS strength is comparatively very weak.		

5.2.2 Load-time plots and featured UCS strength based analysis

Further analysis has been done by plotting load-time curves for all the tested plugs from Rurikfjellet (Fig. 5.1) and Agardhfjellet (Fig. 5.3) formations. These plots show the time dependent load bearing capacity of the tested plugs and the estimated UCS strength is function of their peak loads. This section is divided into two subsections as follow:

5.2.2.1 Rurikfjellet formation

The plug RFF-8A-UCS has the highest time dependent load bearing capacity and UCS strength because it was a good and intact plug as described in previous section (Table 5.5), also it has above average density (2.61 g/cm3). If we look at the SEM analysis that was done

on a thin section from this sample as described in chapter 3 under section 3.3.3 (see Fig. 3.4, Fig. 3.5) where we can see that there are not many microfractures, porosity is just 3% and it has 4.5% heavy minerals. All these factors are good enough to describe this plug as strong and it can bear higher UCS strength as compare to other plugs from this formation. Plug RFF-8B-UCS has the same trend of time dependent loading plot as RFF-8A-UCS because both of these plugs are prepared from same core sample 8 but it has lower values for load and UCS strength than RFF-8A-UCS. Possible reason could be inner pre-existing fractures or defects though density and mineralogy is very similar.

Plugs RFF-18-UCS and RFF-19-UCS have very similar trend and time dependent load capacity though they are not from same core sample but their densities are quite similar. Comparatively they have lower load and UCS strength than the other plugs from this formation. Possible reason could be pre-existing defects and microfractures e.g. there is visible pre-existing fracture in RFF-19-UCS (see pre-test image in Table 5.5). There is evidence of pre-existing microfractures in plug RFF-18-UCS if we look at the SEM analysis that has been done on a thin section from this plug (see Fig. 3.6 and 3.7) and estimated porosity from SEM is 4.2% and 6.1%.

There is no post-failure behavior (like we have noticed in Brazilian test discussed in the previous chapter) in any of the load-time curve of these all tested plugs. After they reach the maximum capacity there is a sudden drop in the load. The possible reason is the dimension of the plug for UCS test as compare the disc shaped plugs used for Brazilian test.

5.2.2.2 Agardhfjellet formation

Plugs AFF-32-UCS and AFF-33-UCS are tested from this formation and the load-times are shown in Fig. 5.3. Plug AFF-32-UCS shows very linear behaviour and highest value in the time dependent loading capacity and there is also a deviation in the trend that would be caused by activation of an inner fracture or may be opening of filled fracture (as observed in core sample in Table 3.2). Also it resulted into strongest UCS strength (87.37 MPa) in the whole set of tested plugs. The reason of strong behaviour can be justified by looking at its exceptional density value (3.15 g/cm^3 and its too high for a shale specimen) due to highest content of Siderite (80.19% analysed by XRD). If we look at the SEM analysis that is done on a thin section from AFF-32-UCS, higher content of Siderite is clearly identified and even at 600 to 40 µm scale there are no microfractures spotted in it (see Fig. 3.8). By performing SEM area measurements we found out that it has very low porosity about 0.8% (Fig. 3.9). Another good reason of this strong behaviour can be greater compaction, cementation and mineral filled fractures because the depth where this core sample belong to a detachment zone (see Fig. 2.7 in stratigraphy section).

Plug AFF-33-UCS shows quite linear trend but it's time dependent load bearing capacity is almost half compare to AFF-32-UCS. As we know both of these plugs are from same formation and the difference between their depths is just 3m but the difference between their density, peak load and UCS strength is very high. The bulk mineralogy estimated from XRD is quite different (see Table 3.5). The possible reason can be weakness plane along bedding as we have observed in its core sample inventory (see image in Table 3.2) and it also belong to the detachment zone, so this portion of Agardhfjellet formation might be newly fractured and haven't been experienced any cementation.

5.2.3 UCS and density versus depth profile

To see the depth dependent variation in the density and UCS strength for the Rurikfjellet and Agardhfjellet formations UCS and density versus depth profile is constructed (Fig. 5.7).Depth dependant variations in density and UCS strength are different in Rurikfjellet formation than Agardhfjellet formation. We can see that density is quite similar and UCS strength is not that stable, it decreasing and also increasing at some points with depth throughout the tested depth of Rurikfjellet formation. Possible reasons could be composition of shale material is quite same if we look at the bulk mineralogy analysis of all the tested plugs from this formation (see Table 3.5) and there are not such evidences of alterations of material due to faulting or filled fractures with heavy minerals as we have noticed in Agardhfjellet formation.

In Agardhfjellet formations variations in density and UCS strength are very sharp. For instance in the upper part density and UCS strength are significantly high and then in the lower part it is totally opposite (decreasing with increasing depth throughout the tested depth). Possible reasons for these variations are; compaction due to detachment zone and fractures filled with heavy minerals such as Siderite as we have discussed earlier.

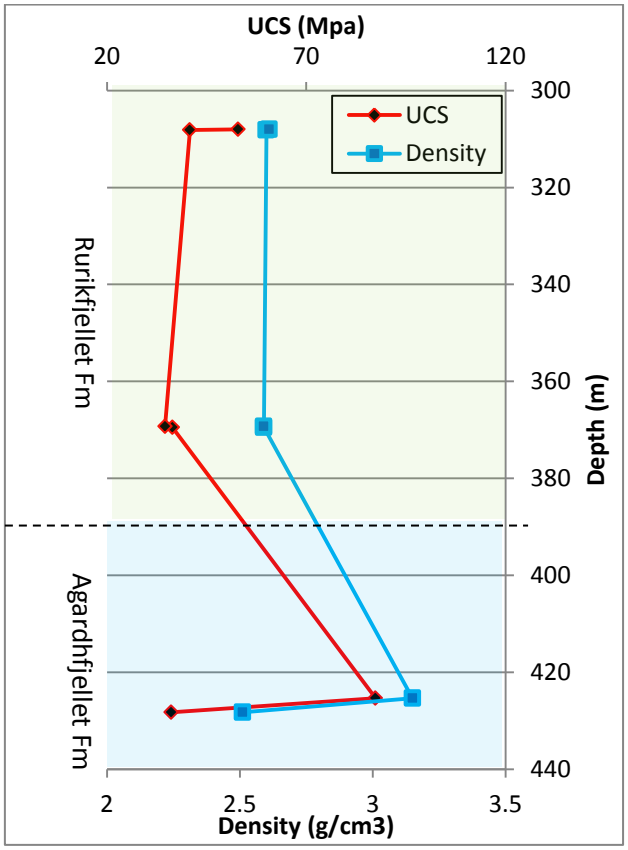

Fig. 5.7: UCS and density versus depth profiles for whole tested plugs from both formations (depth 308-428.28m).

5.2.4 Stress versus axial strain and Young's modulus (E) analysis

Stress-(axial) strain curves are plotted for Rurikfjellet and Agardhfjellet formations to see the deformation behavior and failure type of the materials when it undergoes uniaxial compressive stress. Also Young's modulus is calculated by taking the ratio of stress and axial strain (see Table 5.1).

Deformation behavior of tested materials from Rurikfjellet formation is shown in Fig. 5.2, where we can see that all the plugs have deformed elastically. If we analyze the trend of these curves till the failure point, plug RFF-8B-UCS is showing brittle failure with a high value of E (12.55 MPa) means it is a mechanically stiff material. RFF-8A-UCS is showing transitional behavior between brittle and ductile because there is some plastically deformed part in the curve and E value for this plug is also quite high. Plugs RFF-18-UCS and RFF-19-UCS are deform super elastically as there axial strain deformation is more as compare to the relevant stress values and their E values are lower as compare to the other plugs from this formation.

Stress-strain curves for Agardhfjellet formation are shown in Fig. 5.4, where we can see that deformation behavior of AFF-32-UCS is elastic and it failed in very brittle way. The E value of this plug is 24.34 MPa that is highest in the entire set from both formation just like its exceptionally high density and UCS strength values, so very high E value is another evidence of this plug for being very strong mechanically. Plug AFF-33-UCS shows weak elastic deformation and failure is more likely brittle but its E value is very low comparatively. Reasons for the deformation behavior and failure modes for these plugs from this formation are same as described before in the last section of UCS and density versus depth comparison.

5.2.5 Velocity analysis

P- and S-waves are measured during UCS test for each plug from Rurikfjellet and Agardhfjellet formation as shown in Table 5.4. Further these velocities are plotted versus stress to see the variations as shown in Fig. 5.5 and Fig. 5.6 for Rurikfjellet and Agardhfjellet formations respectively. Observations from these plots show that Vp is increasing more than Vs with increasing stress. The possible answer can be given by comparing the elastic parameters and density based formulas of Vp and Vs as shown in equations Equ. 5. 1and Equ. 5. 2 respectively (Gelius and Johansen, 2010). As we can see that Vp is a function of bulk, K, (pressure/stress dependent) and shear modulus, μ, and Vs is only function of shear modulus, μ. While density, ρ, is common parameter in both Vp and Vs. So on the basis of these statements we can say that Vp will increase more than Vs for a rock sample when it is subjected to stress and that's why in our results as we have observed a higher variations in Vp than Vs with changing compressive strength while testing.

$$\boldsymbol{V_p} = \sqrt{\frac{\boldsymbol{K+4/3\mu}}{\boldsymbol{\rho}}} \qquad \text{Equ. 5. 1}$$

$$\mathbf{V_s} = \sqrt{\frac{\mu}{\rho}} \qquad \text{Equ. 5. 2}$$

Where Vp is P-wave velocity, Vs is s-wave velocity, K is bulk modulus, μ is shear modulus and ρ is density.

The main purpose of velocity analysis for these tested plugs from both formations is to re-assure or cross check the UCS strength or axial stress. As we can see from the empirical relationship of Vp with UCS and Young's modulus (E) described by Horsrud (2001) in Equ. 5. 3 and Equ. 5. 4.

$$\mathbf{UCS = 0.77 \cdot Vp^{2.93}} \qquad \text{Equ. 5. 3}$$

$$\mathbf{E = 0.076 \cdot Vp^{3.23}} \qquad \text{Equ. 5. 4}$$

According to these equations, UCS and E are directly proportional to Vp that means P-wave velocity will change by changing stress/UCS and E. Also Sheraz et al. (2014) has stated that sonic velocities have a direct relationship with the strength of material. So from P-wave velocity versus UCS plots we can see the first breaks in the plugs when P-wave velocity will suddenly drop. Also P-wave velocities are indication of strength and stiffness (E) such as higher the P-wave velocity means higher strength and E and vice versa of the rock same as in our case (Holt et al., 1997).

UCS strength and Young's modulus are plotted versus P-wave velocity to see the correlation between them as shown in Fig. 5.8. We can clearly see that Vp has very linear relationship with UCS and E.

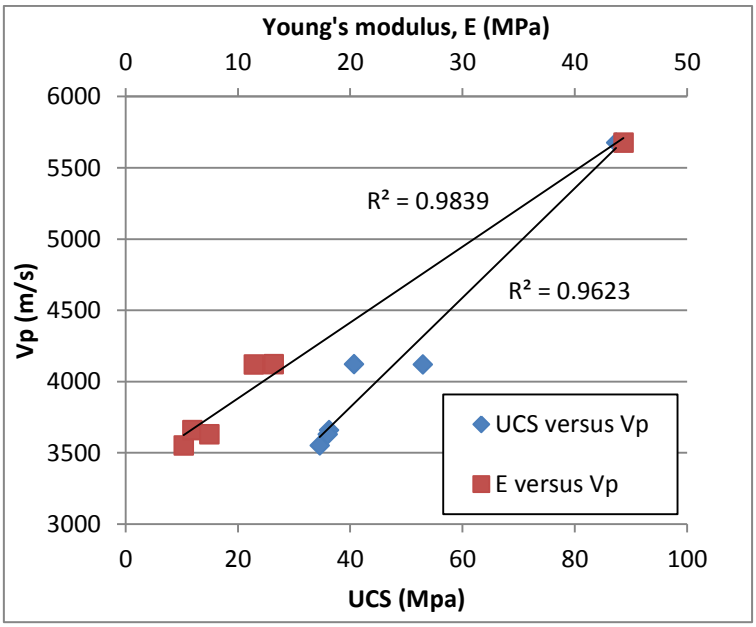

Fig. 5.8: UCS and E versus P-wave velocity of entire set of tested plugs from Rurikfjellet and Agardhfjellet formations.

5.2.6 Comparison with previous work

Recently done geomechanical study (material is from well Dh-4) for UNIS CO2 Lab at NGI are used to compare the results of UCS test from Rurikfjellet and Agardhfjellet formations for this study and plotted in Fig. 5.9. As we can see in these plots that there are not many tested samples from depth range 300-450 m for uniaxial compressive strength test. Only one plug was tested from this depth range and calculated UCS value from this study is matched reasonably well with previous work done at NGI (2014). Similar behavior is also observed for young's modulus-depth relationship.

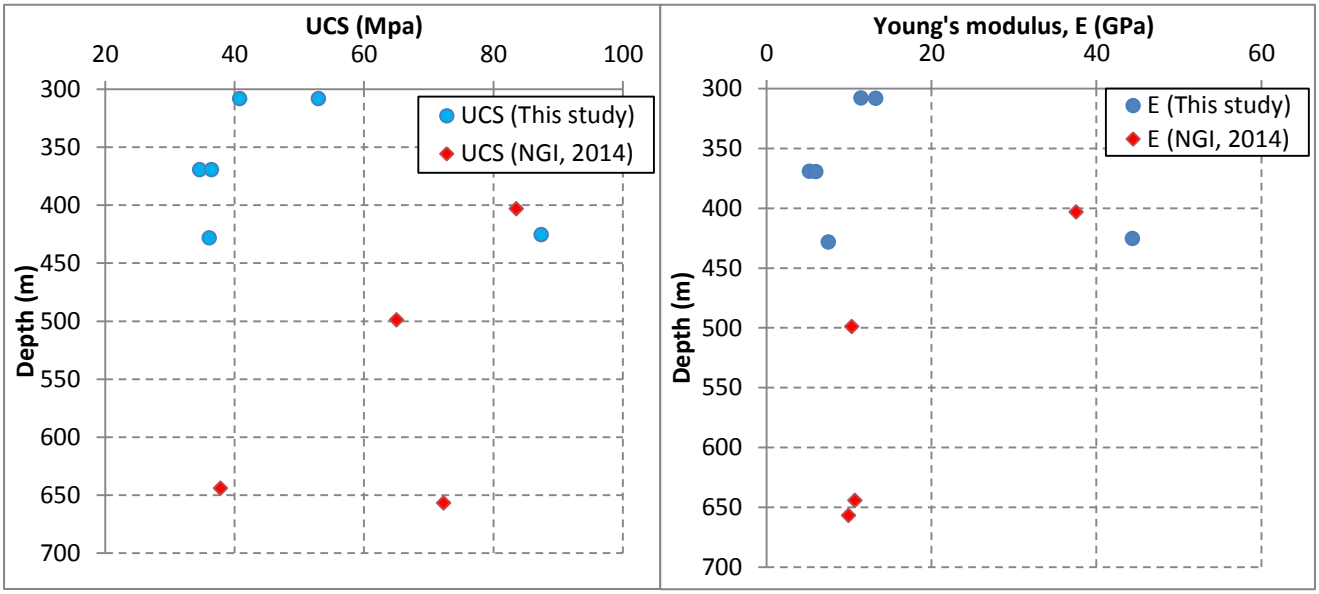

Fig. 5.9: Comparison of UCS and Young's modulus of this study with previous work at NGI is shown.

Furthermore the data acquired in this study from LYB CO2 storage caprock can be compared with previously tested data from the Hekkingen formation, Barents Sea (a nice analogue of Agardhfjellet formation, Svalbard). This formation is well known caprock for different prospects in the Barents Sea. Core samples from a well in Nordkapp basin targeting Hekkingen formation were tested for Geomechanical program at NGI during early 1990 to evaluate the cap rock (NGI, 2012). Mechanical testing for this program is also partly reported by Makurat et al. (1992) Gabrielsen and Kløvjan (1997) and they described that shale from Hekkingen formation is less compacted and cemented due to shallower depth that is subjected to less uplift as compare to shale from Agardhfjellet (Bohloli B. et al., 2014).

Also calculated UCS (MPa) and Young's modulus (GPa) from this study are plotted with previously done comparison by NGI (2012) with an empirical model of Horsrud (2001) for UCS. As we can see in Fig. 5.10 (UCS comparison) and Fig. 5.11 (Young's modulus comparison) that calculated UCS and Young's modulus (GPa) from this study are fitted quite well. If we look at the overall trend of these plots then we can see that UCS and Young's modulus are higher in the deeper depth than shallower depth. Possible reason could be more compaction in rocks in deeper depth (Bohloli B. et al., 2014; NGI, 2012).

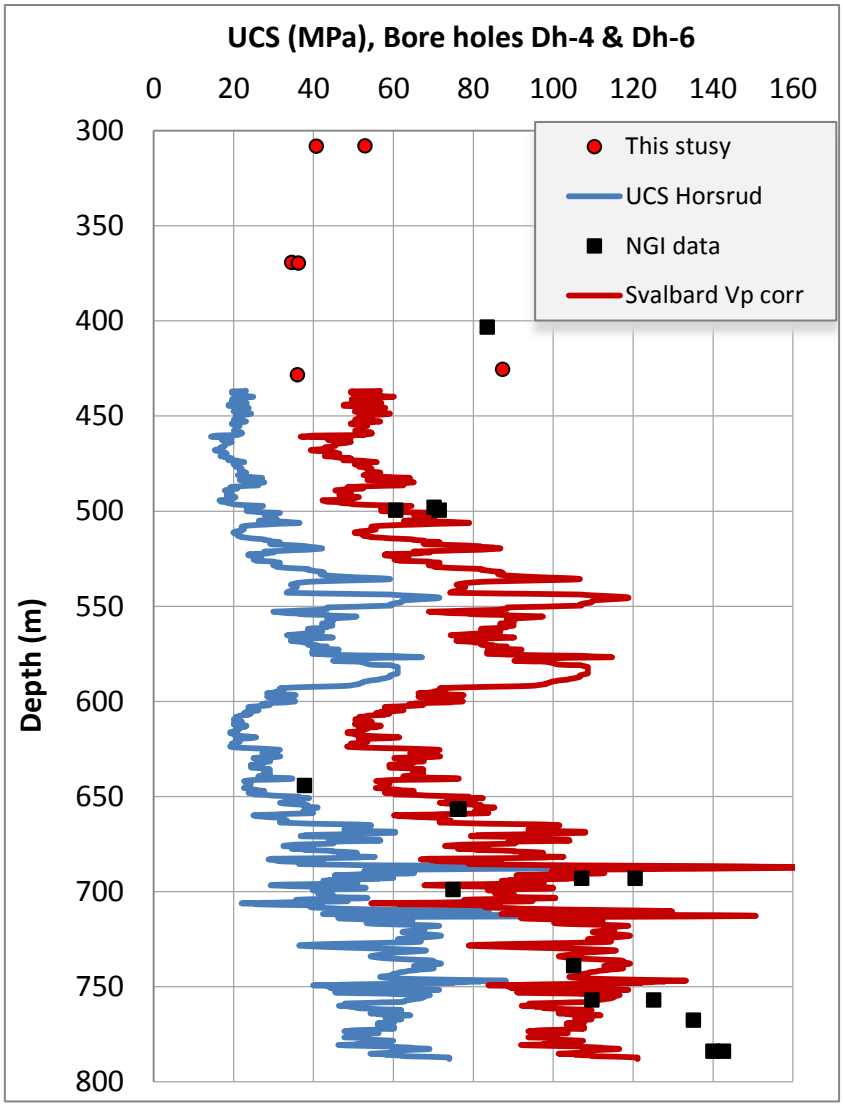

Fig. 5.10: Comparison of UCS of this study with previously made UCS versus depth correlation profile by(NGI, 2012).

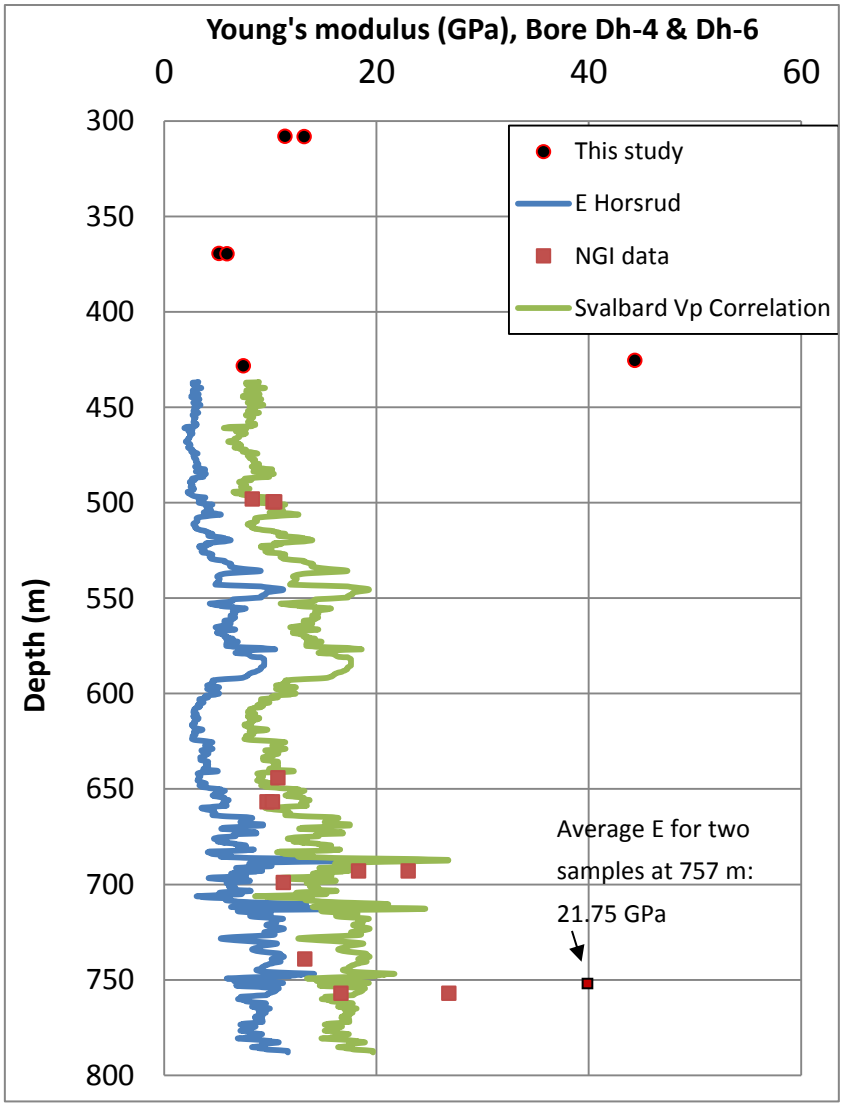

Fig. 5.11: A comparison of calculated Young's modulus of this study with a previously made Young's modulus versus depth profile by (NGI, 2012).

Chapter 6: Summary and conclusions

This chapter presents summary and conclusions of the entire work that has been done for evaluating strength properties of caprock of the Longyearbyen CO_2 Storage Pilot (Svalbard) based on mechanical testing and mineralogical characterization of Rurikfjjellet and Agardhfjellet formations.

6.1 Summary

This study is a small part of ongoing research for CO_2 sequestration at Longyearbyen CO_2 Storage Lab, Svalbard, Norway. The primary aim of this study is to determine geomechanical properties of two important caprock units to assess the integrity of sealing for safe and successful CO_2 storage in the future. Core materials for this study are provided by UNIS CO_2 Lab that previously collected and stored by the Norwegian Geotechnical Institute (NGI). Results from this study are compared with previous work performed by NGI in 2010, 2012 and 2014.

Six core samples were selected from well Dh-6 targeting cap rock unit of Longyearbyen CO_2 storage lab, consists mainly of two geological formations; Rurikfjellet and Agardhfjellet in depth range 308.00-428.28 m. All the samples were well preserved in paraffin sealing and kept in the controlled temperature room at NGI. Samples were unsealed and inspected for any pre-existing defects e.g. fractures or any damage. These cores were cut to make plugs according to the ASTM standard for Brazilian and UCS tests. The diameter and thickness of disc shaped plugs for Brazilian test are 40-40.5mm and 19-21mm respectively. The diameters and heights of cylindrical plugs for UCS tests are 40.4 and 28 mm and 82 and 60 mm respectively. Two geomechanical laboratory tests; Brazilian and Uniaxial compressive strength tests were performed on the prepared plugs to determine tensile and uniaxial compressive strength respectively.

A detailed study of tensile strength was executed on a set of ten disc shaped plugs from two different geological units; Rurikfjellet and Agardhfjellet formations at certain depth ranges 308.00 to 386.89 m and 425.28 to 428.28 m respectively. Before performing laboratory tests on these plugs, density was measured and also a detailed analysis of bulk mineralogy and mineral identification plus micro-structure (only three thin section were made) study was carried out using X-ray diffraction (XRD) and scanning electron microscopy (SEM) respectively. All these plugs were loaded perpendicular to the bedding planes and that is why the calculated strength was called vertical tensile strength. Almost all the plugs were failed in expected time according to ISRM standard and the pattern of produced fractures after the test is also as expected. Variations based on tensile strength are higher in Agardhfjellet formation (2.29-10.35 MPa) as compared to Rurikfjellet formation (3.96-5.53 MPa). Estimation of tensile strength for a cap rock can be very important aspect, especially when it is subjected to a fluid injection into a subsurface reservoir. The information of tensile strength can be used to avoid hydraulic fracturing caused by fluid injection, also fracture propagation and its nature can be determined.

Uniaxial compressive strength test is also performed on a set of six plugs. Four of the plugs were tested from Rurikfjellet Formation (depth range 308.00 to 369.53 m) and two plugs were

tested from Agardhfjellet Formation (depth range 425.28 to 428.28 m). Most of the tested plugs were failed within the time frame mentioned in ASTM standards for UCS test and few of the plugs show very clear shear failure. Mainly geomechanical parameters [uniaxial compressive strength (σ), Young's modulus (E) for axial deformation] and P- and S-wave velocities are measured from this test. Variations of these all three measurements are analyzed within each formation and also compared with each other. Agardhfjellet Formation has highest values in these measurements as compared to Rurikfjellet Formation. Index test from UCS can be utilized to estimate overburden pressure of rocks and behavior of material when it is subjected to compression in uniaxial directions. Furthermore this data can be used for various modelling of the caprock/seal evaluation.

Finally results from Brazilian and uniaxial compressive strength test are compared with previous work performed at NGI. The previous work of NGI was done on core samples from wells Dh-2, Dh-4 and Dh-6 from different formations, also including Rurikfjellet and Agardhfjellet formations at different depths. Results from this study from similar depth are matching with previous results. The overall rock strengths (UCS and tensile strength) are higher at deeper intervals. Reasons can be the compaction, cementation, etc.

For more accurate and better understandings of caprock integrity to ensure safe CO_2 storage, further research is required than this study. For instance, more core samples should be tested from Agardhfjellet formation because in this study only two were tested and both are very different in all reported parameters. Therefore, evaluation of an entire formation would not be appropriate on the basis of few tested samples. Fracture analysis could be done for both macro and micro levels but it was not considered here due to limited data sources, laboratory facilities and time constraint, though it is highly recommended and can be very useful for the leakage risk assessment in the caprock.

6.2 Conclusions

Based on assessment of caprock integrity by utilizing two standard geomechanical testing programs the following conclusions are made from this study:

- Calculated vertical tensile strength values for both formations are very different. The tensile strength values throughout the Rurikfjellet formation have relatively less difference but overall these values have decreased gradually with increasing depth. Agardhfjellet formation has extreme nature of vertical tensile strength values such as reported highest values and lowest values belong to this formation in the entire set of tested data under Brazilian test.

- The intermediate values of Uniaxial (unconfined) Compressive Strength are reported throughout the caprock intervals except the upper part of Rurikfjellet formation where a high UCS is observed. The upper part of Agardhfjellet formation has exceptionally high strength. Overall UCS values of two tested caprocks decreased with increasing depth except one depth range at 425.28-425.43 m.

- Mechanical stiffness of the cap rock material is defined by Young's modulus and it has similar trend in variations like other geomechanical parameters (UCS and vertical tensile strength mentioned earlier).

- Calculated P-wave velocities for all the plugs from both formation has greater variations with changing pressure (Stress, MPa) than S-waves velocities which are almost constant and shows flat trend in their plot versus depth.

- Measured densities for the upper part of caprock (Rurikfjellet formation) are above average according to the density range for a shale rock and have fewer variations throughout the whole unit. Lower unit (Agardhfjellet formation) that is in direct contact with the CO_2 storage reservoir has very high density values at certain depths and also lowest values in the entire tested depth. Overall there are no such variations observed in density except for Agardhfjellet formation at depth range 425.28-425.43 m and it is because of high content of heavy minerals.

- Mineralogy of the samples is quite similar with small variations in mineral type and percentage except one core sample from Agardhfjellet formation that contains 81% Siderite.

References

Anell, I., Braathen, A., and Olaussen, S., 2014, The Triassic-Early Jurassic of the northern Barents Shelf: a regional understanding of the Longyearbyen CO2 reservoir: NORWEGIAN JOURNAL OF GEOLOGY, v. 94, no. 2-3, p. 83-98.

Bælum, K., Johansen, T. A., Johnsen, H., Rød, K., Ruud, B. O., and Braathen, A., 2012, Subsurface structures of the Longyearbyen CO2 Lab study area in

Central Spitsbergen (Arctic Norway), as mapped by reflection seismic data: Norwegian Journal of Geology, v. 92.

Birch, F., 1961, The velocity of compressional waves in rocks to 10 kilobars: 2: Journal of Geophysical Research, v. 66, no. 7, p. 2199-2224.

Bohloli B., Skutveit E., Grande L., Titlestad, G. O., Børresen M.H., J. Ø., and A., B., 2014, Evaluation of reservoir and cap-rock integrity for the Longyearbyen CO2 storage pilot based on laboratory experiments and injection tests: Norwegian Journal of Geology v. 94, p. 171-187.

Braathen, A., Bælum, K., Christiansen, H. H., Dahl, T., Eiken, O., Elvebakk, H., Hansen, F., Hanssen, T. H., Jochmann, M., and Johansen, T. A., 2012a, The Longyearbyen CO 2 Lab of Svalbard, Norway—initial assessment of the geological conditions for CO 2 sequestration: Norwegian Journal of Geology/Norsk Geologisk Forening, v. 92, no. 4.

Braathen, A., and Bergh, S. G., 1995, Kinematics of Tertiary deformation in the basement-involved fold-thrust complex, western Nordenskiöld Land, Svalbard: tectonic implications based on fault-slip data analysis: Tectonophysics, v. 249, no. 1, p. 1-29.

Braathen, A., Hansen, F. S., Noormets, R., Ogata, K., Olaussen, S., Rønneberg, R., Sand, G., Aker, E., Elvebakk, H., and Johansen, H., 2012b, The Longyearbyen CO.

Bresciani, E., Barata, T. d. J. E., Fagundes, T. C., Adachi, A., Terrin, M. M., and Navarro, M. F. d. L., 2004, Compressive and diametral tensile strength of glass ionomer cements: Journal of applied oral science, v. 12, no. 4, p. 344-348.

Dallmann, W., 1999, Lithostratigraphic Lexicon of Svalbard: Upper Paleozoic to Quaternary Bedrock. Review and Recommendation for Nomenclature Use, Norwegian Polar Institute, Tromsø.

Dallmann, W. K., 2007, Geology of Svalbard: Geology of the land and sea areas of northern Europe. Norges Geologiske Undersøkelse Special Publication, v. 10, p. 87Á89.

Dimakis, P., Braathen, B. I., Faleide, J. I., Elverhøi, A., and Gudlaugsson, S. T., 1998, Cenozoic erosion and the preglacial uplift of the Svalbard–Barents Sea region: Tectonophysics, v. 300, no. 1, p. 311-327.

Eldholm, O., Faleide, J. I., and Myhre, A. M., 1987, Continent-ocean transition at the western Barents Sea/Svalbard continental margin: Geology, v. 15, no. 12, p. 1118-1122.

Faleide, J. I., Solheim, A., Fiedler, A., Hjelstuen, B. O., Andersen, E. S., and Vanneste, K., 1996, Late Cenozoic evolution of the western Barents Sea-Svalbard continental margin: Global and Planetary Change, v. 12, no. 1, p. 53-74.

Gabrielsen, R., and Kløvjan, O., 1997, Late Jurassic—early Cretaceous caprocks of the southwestern Barents Sea: fracture systems and rock mechanical properties: Norwegian Petroleum Society Special Publications, v. 7, p. 73-89.

Gelius, L.-J., and Johansen, T. A., 2010, Petroleum geophysics: Bergen, Unigeo.

Hangx, S. J., Spiers, C. J., and Peach, C. J., 2010, Mechanical behavior of anhydrite caprock and implications for CO2 sealing capacity: Journal of Geophysical Research: Solid Earth (1978–2012), v. 115, no. B7.

Harland, W., and Wright, N., 1979, Alternative hypothesis for the pre-Carboniferous evolution of Svalbard: Norsk Polarinstitutt Skrifter, v. 167, p. 89-117.

Helland-Hansen, W., 2010, Facies and stacking patterns of shelf-deltas within the Palaeogene Battfjellet Formation, Nordenskiöld Land, Svalbard: implications for subsurface reservoir prediction: Sedimentology, v. 57, no. 1, p. 190-208.

Holt, R., Furre, A.-K., and Horsrud, P., 1997, Stress dependent wave velocities in sedimentary rock cores: Why and why not?: International Journal of Rock Mechanics and Mining Sciences, v. 34, no. 3, p. 128. e121-128. e112.

Horsrud, P., 2001, Estimating mechanical properties of shale from empirical correlations: SPE Drilling & Completion, v. 16, no. 02, p. 68-73.

ISRM, Ulusay, R., and Hudson, J. A., 2007, The complete ISRM suggested methods for rock characterization, testing and monitoring: 1974-2006, International Society for Rock Mechanics, Commission on Testing Methods.

Larssen, G., Elvebakk, G., Henriksen, L. B., Kristensen, S., Nilsson, I., Samuelsberg, T., Svånå, T., Stemmerik, L., and Worsley, D., 2002, Upper Palaeozoic lithostratigraphy of the Southern Norwegian Barents Sea: Norwegian Petroleum Directorate Bulletin, v. 9, p. 76.

Lin, W., 1983, Mechanical Properties of Mesaverde Sandstone and Shale at High Pressure, p. 37.

Makurat, A., Torudbakken, B., Monsen, K., and Rawlings, C., Cenezoic uplift and caprock seal in the Barents Sea: fracture modelling and seal risk evaluation, *in* Proceedings SPE Annual Technical Conference and Exhibition1992, Society of Petroleum Engineers.

NGI, 2010, Mechanical Testing of material from Dh4, Longyearbyen CO2 Lab.: Report No. 20081351-00-19-R. 36 p.

NGI, 2012, Geomechanical characterization of the cap rock shale in the LYB CO2 pilot based on core and log data in Dh1, Dh2 and Dh4 wells: Report No. 20081351-00-25-R. 53 p.

NGI, 2014, Geomechanical study for UNIS CO2 LAB: Rock Mechanical testing program.: Report No. 20120649-02-R. 33 p.

Nøttvedt, A., Livbjerg, F., Midbøe, P., and Rasmussen, E., 1993, Hydrocarbon potential of the central Spitsbergen basin: Arctic Geology and Petroleum Potential, v. 2, p. 333-361.

Ogata, K., Senger, K., Braathen, A., Tveranger, J., and Olaussen, S., Natural Fractures in a Tight Reservoir for Potential CO2 Storage (Spitsbergen, Svalbard)-Preliminary Results from Cores, *in* Proceedings 1st EAGE Sustainable Earth Sciences (SES) Conference and Exhibition2011.

Ogata, K., Senger, K., Braathen, A., Tveranger, J., and Olaussen, S., 2014a, Fracture systems and meso-scale structural patterns in the siliciclastic Mesozoic reservoir-caprock succession of the Longyearbyen CO2 Lab project: implications for geologic CO2 sequestration on Central Spitsbergen, Svalbard: Norwegian Journal of Geology, v. 94, no. 2-3, p. 121-154.

Ogata, K., Senger, K., Braathen, A., Tveranger, J., and Olaussen, S., 2014b, The importance of natural fractures in a tight reservoir for potential CO2 storage: a case study of the upper Triassic–middle Jurassic Kapp Toscana Group (Spitsbergen, Arctic Norway): Geological Society, London, Special Publications, v. 374, no. 1, p. 395-415.

Sand, G., Braathen, A., and Olaussen, S., 2014, Longyearbyen CO2 Lab-tales of research and education: NORWEGIAN JOURNAL OF GEOLOGY, v. 94, no. 2-3, p. 77-82.

Senger, K., Planke, S., Polteau, S., Ogata, K., and Svensen, H., 2014, Sill emplacement and contact metamorphism in a siliciclastic reservoir on Svalbard, Arctic Norway: NORWEGIAN JOURNAL OF GEOLOGY, v. 94, no. 2-3, p. 155-169.

Sheraz, A., Emad, M., Shahzad, M., and Arshad, S., 2014, RELATION BETWEEN UNIAXIAL COMPRESSIVE STRENGTH, POINT LOAD INDEX AND SONIC WAVE VELOCITY FOR DOLERITE: Pakistan Journal of Science, v. 66, no. 1.

Steel, R., 1985, The Tertiary strike-slip basins and orogenic belt of Spitsbergen: Society of Economic Paleontologists and Mineralogists, v. 37, p. 339-360.

Stemmerik, L., and Worsley, D., 1995, Permian history of the Barents Shelf area, The Permian of Northern Pangea, Springer, p. 81-97.

Throndsen, T., 1982, VITRINITE REFLECTANCE STUDIES OF COALS AND DISPERSED ORGANIC MATTER IN TERTIARY DEPOSITS IN THE ADVENT-DALEN AREA, SVALBARD: Polar Research, v. 1982, no. 2, p. 77-91.

UiO Natrual history museum, 2015, Lithostratigraphic Lexicon of Svalbard *in* DALLMANN, W. K., Birkenmajer, K., Dypvik, H., Gee, D., Gjelberg, J., Harland, W. B., Heintz, N., Hjelle, A., Keilen, H., Krasil'ščikov, A. A., Mørk, A., Nagy, J., Nøttvedt, A., Ohta, Y., Pčelina, T. M., Steel, R., and Worsley, D., eds., Volume 2015.

Worsley, D., 2008, The post-Caledonian development of Svalbard and the western Barents Sea: Polar Research, v. 27, no. 3, p. 298-317.

Appendix I (Extended abstract)

Extended abstract submitted and accepted in 77th EAGE Conference & Exhibition 2015, Madrid, Spain.

TITLE
Brazilian tensile strength test: post-failure behavior of Jurassic and Cretaceous shales from Svalbard

AUTHORS
Mohsin Abbas[1], Bahman Bohloli[2], Elin Skurtveit[2], Nazmul Hague Mondol[1, 2], Lars Grande[2]
[1]University of Oslo, Department of Geosciences
[2] Norwegian Geotechnical Institute (NGI),

ABSTRACT
This study presents results of indirect tensile tests on cap rock shale samples from Svalbard CO2 storage pilot. It elaborates on tensile strength and the relationship between loading direction and post-failure behaviour of cap rock shale samples. Several test plugs were sampled from Jurassic and Creataceous Age cores of borehole Dh2, Dh4 and Dh6 from depth range of about 400 to 700 m. Samples were tested both parallel and perpendicular to bedding plane. Result of the tests showed that cap rock shale samples subjected to the Brazilian test in different directions relative to bedding planes differs not only in terms of the peak strength but also in the shape of the post-failure curve. The cap rock shale loaded perpendicular to bedding has higher strength and those loaded parallel with bedding show lower strengths. Samples loaded perpendicular to bedding bear load up to a maximum peak followed by a large drop and never reaches the maximum peak load again. For samples loaded parallel with bedding a maximum load is reached at failure followed by sudden drop, but load can increase to the same or higher level than the initial failure stress.

Introduction

Mechanical anisotropy, deformation behaviour and post-failure behaviour of cap rock shales are of paramount importance in various engineering problems such as subsurface excavations, petroleum production and CO2 storage (Hudson and Harrison 1997, Tutlouglu et al. 2015). Strength anisotropy, pre-failure and post-failure behaviours of rock can be determined using laboratory tests such as the Brazilian tensile strength test. A disc-shaped specimen is subjected to compression across the diameter, which results in a tensile stress field inside the specimen, and leads to failure of specimen in tension. Deformation of test specimen can be studied in detail and be related to loading direction and failure processes.

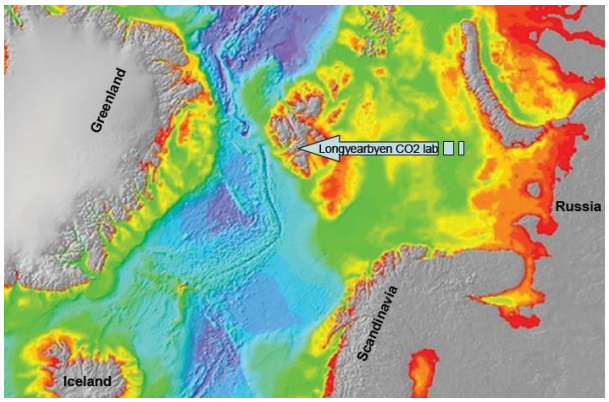

Figure 1 *Location of the study area, Longyearbyen CO2 Lab, 78 degrees North.*

Mechanical characterisation of cap rock shales from three bore holes (Dh2, Dh4 and Dh6) from the Longyearbyen CO_2 Lab (Braathen et al. 2012) (Fig. 1) has been presented in Bohloli et al. (2015), where the main focus was the strength values rather than failure behaviour of the shale samples. The current research extends beyond tensile strength anisotropy and focuses on the relationship between loading direction and post-failure behaviour of cap rock shale samples loaded in different directions relative to bedding plane. Several test plugs were sampled from cores of borehole Dh2, Dh4 and Dh6 from depth range of about 400 to 700 m (see Table 1 for details). They cover three geological formations; Rurikfjellet, Agardfjellet and Knorringfjellet of Jurassic and Creataceous Age.

Methodology

We use the Brazilian tensile strength test, also known as indirect tensile strength test, to determine tensile strength of cap rock shales and measure their deformation properties (e.g. pre- and post failure). Brazilian test is one of the widely used methods in engineering practice to determine the tensile strength of rocks indirectly. A disc-shaped specimen is loaded diametrically by two steel jaws that cover an arc of contact of approximately 10º at failure (ISRM, 2007) as shown in Fig. 2. Height of specimens is in most samples close to radius of specimen according to ISRM recommendation. Details on specimen dimensions are given in Table 1. One layer of masking tape was wrapped around the specimens. Load is applied continuously at a constant rate such that failure is reached typically within 30 seconds. Axial load versus time is recorded and plotted for tested specimens.

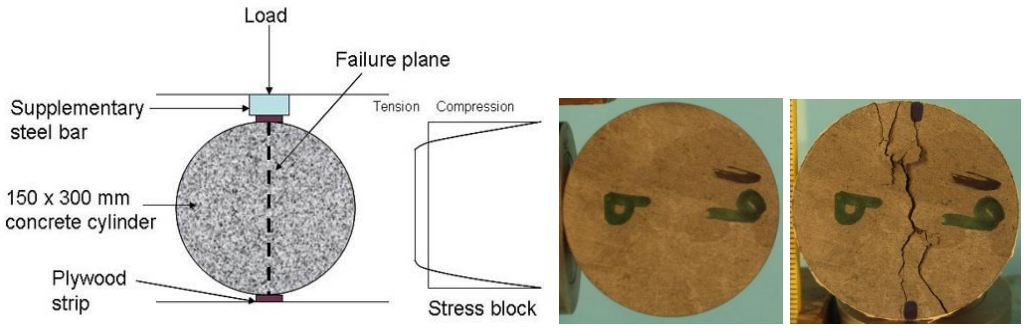

Figure 2 *Left: schematic illustration of Brazilian test (Courtesy of the Concrete Portal, 2015) and right: photograph of a shale sample 19b before and after testing.*

The tensile strength σ_t (MPa) is calculated using the following equation:

$$\sigma_t = \frac{0.636 \cdot P}{D \cdot t}$$

where P is the axial load at failure (N), D is the diameter of the specimen (mm) and t is the thickness of the specimen (mm).

Results and Discussion

Tensile strength of cap rock shale samples

Tensile strength of Rurikfjellet samples of Cretaceous Age from the depth of 308 through 425 m varies between 4.05 and 10.71 MPa perpendicular to bedding. Samples 32A and 32B from depth of 425 m show significantly higher tensile strength than the others. These samples have a high density of 2.85 g/cm^3 and might be related to a fault zone, well known in the well logs. Strong cementation associated with the fault rocks are suggested as the explanation for the higher strengths (see Bohloli et al. 2015). No sample parallel to bedding is available from Rurikfjellet formation. From Knorringfjellet and Agardfjellet formations specimens of Jurassic Age were tested both parallel and perpendicular to the bedding planes. Comparison of test results shows that tensile strength parallel to bedding is lower than that of perpendicular to bedding.

Table 1: *Specifications and tensile strength of cap rock shale samples from Rurikfjellet, Agardhfjellet and Knorringfjellet formations of bore holes Dh2, Dh4 and Dh6.*

Depth (m)	*Sample ID*	*Diameter D (mm)*	*Thickness t (mm)*	*Density g/cm3*	*Tensile strength σ_t (MPa)*	*Load direction*
308	8A	40.4	21	2.58	5.76	Perpendicular to bedding
308	8C	40.4	21	2.58	5.60	
369	18	40.4	21	2.60	4.94	
369	19A	40.3	19	2.54	4.57	
386	25B	40.0	20	2.60	4.05	
425	32A	28.5	15	2.85	10.71	
425	32B	28.5	15	2.85	8.33	
685	C1	25.25	12.49	2.64	4.35	
685	C2	25.19	12.59	2.64	2.38	
699	E1	25.26	12.14	2.39	3.02	
699	E2	25.26	09.13	2.56	2.24	
685	A1	25.10	12.35	2.65	2.80	Parallel with bedding
685	A2	25.14	12.30	2.58	2.44	
685	B1	25.12	12.29	2.58	6.65	
685	B2	25.16	12.33	2.63	3.08	
699	D1	25.26	12.59	2.57	2.94	
699	D2	25.21	12.56	2.28	5.06	

Post-failure behavior of cap rock shale samples

A typical failure curve shows a stress increase up to a peak load where specimen cracks and load sharply drops to a relatively low level (Tutluoglu et al., 2015). We observed that post-failure behavior of the samples loaded parallel to bedding is different from those loaded perpendicular to bedding. For the first group, it shows a first peak load (failure load) followed by a small load drop and several subsequent peak loads. These secondary and tertiary peaks can reach or even exceed the first peak load (Fig. 3). This indicates that after the first cracking, failure develops and the sample can bear loads that are significantly larger than the first

failure load. This behavior is observed for all samples loaded parallel to bedding irrespective of their strength (Fig. 3).

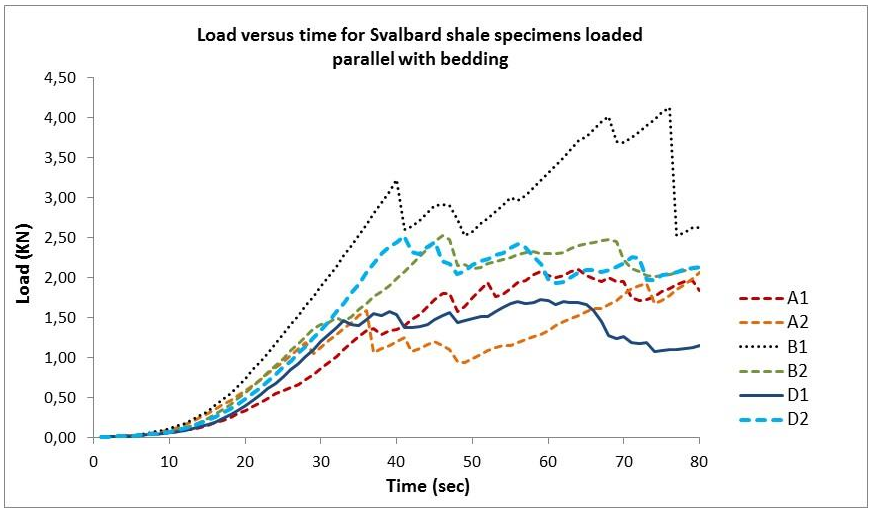

Figure 3 *Load versus time for shale samples loaded parallel with bedding plane. Sample B1 (black-dashed line) reaches the first peak load and fails at around 40 seconds. Further failure development results in peak loads that are higher than the failure peak. A similar trend is also observed for other samples where post-failure peaks are almost as big as the failure peak.*

Specimens loaded perpendicular to bedding plane show almost a typical failure curve throughout the loading time. First, a peak load is reached which indicates cracking of the specimen. Then a sharp load drop is observed (Fig. 4). For some specimens, e.g. 8A and 8C, two peak loads are registered but after these peaks of almost the same magnitude, load decreases significantly and no recovery of load versus time is registered. This shows that first failure/crack in such specimens requires a large load but development of subsequent fractures requires much less stress. Thus, cap rock shale samples tested in the laboratory by the Brazilian tests method that fail perpendicular to bedding plane can't bear large loads in the post-failure region.

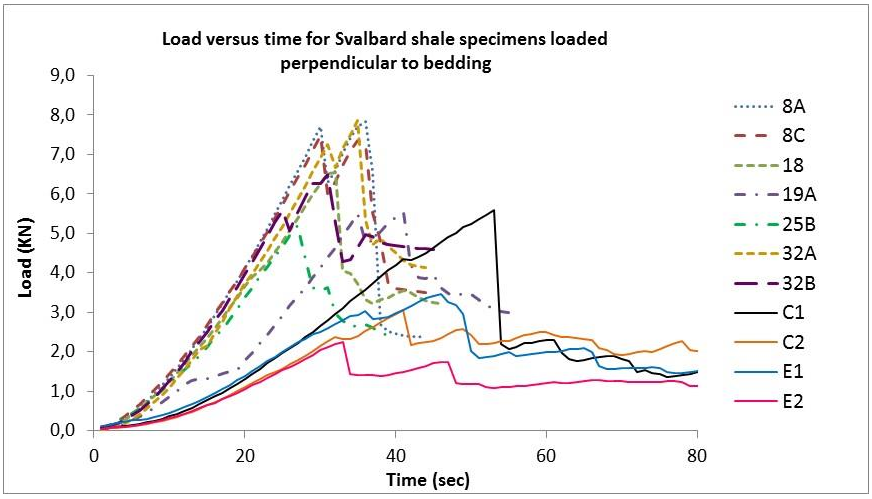

Figure 4 *Load versus time for shale samples loaded perpendicular to bedding plane. Failure of samples is indicated by the first peak load followed by a sudden drop. After the drop, sample bear some loads but never reaches the same level as the failure peak.*

From our experiments it can be stated that the post-failure behavior of cap rock shale specimens tested is dependent on loading direction. This observation implies that samples that fails parallel to bedding plane can bear relatively large load/stress in the post-failure region. On the other hand, samples that fail perpendicular to bedding plane have higher strength but bear quite small loads in the post-failure region.

Post-failure behavior of rocks may be monitored by acoustic/microseismic measurements. Each failure, indicated by a peak load followed by sudden stress drop, makes an acoustic event. This happens in the post-failure region too. Assuming a shale loaded parallel to bedding plane and similar to the Brazilian testing conditions, it may create a first acoustic emission then followed by several events. The magnitude of post-failure events may exceed that of the first acoustic event. In contrary, if a shale fails perpendicular to bedding, it may produce a major acoustic emission (or two) followed by much smaller events. This can be a potential application of post-failure data for microseismic monitoring. However, it has not been validated in the laboratory yet and requires further investigation.

Conclusions

Shale samples subjected to the indirect tensile test in different directions relative to bedding differs not only in terms of the peak strength but also in the shape of the post-failure curve. This study shows that cap rock shale specimens from Svalbard CO2 storage site loaded perpendicular to bedding have higher strength and those loaded parallel with bedding show lower strengths, as is well known from previous studies due to general anisotropic behaviour of shales. However, for samples loaded perpendicular to bedding, they bear load up to a maximum peak followed by large drop, which never reaches the maximum peak again in time domain. For samples loaded parallel with bedding, on the other hand, a maximum load is reached at failure followed by sudden drop which can increase to the same or higher level than the initial failure stress. This information from laboratory can be of importance also for seismic monitoring in field, although, in-situ boundary conditions might affect the post peak behavior compared to tests performed in the laboratory.

Acknowledgements

This work was financed by Research Council of Norway, Total E&P Norway, RWE DEA, SUCCESS, University of Bergen and University of Oslo through PROTECT (Protection of Caprock Integrity for Large-Scale CO2 Storage) project. Authors acknowledge UNIS CO2 Lab for access to core material.

References

Bohloli B., Skutveit E., Grande L., Titlestad, G.O., Børresen M.H., Johnsen Ø., Braathen A., 2015. Evaluation of reservoir and cap-rock integrity for the Longyearbyen CO2 storage pilot based on laboratory experiments and injection tests. Norwegian Journal of Geology 94, p. 171-187.

Braathen A., Balum K., Christiansen H., Dahl T., Eiken O., Elvebakk H., Hansen F., Hanssen T., Jochmann M. & Johansen T. 2012. The Longyearbyen CO2 Lab of Svalbard, Norway−initial assessment of the geological conditions for CO2 sequestration. Norwegian Journal of Geology 92, 353–376.

Concrete Portal, 2015. Available through: http://www.theconcreteportal.com/hard_strength.html

Hudson J.A. and Harrison J.P., 1997. Engineering rock mechanics: an introduction to the principles, 1st edn. Pergamon, an imprint of Elsevier Science, Oxford, UK.

ISRM, International Society for Rock Mechanics, 2007. The complete ISRM suggested methods for rock characterization, testing and monitoring: 1974-2006. Ulusay P. and Hudson J.A. (edits.), 627 p.

Tutluoglu L., Öge I.F., Karpuz C., 2015. Relationship Between Pre-failure and Post-failure Mechanical Properties of Rock Material of Different Origin. Rock Mech Rock Eng 48, p. 121-141.